SHEAR AND VOLUMETRIC STRAINING RESPONSE OF ÇİNE SAND

A THESIS SUBMITTED TO
THE GRADUATE SCHOOL OF NATURAL AND APPLIED SCIENCES
OF
MIDDLE EAST TECHNICAL UNIVERSITY

BY

AHMET CAN KORKUSUZ

IN PARTIAL FULFILLMENT OF THE REQUIREMENTS
FOR
THE DEGREE OF MASTER OF SCIENCE
IN
CIVIL ENGINEERING

JANUARY 2021

Approval of the thesis:

SHEAR AND VOLUMETRIC STRAINING RESPONSE OF ÇİNE SAND

submitted by **AHMET CAN KORKUSUZ** in partial fulfillment of the requirements for the degree of **Master of Science** i**n Civil Engineering, Middle East Technical University** by,

Prof. Dr. Halil Kalıpçılar
Dean, Graduate School of **Natural and Applied Sciences**

Prof. Dr. Ahmet Türer
Head of the Department, **Civil Engineering**

Prof. Dr. Kemal Önder Çetin
Supervisor, **Civil Engineering, METU**

Examining Committee Members:

Prof. Dr. Erdal Çokça
Civil Engineering, METU

Prof. Dr. Kemal Önder Çetin
Civil Engineering, METU

Prof. Dr. Zeynep Gülerce
Civil Engineering, METU

Prof. Dr. Berna Unutmaz
Civil Engineering, Hacettepe Uni.

Assoc. Prof. Dr. Nabi Kartal Toker
Civil Engineering, METU

Date: 19.01.2021

I hereby declare that all information in this document has been obtained and presented in accordance with academic rules and ethical conduct. I also declare that, as required by these rules and conduct, I have fully cited and referenced all material and results that are not original to this work.

Name, Last name : Ahmet Can Korkusuz

Signature :

ABSTRACT

SHEAR AND VOLUMETRIC STRAINING RESPONSE OF ÇİNE SAND

Korkusuz, Ahmet Can
Master of Science, Civil Engineering
Supervisor : Prof. Dr. Kemal Önder Çetin

January 2021, 144 pages

The response of sandy soils under monotonic loading depends on size, shape and mineralogy of particles, fabric, stress and density states of mixtures. Researchers around the world have studied their local sands and calibrated their responses (e.g., Toyoura sand-Japan, Ottawa sand-Canada, Sacramento sand-US, Sydney sand-Australia, etc.). However, there are not many studies that have focused on regional sands from Turkey. This research study aims to introduce a local sand, Çine sand, to literature as a "standard sand" from Turkey. For this purpose, shear and volumetric straining responses of Çine sand samples were investigated by a series of consolidated undrained monotonic triaxial and oedometer tests. Specimens with relative densities of 25-47-60-70 and 85 %, were prepared by tapped funnel deposition and wet tamping methods and consolidated under 50 kPa, 100 kPa, 200 kPa ve 400 kPa cell pressures, followed by undrained shearing. Test results were presented by four-way plots, which enable the individual variations of axial load, cell pressure, pore water pressure, and axial deformation along with the progress of the stress paths relative to failure envelopes. On the basis of test results, linear and nonlinear elastic-perfectly plastic constitutive modelling parameters, including but not limited to stress and relative-density dependent modulus and effective stress based angles of shearing resistance, were estimated.Çine sands' angles of shearing resistance values of 24.2˚-39.5° were observed. Triaxial modulus values fall in the range of ~10 and ~60 MPa.

Similarly, samples with varying relative densities, prepared tapped funnel deposition method, were tested in a conventional oedometer device under stresses starting from ~23 kPa increasing up to ~29 MPa. During tests, unloading and reloading cycles were performed. Based on these test results, particle crushing-induced yield stresses of Çine sands along with their C_c, C_α values were estimated as ~1.3-3.1 MPa, $\sim 1\times10^{-2}$-25×10^{-2}, and $\sim 1\times10^{-5}$–1×10^{-3}, respectively. It was concluded that Çine sand exhibited Type B volumetric compression response as defined by Mesri and Vardhanabhuti (2009).

Keywords: Çine sand, Triaxial test, Oedometer test, Undrained behavior, One dimensional loading behavior

ÖZ

ÇİNE KUMUNUN KAYMA VE HACİMSEL BİRİM DEFORMASYON DAVRANIŞI

Korkusuz, Ahmet Can
Yüksek Lisans, İnşaat Mühendisliği
Tez Yöneticisi: Prof. Dr. Kemal Önder Çetin

Ocak 2021, 144 sayfa

Kumlu zeminlerin statik yükleme altındaki davranışı dane boyutu, şekli, mineralojisi, dokusu, gerilme ve sıkılık durumları gibi bir çok etken tarafından kontrol edilmektedir. Araştırmacılar kendi yerel bölgelerinde bulunan kumları çalışarak kalibre etmiş ve standart kumlar olarak literatüre sunmuşlardır (örneğin; Toyoura kumu- Japonya, Ottawa kumu- Kanada, Sacramento kumu- ABD, Sydney kumu- Avusturalya, vb.). Ancak Türkiye'de yerel kumlar üzerinde standart bir kum geliştirmeye odaklı fazla sayıda çalışma bulunmamaktadır. Bu çalışma yerel Çine kumunu literatüre standart bir kum olarak sunmayı amaçlamaktadır. Bu amaca yönelik olarak Çine kumunun kayma ve hacimsel birim deformasyon davranışı konsolidasyonlu-drenajsız statik üç eksenli ve odometre deneyleri ile incelenmiştir. Bağıl yoğunlukları % 25-47-60-70 ve 85 olan, kuru huni depolama ve nemli sıkıştırma yöntemleri ile hazırlanmış, ve 50 kPa, 100 kPa, 200 kPa ve 400 kPa hücre basınçları altında konsolide edilen numuneler, drenajsız yükler altında test edilmiştir. Sonuçlar, deney süresince numunenin eksenel yükleme, birim deformasyon, boşluk suyu basınç birikiminin izlenmesine imkan veren ve gerilme izini yenilme zarfı ile ilişkilendirebilen 4 yönlü grafikler kullanılarak sunulmuştur. Bu veriler esas alınarak, doğrusal ve doğrusal olmayan elastik-mükemmel plastik bünye modeli parametreleri belirlenmiş, bu parametrelerden modül ve efektif kayma direnci açısı gerilme ve bağıl sıkılık ile değişecek şekilde modellenmiştir. Çine kumunun kayma direnci açısının 24.2°-39.5° aralığında olduğu belirlenmiştir. Üç eksenli modül değerileri ise 10 ve 60 MPa aralığında değişmektedir.

Benzer olarak, farklı bağıl sıkılıklarda, kuru huni depolama yöntemi ile hazırlanan numuneler odometre düzeneğinde 23 kPa'dan başlayıp 29 MPa'a kadar artan düşey yükler altında test edilmiştir. Deney sırasında yükleme ve boşaltma tekrarları uygulanmıştır. Çine kumunun, danelerin kırılmaya başladığı yenilme gerilmelerinin ve C_c, C_α indis değerlerinin sırası ile ~1.3 ve ~3.1 MPa, $\sim 1\times10^{-2}$ ve $\sim 25\times10^{-2}$, $\sim 1\times10^{-5}$ ve $\sim 1\times10^{-3}$, mertebelerinde olduğu belirlenmiştir. Çine kumunun hacimsel birim deformasyon davranışının, Mesri and Vardhanabhuti (2009) tarafından tanımlanan, Tip B davranış grubuna dahil olduğu sonucuna varılmıştır.

Anahtar Kelimeler: Çine kumu, Üç eksenli deney, Odometre deney, Drenajsız davranış, Tek boyutlu sıkıştırma davranışı

To my family

ACKNOWLEDGMENTS

I would like to express my deepest gratitude to my supervisor Prof. Dr. Kemal Önder Çetin for his guidance, encouragement, patience, and support throughout my study.

I would like to thank Elife Çakır for her all supports.

I would like to thank Kamber Bilgin for his technical supports.

TABLE OF CONTENTS

CHAPTERS

LIST OF TABLES

TABLES

LIST OF FIGURES

FIGURES

LIST OF ABBREVIATIONS

ABBREVIATIONS

3-D	Three – Dimensional
ASTM	American Society for Testing and Materials
AG	Angular Glass
BG	Glass Ballotini
CU	Consolidated Undrained
IDL	Initial Dividing Line
L	Locking
LVDT	Linear Variable Displacement Transducer
MD	Machine Deflection
METU	Middle East Technical University
QSSL	Quasi Steady State Line
SP	Poorly Graded Sand
SSL	Steady State Line
UL	Unlocking
USCS	Unified Soil Classification System

LIST OF SYMBOLS

SYMBOLS	
A	Area of the sample
A_0	Initial area
A_c	Area after consolidation
A^*_c	Corrected area
B	The pore-pressure coefficient
c	Cohesion
C_c	Coefficient of curvature
C_c	Compression index
CO_2	Carbon dioxide
C_r	Recompression index
C_u	Coefficient of uniformity
C_α	Secondary compression index
D	Diameter
D_0	Initial diameter
D_{10}	Diameter corresponding to 10% finer
D_{30}	Diameter corresponding to 30% finer
D_{60}	Diameter corresponding to 60% finer
D_c	Diameter after consolidation
D_r, D_R, RD	Relative density

e	Void ratio
e_0	Initial void ratio
e_1	Void ratio after primary consolidation
e_f	Void ratio after primary + secondary consolidation
e_{max}	Maximum void ratio
e_{min}	Minimum void ratio
E_i	Initial elastic modulus
E_m	Modulus of elasticity of the rubber membrane
E_{trx}	Elastic modulus from triaxial test results
F_c	Corrected vertical load
F_v	Total vertical force
G_s	Specific gravity
H	Height
H_0	Initial height
H_c	Height after consolidation
h_t	Total height of the specimen
K	Modulus number
M	Constrained modulus
MC	Maximum curvature
M_{max}	Maximum constrained modulus
n	Modulus exponent
n	Number of layer being considered for undercompaction

n_t	Total number of layers for undercompaction
p'	Mean effective stress
P_a	Atmospheric pressure
q	Half of deviatoric stress
q/p'	Effective stress ratio
R_f	Failure ratio
t_0	Initial thickness of the rubber membrane
t_1	Time of primary compression
t_f	Time of primary + secondary compression
u	Pore pressure
U_{ni}	Percent undercompaction selected for first layer
U_{nt}	Percent undercompaction selected for final layer
U_n	Percent undercompaction for layer being considered
Δe_1	Void ratio change after primary consolidation
Δe_f	Void ratio changer after primary + secondary consolidation
Δh	Change in height
ΔH_1	Change in height after primary consolidation
ΔH_f	Change in height after primary + secondary consolidation
Δu	Pore pressure change
$\Delta \varepsilon_v$	Vertical strain change
$\Delta \sigma_3$	Change in cell pressure
$\Delta \sigma_{dcorr}$	Deviatoric stress membrane correction

$\Delta\sigma'_v$	Vertical stress change
$\Delta\varphi$	Change in the angle of friction
ε_1	Vertical strain after primary consolidation
ε_a	Axial strain
ε_f	Failure strain
ε_f	Vertical strain after primary + secondary consolidation
ε_r	Radial strain
ε_v	Volumetric strain
υ	Poisson's ratio
σ	Normal stress
σ_1	Major principal stress
σ_3	Minor principal stress
$(\sigma_1 - \sigma_3)_{ult}$	Asymptotic stress
σ_c	Cell pressure
σ_d	Deviatoric stress
σ_{dcorr}	Corrected deviatoric stress
σ_v	Vertical normal stress
σ'_1	Effective major principal stress
σ'_3	Effective minor principal stress
σ'_c	Effective consolidation pressure
σ'_v	Effective vertical stress
σ'_y	Yield stress

$(\sigma'_{v})_{MC}$	Effective vertical stress at maximum curvature
$(\sigma'_{v})_{Mmax}$	Effective vertical stress at maximum constrained modulus
φ_0	Angle of friction when confining pressure is equal to atmospheric pressure
φ'	Effective friction angle
ψ	Dilatancy angle

CHAPTER 1

INTRODUCTION

1.1 Research Statement

There exists a number of research studies regarding the mechanical behavior of clean sands. These studies confirm that sand behavior is complex, and its mechanical behavior depends on the size and shape of particles, mineralogy, and packing of the particles, stress and density states of the sand. Depending on these factors, the response of sand can be significantly different.

Sand behavior under high stress levels is also a concern with advances in the construction of high-rise buildings, high earth-fill dams, and deep tunnels, etc. Stress levels on foundation soils can reach to MPa levels. At these high stress levels, sand may be subjected to grain crushing. After crushing, both the physical and engineering properties of sand may significantly differ from their initial configuration. Therefore, it is essential to identify the crushing stress levels and understand the behavior of sand after crushing.

Researchers from different regions have studied their local sands and calibrated their responses (Toyoura sand-Japan, Ottawa sand-Canada, Sacramento sand-US, Sydney sand-Australia, etc.). However, there are not many studies that focus on regional sands from Turkey. The aim of this research study is to investigate the shear and volumetric straining response of Çine sand, and introduce this sand to the literature as a "standard sand" from Turkey. It is not a widely studied sand in the literature. Therefore, a laboratory testing program was designed to assess physical and mechanical properties of this sand. In the testing program, 20 monotonic strain-controlled consolidated undrained triaxial tests, 6 one-dimensional compression tests and soil index tests (minimum and maximum void ratio determination, grain size distribution and specific gravity determination) were performed.

1.2 Research Objectives

The research objectives are:

- To investigate the effects of stress states on the two-dimensional (triaxial) stress-strain behavior and strength of relatively loose and dense Çine sand specimens.
- To investigate the effects of density states on the two-dimensional (triaxial) stress-strain behavior and strength of Çine sand specimens consolidated to different confining pressures.
- To investigate the effects of density states on one-dimensional compression behavior of Çine sand.
- To define stiffness (E_{trx}) correlations for Çine sand on the basis of elasto-plastic constitutive models.

1.3 Scope of the Thesis

After introduction, a brief summary of the test system and available literature focusing on the sand behavior in terms of shearing and volumetric responses, and aspects that affect these behaviors is presented in Chapter 2.

Test systems are detailed in Chapter 3.

Test results and their interpretation are presented in Chapter 4.

In Chapter 5, the conceptualized constitutive modeling of Çine sand is presented. Linear and nonlinear elastic-perfectly plastic constitutive modeling parameters are developed on the basis of triaxial test results.

In Chapter 6, summary of the research is presented.

CHAPTER 2

LITERATURE REVIEW

During the geotechnical design processes, estimating how the granular soils behave under loading has been a problem for many years. Researchers have been working for a long time to understand the behavior of granular soils under different loading conditions. However, since many factors affect the behavior of granular soils under loading, researchers have difficulty categorizing these behaviors. For a typical granular soil type, the main factors affecting soil behavior are listed below:

- Void ratio
- Stress state before and during the loading
- Stress history
- Drainage situation
- Degree of saturation
- Fine content
- Permeability
- Mode of loading (monotonic or dynamic loading)
- Physical properties of soils (size, shape, angularity, mineralogy)

Since these factors differ, it is difficult to predict accurately the behavior of the granular soils under loading. Therefore, to understand each factor's effect on the behavior, researchers perform experiments by changing a factor within a specific range and keeping all other factors constant. The effect of void ratio and stress states onstress and straining response of Çine sand is the aim of this research study. Therefore, after the literature test system review, the literature theory review will be based on the effects of void ratio and stress state on granular soils' behavior.

2.1 Triaxial Testing System

2.1.1 Short History

The triaxial testing system is used for more than a century to understand the soils and rocks’ mechanical properties. The test system was first developed in 1910-1911 by Hungarian-American engineer Theodore von Kármán to understand rock samples’ mechanical properties. The systematic view is shown in Figure 2.1. With this experimental system, axial and confining pressures were changed separately, and the strength of rock samples was investigated. In the test system, confining pressure was generated by compressing the water in chamber “a”. This compression was transmitted by piston D_1 to chamber “b”. Rock samples were held between chamber “c” and chamber “b”. The longitudinal force was applied with a D_2 piston’s help, which directly transmits force to the rock sample. In the system, 600 MPa confining pressure could be generated. Force and deformations were measured with the help of a manometer and micrometer gauges (Deák et al., 2012).

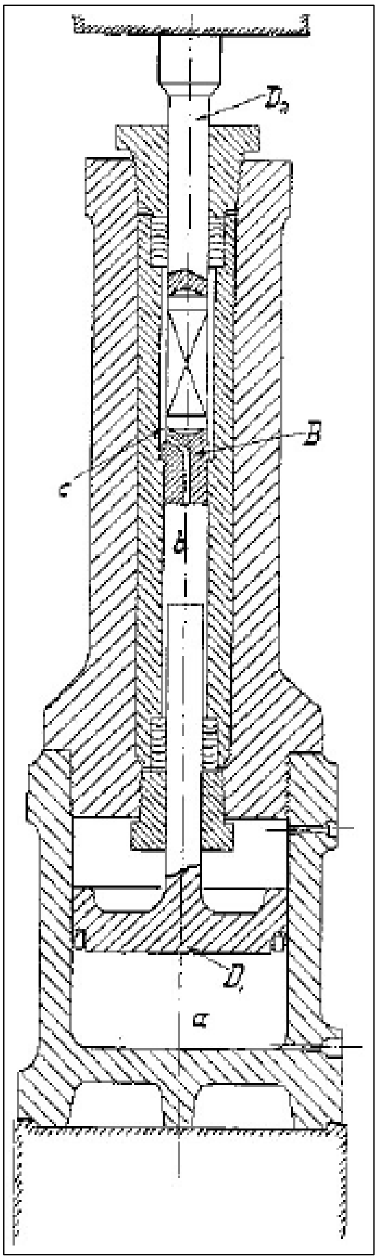

Figure 2.1. Schematic illustration of first triaxial test system developed by Theodore von Kármán (Deák et al., 2012)

2.1.2 Automated Triaxial Test System

Over the years, the triaxial test system has begun to be used to understand soil samples' behavior. As the factors that affect the soils' behavior were understood in more detail, the test system was improved. Also, to minimize human errors, automated systems were constituted.

With a triaxial test system, intact or reconstituted samples prepared in the laboratory are consolidated to a specific stress state and then loaded until a certain strain level. With this test system, soil behaviors such as stress-strain behavior, volume change, pore pressure change are investigated. There are several advantages and disadvantages of the test system (Lade, 2016), as explained below.

The advantages are:

- Drainage system control
- Volume change measurement
- Pore pressure measurement
- Deformation measurement
- Specimens can be brought to the desired stress state before the test.

The disadvantages are:

- Stress concentrations caused by friction at the upper and lower caps of the specimen can cause nonuniform strains and stresses.
- While axisymmetric stress conditions can be created with the triaxial testing system, 3-D unsymmetrical stress conditions occur in the field.

Triaxial tests can be carried out in two different ways, monotonic (compression, extension, or shear) and cyclic. Since consolidated undrained (CU) monotonic compression tests will be carried out within this research scope, the literature review will be based on the monotonic compression under undrained situation concept in the following parts.

2.1.3 Consolidated Undrained (CU) Triaxial Testing System Under Monotonic Compression

In general, CU tests start by applying a certain all-around pressure (σ_3) to the specimen and consolidate the specimen to a specific stress state. Then additional axial stress is applied. This additional stress is called deviatoric stress. During the loading, total axial stress is the sum of all-around pressure and deviatoric stress, as shown in Figure 2.2. By observing the changes in deviatoric stress and pore pressure with increasing axial strain, soils' behavior is investigated.

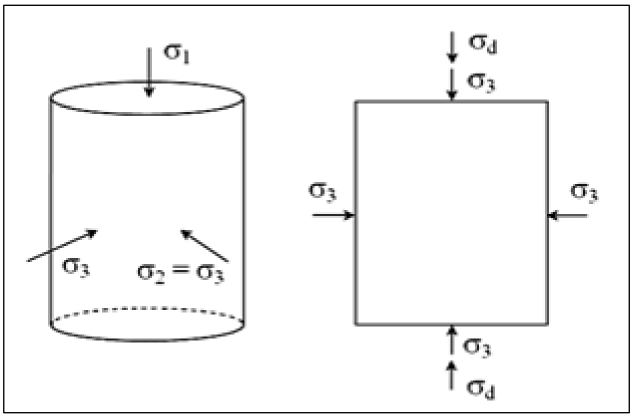

Figure 2.2. Stress states during monotonic triaxial compression tests

Consolidated undrained (CU) triaxial tests consist of 4 main stages, specimen preparation, saturation, consolidation, and shear stage, as explained following parts.

2.1.3.1 Specimen Preparation

The soils in the field have a heterogeneous structure. Specimens prepared for the triaxial test system should adequately reflect the situation in the field. Therefore, the geometric properties of the specimens are essential for the reliability of the results. Since the soils are quite heterogeneous, the larger the size of the samples prepared, the closer the real situation is. However, in terms of the test systems' capacity and the tests' practicality, the samples' geometric properties must be within certain limits.

As a result of the studies, some geometric properties that can be considered optimum for the specimens were determined. These features can be listed as follows:

- Generally, cylindrical specimen shapes with diameters ranging from 35 mm to 150 mm are used in practice. Nevertheless, square and rectangular samples can also be used (Lade, 2016).
- It is recommended to prepare the sample diameter at least six times the maximum particle size for uniformly graded soils, and eight times for well-graded samples to reduce the not suitable sized particles in the sample. (Marachi et al., 1972; Wong et al., 1975).

It is recommended to have a H/D ratio between 2 and 2.5 to reduce nonuniform stress and strain due to friction between sample and cape & base. Nonuniform stress and strains may result in shear bands, which may affect the samples' peak strength. However, using lubricated endplates, nonuniformity in strain and stress decreases in samples with a H/D ratio smaller than 2. In other words, in the tests performed with lubricated endplates, consistent stress-strain behavior is observed in samples with H/D ratio smaller than 2 (Lade & Wasif, 1988; Wang & Lade, 2001). Figure 2.3 shows that for non-lubricated endplates samples in cases where the H/D ratio is two or more, the maximum angle of shearing resistance does not change. In cases where H/D is less than 2, the maximum angle of shearing resistance value increases with decreasing H/D ratio. It is also seen from Figure 2.3 that when appropriately lubricated ends are used, there is no change in the maximum angle of shearing resistance value even for a H/D ratio of 1.

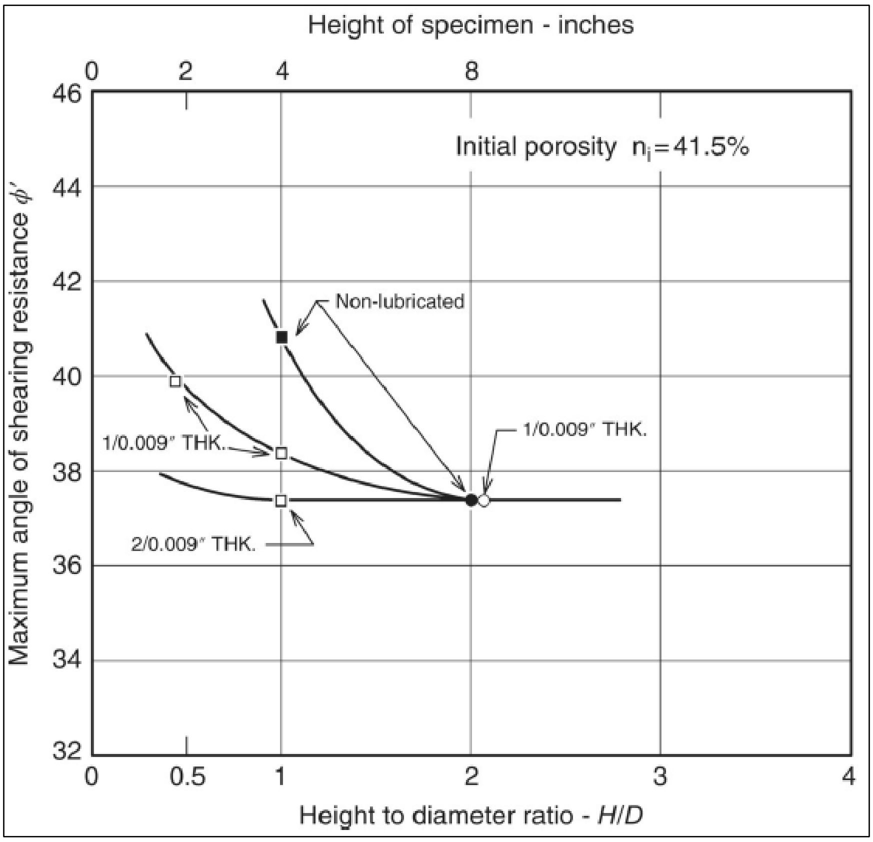

Figure 2.3. Effects of H/D ratio and lubricated end plates on the behavior of samples (Lade, 2016)

The use of consistent and representative specimen preparation methods are crucial to get realistic results from triaxial tests. The void ratio in the specimen should be as uniform as possible. Otherwise, unrealistic behaviors can be obtained. Specimens are generally prepared in two different ways for the triaxial test systems. The first way is to use an intact specimen taken directly from the field and prepared for the tests under suitable transportation and storage conditions. This method is generally used for cohesive materials, which is not the scope of this research. The other way is preparing reconstituted specimens in the laboratory. Granular soils are generally reconstituted in the laboratory since they do not have enough effective stress to hold themselves. Within this research scope, Çine sand samples will be reconstituted in the laboratory for tests. Therefore, laboratory reconstituted specimen preparation techniques for sands will be examined in the following parts. Generally, sand specimens' preparation techniques are divided into two main groups, pluviation (or deposition) and tamping techniques.

2.1.3.1.1 Pluviation or Depositional Techniques

Air Pluviation

The air pluviation technique is one of the sample preparation techniques used to represent the formation of layers of sand in the laboratory. It is carried out by pouring sand from a certain height at a specific rate into the mold. Depending on the height and pouring rate, specimens with the desired void ratio can be obtained. Vaid & Negussey (1984) worked with Ottowa sand to investigate the effect of drop height on the void ratio. In Figure 2.4 and 2.5, the results of Ottowa Sand and its comparisons with Leighton Buzzard Sand are shown.

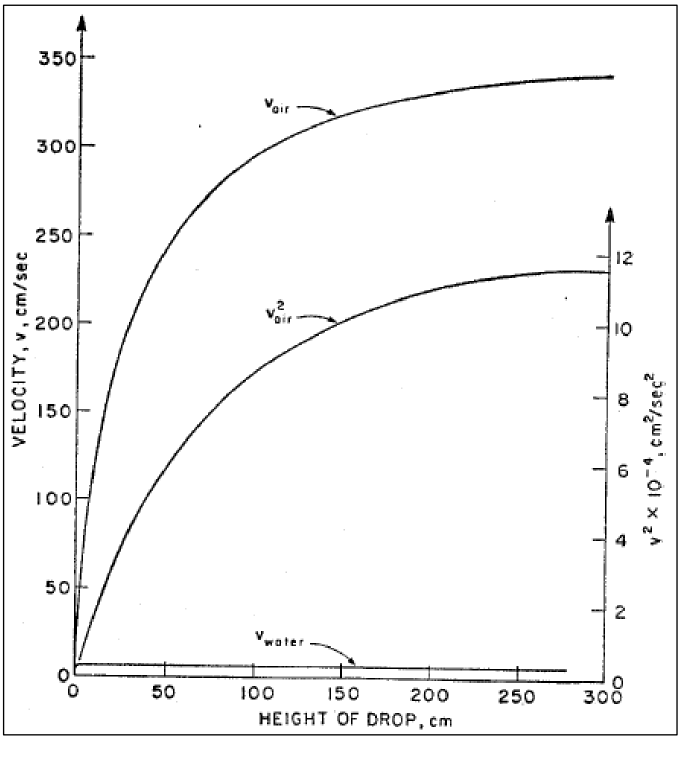

Figure 2.4. The effect of drop height on the velocity of particles in air pluviation specimen preparation method (Vaid & Negussey, 1984)

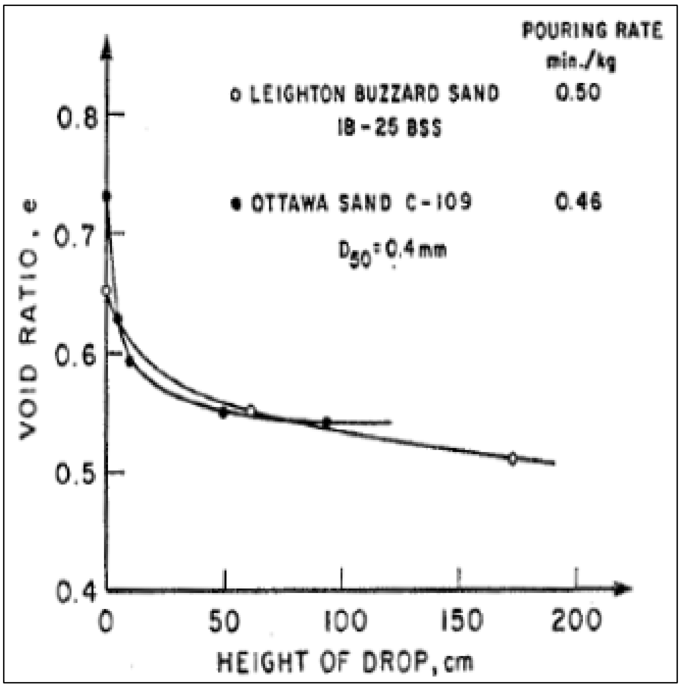

Figure 2.5. The effect of drop height on the void ratio in air pluviation specimen preparation method (Vaid & Negussey, 1984)

As shown in Figure 2.4, the particles' velocity increases up to a specific drop height. At higher velocities, the particles have more compaction energy, resulting in denser specimen. Therefore, specimen density increases up to a particular drop height. The value at which velocity change with drop height to be minimal, is called terminal velocity. Even if drop height increases, the void ratio change will be very small after reaching terminal velocity. The height of the drop effect on the void ratio is shown in Figure 2.5. Until a certain drop height, the void ratio is decreasing, and after that point, the void ratio change is very small. To get a uniform void ratio in the specimen, drop height should be kept constant during pouring. The rate of pouring effect is opposite to the drop height effect. As the pouring rate decreases, denser specimens are obtained. (Vaid & Negussey, 1984).

Dry Funnel Deposition

The dry funnel deposition method may be considered as a modified version of the air pluviation method. In this method, the sample is filled into the funnel. The funnel is lifted symmetrically upwards, starting from the bottom of the mold. Without drop height, the specimen is deposited in a low energy state. A slow and symmetrical vibration is applied from the edges of the mold to reach high density, which is called "Tapped Funnel Deposition". In Figure 2.6 (a), a schematic representation of the dry funnel deposition method prepared by Wood et al. (2008) is shown.

Water Sedimentation

It is a method performed by pouring dry or saturated sand into the mold, which is filled with water. Sand is deposited with the help of a volumetric flask. The deposition is performed by lifting the flask symmetrically and slowly. As sand pours from flask to mold, the vacuum builds up due to the flask's void, and the water in the mold moves towards the flask. At the end of the method, the sand remaining in the flask is dried, and its weight is determined. In this way, the total amount of sand in the specimen is found. The technique represents layer formation in the field as in the air pluviation method. In Figure 2.6 (b), a schematic representation of the water sedimentation method prepared by Wood et al. (2008) is shown.

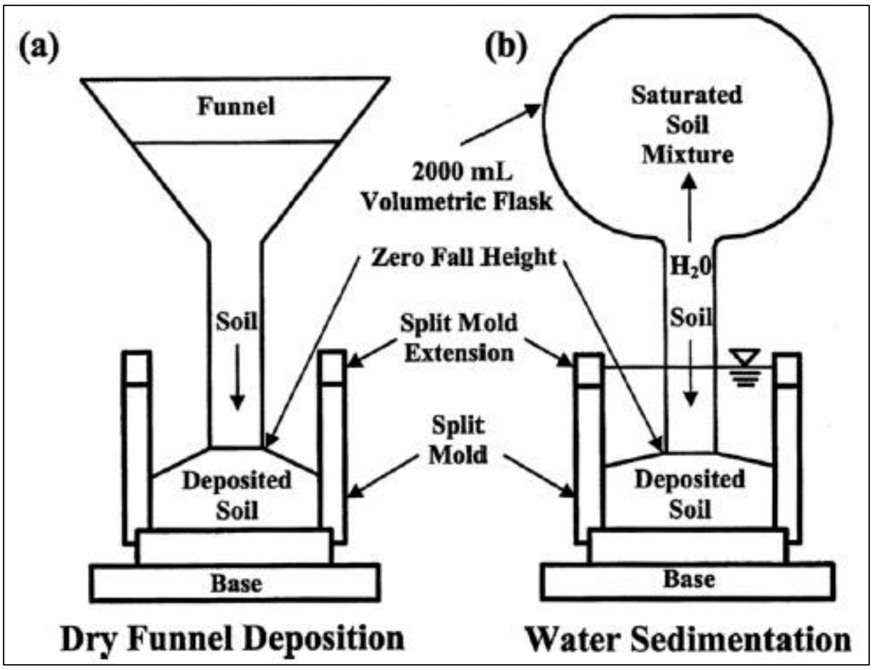

Figure 2.6. Schematic representation of (a) dry funnel deposition and (b) water sedimentation techniques (Wood et al., 2008)

2.1.3.1.2 Tamping Techniques

Moist Tamping

It is a sample preparation method that is carried out by placing the sand with a certain water content into the split mold and tamping it to a predetermined height. In general, the tamping in the lower layers is less than the tamping in the upper layers to have a uniform density. The reason is that the lower layers are also affected by tamping of the upper layers.

Due to the capillary effect between the soil particles, very loose sand samples can be prepared with the moist tamping method. In some cases, specimens can be prepared with a larger void ratio than the maximum void ratio found according to ASTM - max void ratio standard. Strain softening behavior can be easily observed in samples prepared with this method (Konrad, 1990).

Vaid et al. (1999) show the comparison of density uniformity of samples prepared with moist tamping and water sedimentation in Figure 2.7. As shown from Figure 2.7, Fraser River Sand, which is prepared with moist tamping, and Ottowa Sand (Vaid & Negussey, 1988), which is prepared by the water sedimentation method, show different density uniformity along with the height. The variation of the void ratio along the samples' height prepared with water sedimentation is less than the moist tamping method. In other words, samples prepared with the water sedimentation method have a more uniform density along with the height.

To minimize the density difference between the layers, Ladd (1978) also developed the undercompaction method by modifying the moist tamping method. Sands are mixed with water to reach certain water content. The amount of sand-water mixture is defined to reach the desired density. Then, the number of layers and layer thicknesses are defined for uniform density along with the specimen's height. With this method, a more uniform density along the height is obtained.

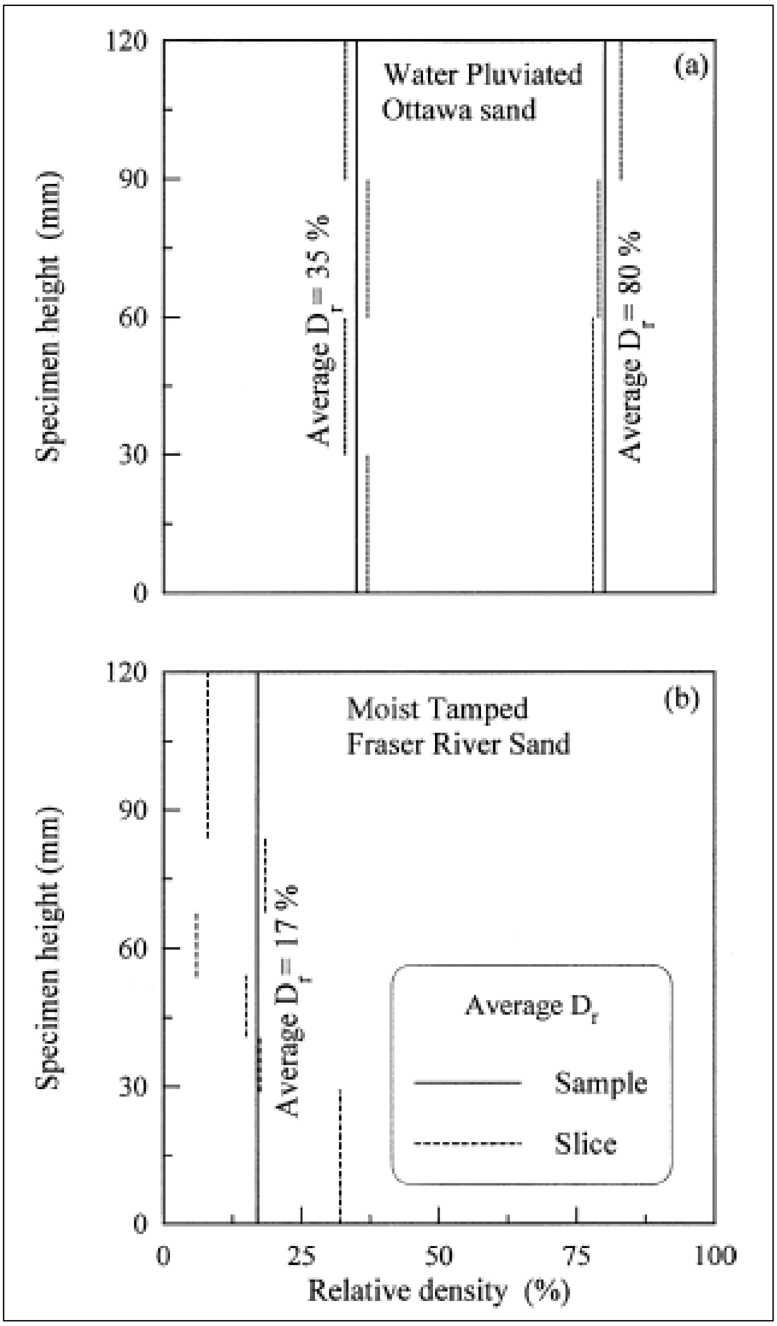

Figure 2.7. Relative density change along with specimen height for Ottowa sand (prepared by water sedimentation method) and Fraser River Sand (prepared by moist tamping method) (Vaid et al., 1999)

2.1.3.2 Saturation Stage

Saturation is applied to fill all the voids with water in the soil. With full saturation, pore water pressure (in undrained tests) and volume change (in drained tests) can be measured correctly during the test. In general, three methods are used to saturate the samples in the laboratory. These methods are:

Percolation with water:

It is a system that percolates water through the specimen by applying pressure. The aim is to get the air bubbles out from voids and fill all voids with water. A vacuum can be applied from the outlet of the water to help saturation. With this method, it is not easy to fully saturate the soil. Even in high permeable clean sands, air bubbles can be trapped between the particles and prevents full saturation with this system. Also, since the system requires much time, it is not practical. For these reasons, this system is not preferred alone to saturate the soils. Nevertheless, the system can be used to help other methods (CO_2 & back pressure methods) (Lade, 2016).

CO_2 Method:

This method is performed by percolating CO_2 gas through the specimen for a particular time. The aim is to fill the voids inside the soil with lighter gaseous CO_2. CO_2 dissolves in water faster than air. After the CO_2 percolation, the de-aired water is passed through the specimen, and CO_2 gas in the voids is replaced with water. The remaining CO_2 in the voids dissolves in water. In this way, the soil is tried to be fully saturated. In this method, the rate of CO_2 transmission is important. In the case of fast passing, effective stress will change as the pressure will increase in the region where the passing begins, and this situation may affect the behavior. Lade & Abelev (2005) set up a system for the CO_2 method that is shown schematically in Figure 2.8. As can be seen from the Figure, water percolation and vacuum systems can also be applied to help this method. The CO_2 method may not be effective if air bubbles are trapped in water on partially saturated soils. For this reason, this method is more effective on dry and permeable soils.

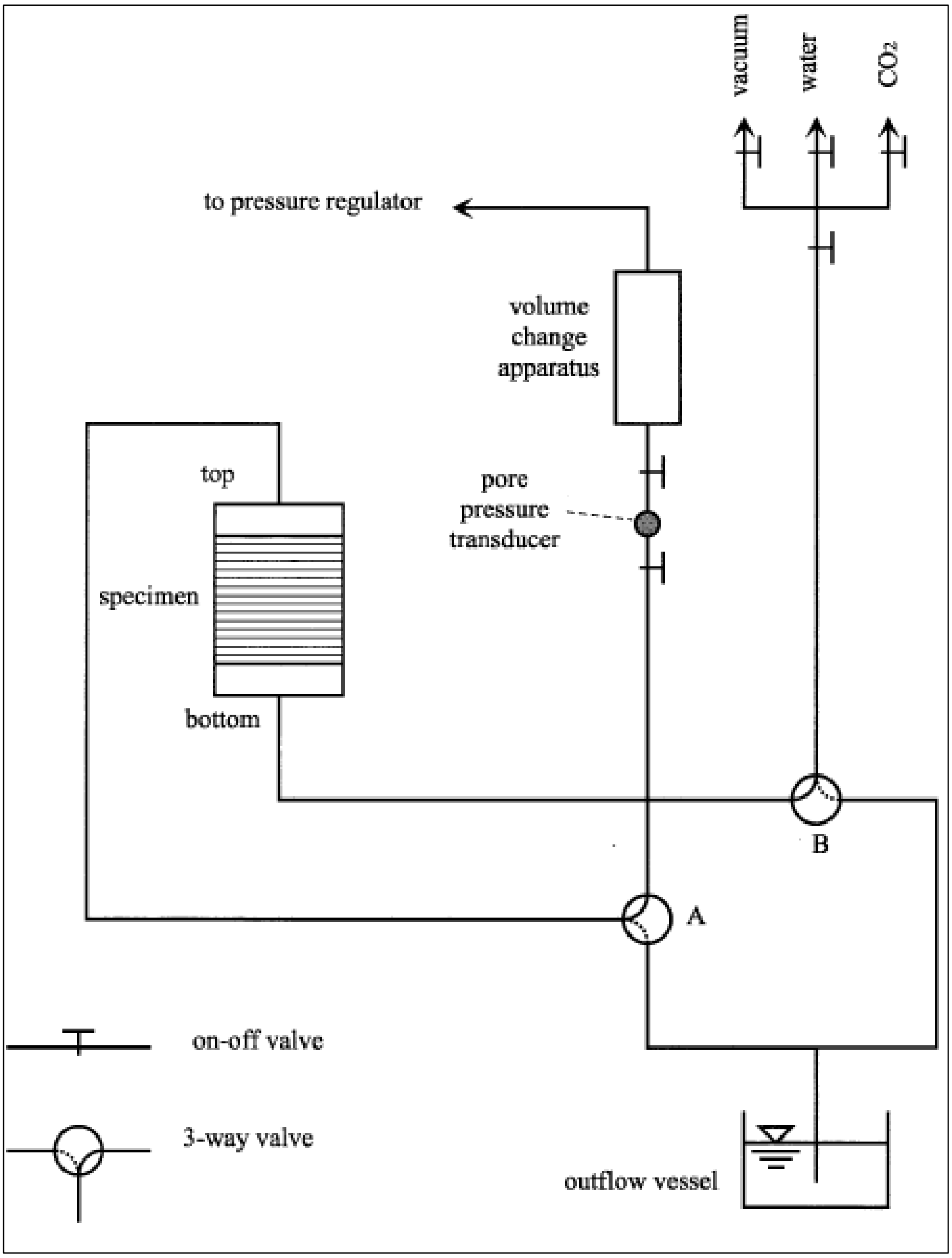

Figure 2.8. Schematic representation of CO_2 Method (Lade & Abelev, 2005)

Application of Back Pressure:

With this method, positive pore pressure is created by applying pressure into the soil, and the soil is tried to be saturated. According to Boyle's law, the pressure and volume product is constant for ideal gases. In other words, if the pressure is increased, the volume of the gas will decrease. In this way, by increasing the specimen's pore pressure, the gas volume is reduced, and high saturation can be achieved. According to Henry's law, the amount of gas that can be dissolved in water under constant temperature is proportional to pressure. With the back pressure method, high saturation can be achieved by increasing the specimen's pressure and dissolving the gas in the voids with water.

With the back pressure method, the degree of saturation can be determined by gradually determining the Skempton B value during the saturation. After waiting for a specific time under back pressure, while all drain valves are closed, cell pressure is increased by a certain amount (≈ 50 kPa), and the change in pore water pressure is calculated. This value is called B.

$$B = \frac{\mathit{\Delta} u}{\Delta\sigma_3} \qquad \text{Eqn. 2.1}$$

If the B value is greater than 0.93-0.95, it is considered that the sample has reached full saturation.

2.1.3.3 Consolidation Stage

Since the soils' behavior depends on the stress state before the loading, the soils are consolidated to a specific stress state before starting the shear stage in the triaxial test system. Specimens should be close to the field's conditions to achieve realistic results with the triaxial test system. For this reason, the consolidation pressure to be chosen should be compatible with the situation on the field. While high consolidation pressures are applied to understand deep soils' behavior, lower consolidation pressure should be applied to understand shallow soils' behavior.

Naturally, the soils in the field are under anisotropic stress state. Therefore, bringing samples to an anisotropic stress state in the consolidation stage will enable us to obtain more realistic behaviors. However, applying anisotropic consolidation in the triaxial test system is challenging and not practical; therefore, isotropic consolidation is generally employed. Isotropic consolidation means the application of same stress to the sample from all axes. In other words, the three principal stresses are equal, and they are equal to cell pressure value ($\sigma_1 = \sigma_2 = \sigma_3 = \sigma_c$).

After the B value exceeds 93-95% at the saturation stage, the back-pressure valve is closed to keep the back-pressure constant, and the cell pressure is increased until the desired consolidation pressure is reached. Then the back-pressure valve is opened. Water comes out, and pore pressure in the specimen is fixed. After the water is fixed, its amount is measured, and new dimensions of the specimen are recorded. Finally, the sample is ready to the shearing stage (ASTM D4767 – 11).

2.1.3.4 Shearing Stage

The shearing stage is the last stage of the triaxial test system. In this stage, soil responses (deviatoric stress & excess pore pressure change with axial strain) are assessed. The stage can be carried out in two different ways; strain and stress controlled. In stress-controlled tests, the sample is loaded with a specific stress increment. In this approach, peak stress values are uncertain and can only be indirectly predicted. Therefore, they are less preferred than strain-controlled tests. On the other hand, in strain-controlled tests, the sample is loaded with a specific strain rate, and peak stresses can be determined precisely. The strain rate to be applied varies depending on the type of test and soil. In granular soils, relatively high strain rates can be applied due to their higher permeability.

During the shearing stage, deviation from the specimen axis should be as low as possible. Otherwise, non-uniform stress-strains may lead to misunderstanding of behavior. There are several ways to prevent deviating from their axis along the shear stage. During the specimen preparation, the specimen should have a uniform void ratio along with the height. Piston and top cap should be compatible with each other, and the top cap diameter must be equal to the specimen diameter. An appropriate H/D ratio (2-2.5) should also be selected to prevent end restraint effects. If a lower H/D ratio would be prepared, lubricated ends should be employed.

The shearing stage starts after the specimens are bought to the desired stress state at the consolidation stage. Since the test is undrained, all valves (except the cell pressure valve) are closed during loading to prevent water in or out of the sample. Then the strain rate is chosen. The loading continues until the strain level at which behavior is desired to be assessed. Then the shearing stage is completed.

2.1.4 Undrained Behavior of Clean Sands Under Monotonic Loading

Under stresses, granular soils tend to change their volume because of particle rearrangement. Volume change tendency with stress is called dilatancy. Rearrangement of particles depends on two mechanisms, crushing of particles and particles’ motion (sliding and rolling). Sliding and rolling of particles determine dilatancy tendency at stress levels where particle crushing is not essential. With sliding motion, particles try to fill voids in the soil and decrease the soil’s volume. This behavior is also called contractive behavior. With contractive behavior, soils tend to reach to a denser structure. Since particles’ movement is in the direction of the applied stresses, sliding behavior starts from the first stages of loading. On the other hand, particles try to move over nearby particles with a rolling motion and increase the soil’s volume. This behavior is also called dilative behavior. With dilative behavior, soils tend to get a looser structure. Unlike the sliding behavior, rolling behavior starts only after a certain amount of deformation. (Lambe & Whitman, 1969; Ishihara, 1996).

Dilatancy is primarily dependent on the initial void ratio and stress state. Generally, loose sands or sands under relatively high confining stresses exhibit contractive behavior, while dense sands or sands under relatively low confining stresses exhibit dilative behavior. Therefore, it can be concluded that dilatancy is governed by a combination of void ratio and confining stress states. Castro (1969) studied with Banding sand and carried out isotropically consolidated undrained triaxial tests. The results of the tests are shown in Figure 2.9. From these results, the effects of void ratio and stress state on dilatancy, and hence on the undrained behavior sands are clearly observed.

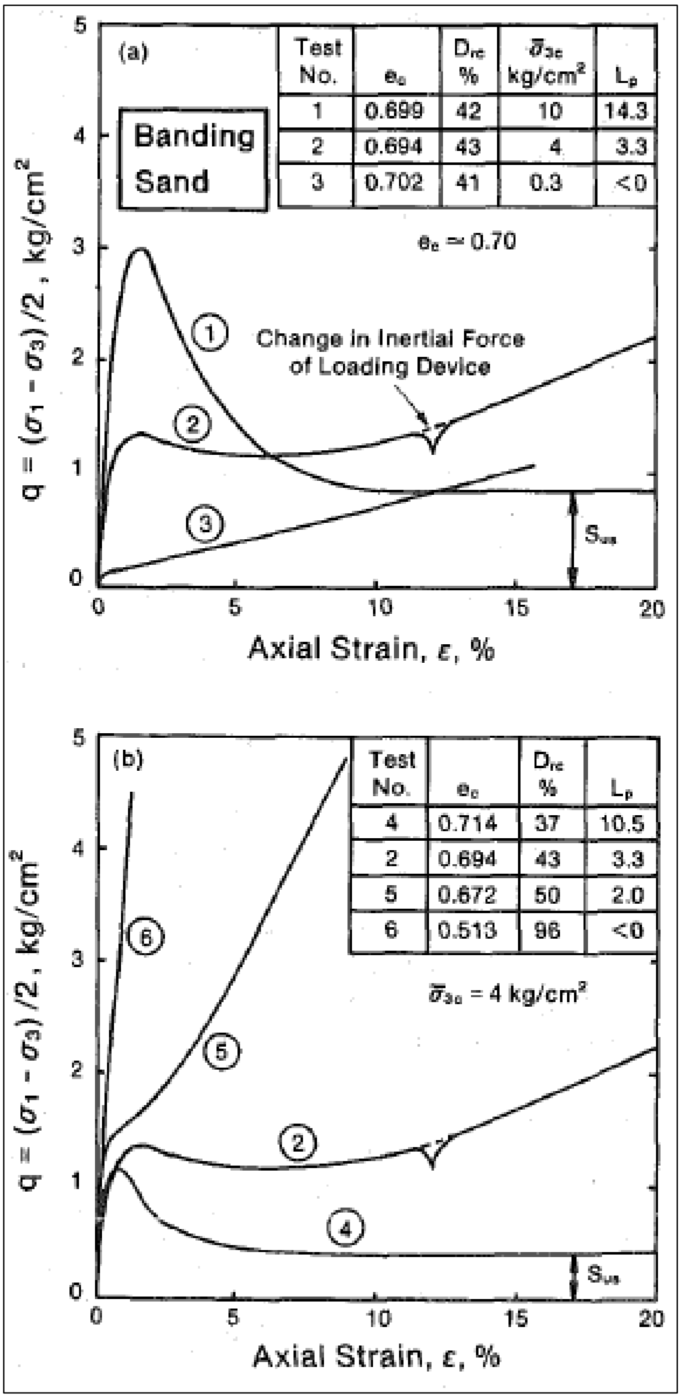

Test No.	e_c	D_{rc} %	$\bar{\sigma}_{3c}$ kg/cm^2	L_p
1	0.699	42	10	14.3
2	0.694	43	4	3.3
3	0.702	41	0.3	<0

Test No.	e_c	D_{rc} %	L_p
4	0.714	37	10.5
2	0.694	43	3.3
5	0.672	50	2.0
6	0.513	96	<0

Figure 2.9. Effects of void ratio and confining stress on the undrained behavior of Banding Sand (Castro, 1969)

It can be concluded from these results that in lower void ratios (“dense” conditions), the particles try to roll over each other with loading, and thus volume expansion tendency occurs. However, since there is no volume change in undrained systems, this volume change tendency turns into negative excess pore pressure in the undrained systems to achieve force equilibrium in the sand structure. With negative excess pore pressure, effective stress will increase during loading. In this situation, strength will increase with axial strain. This response is called strain hardening, as shown in Figure 2.9, test no 6. On the other hand, in “loose” conditions, particles try to fill voids with loading, and volume contraction tendency occurs. In the same way, since there is no volume change in undrained systems, particles transmit the load on to water, resulting in positive excess pore water pressure buildup in the soil. With positive excess pore water pressure, effective stress decreases during loading. In this case, strength will decrease with axial strain. This response is called strain-softening, as shown in Figure 2.9, test no 4.

Figure 2.9 also shows how undrained response changes with confining stress. For the same relative density samples, in higher consolidation pressure, more contractive behavior is observed. The reason is that as the confining stress increases, the stiffness of the soil increases too. In this case, it will be difficult for the particles to roll over each other due to the high confining pressure. This results in more contractive behavior in higher consolidation pressures.

As a result of the particle rearrangement concept in undrained systems, if particles tend to slide and fill voids, contractive behavior is observed, resulting in an overall strain softening response. On the other hand, if particles tend to roll over each other, dilative behavior is observed, resulting in strain hardening response. During loading, sliding and rolling tendencies occur independent of each other. If the rolling tendency is dominant, dilative behavior is observed, while if sliding tendency is dominant, contractive behavior is observed. This dominance may change during loading, and hence undrained behavior changes during loading. In this context, Yoshimine & Ishihara (1998) explain general undrained behavior under large deformations, as shown in Figure 2.10.

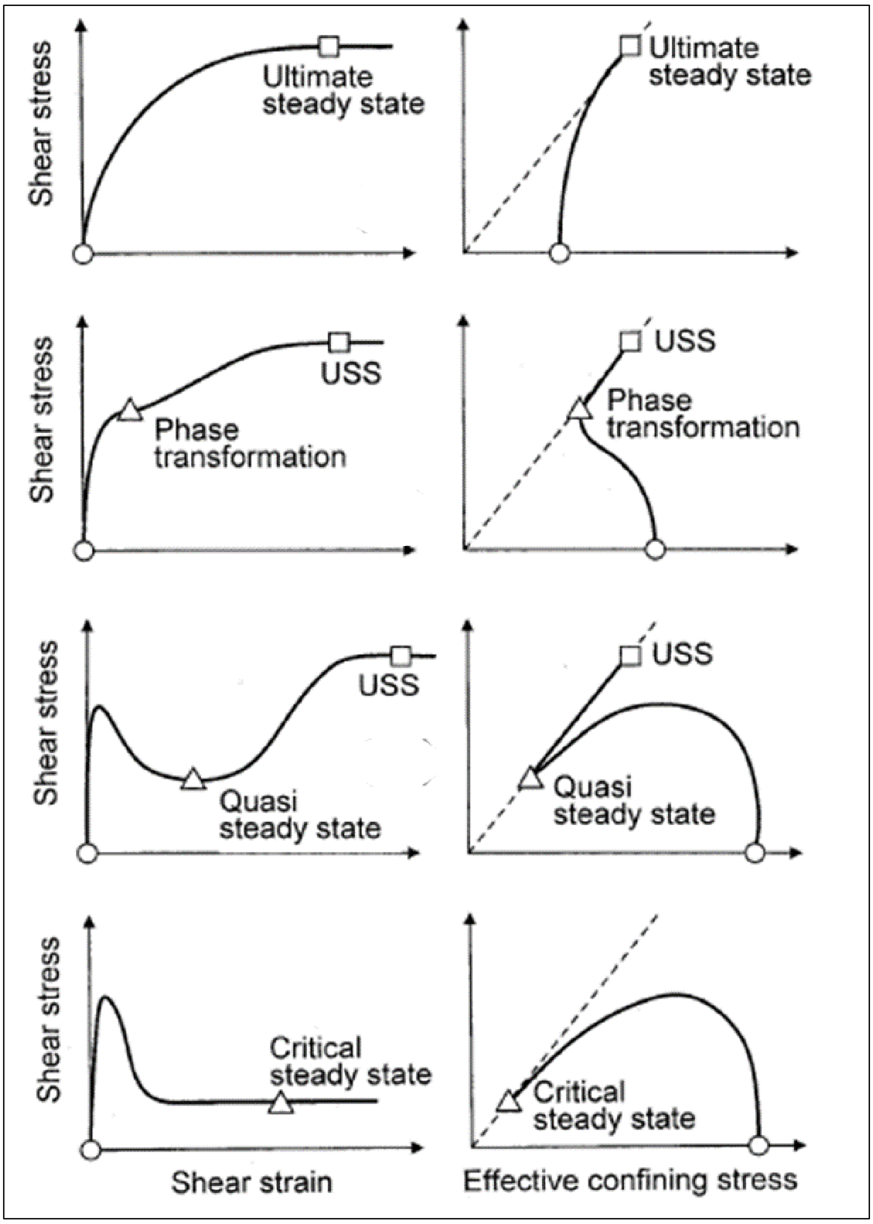

Figure 2.10. Types of Generalalized Undrained Behavior of Sands (Yoshimine & Ishihara, 1998)

As shown in Figure 2.10, four generalized responses are observed as part of undrained behavior of clean sands subjected to monotonic loading.

Case 1:

During loading, dilative behavior is always dominant, and therefore strain hardening takes place until reaching ultimate steady state. The ultimate steady state is defined as the state of continuous deformation of soils under constant shear and mean stresses, independent of the initial fabric, and confining stress (Verdugo & Ishihara, 1996). Soils usually reach this state at relatively higher strain levels (> 20-25% strain levels). The strength of soil at the ultimate steady state is called residual strength. For each void ratio, the stress state in the ultimate steady state is unique. If the void ratio, e, and effective mean stress, p′ values at the ultimate steady state are jointly considered in the e–p′ plane, the steady state line is obtained as shown in Figure 2.11, which shows the steady state line of Toyoura sand (Ishihara, 1996). The steady state line is a unique line for the soils, and it is independent of the initial state and the initial fabric (Ishihara, 1993).

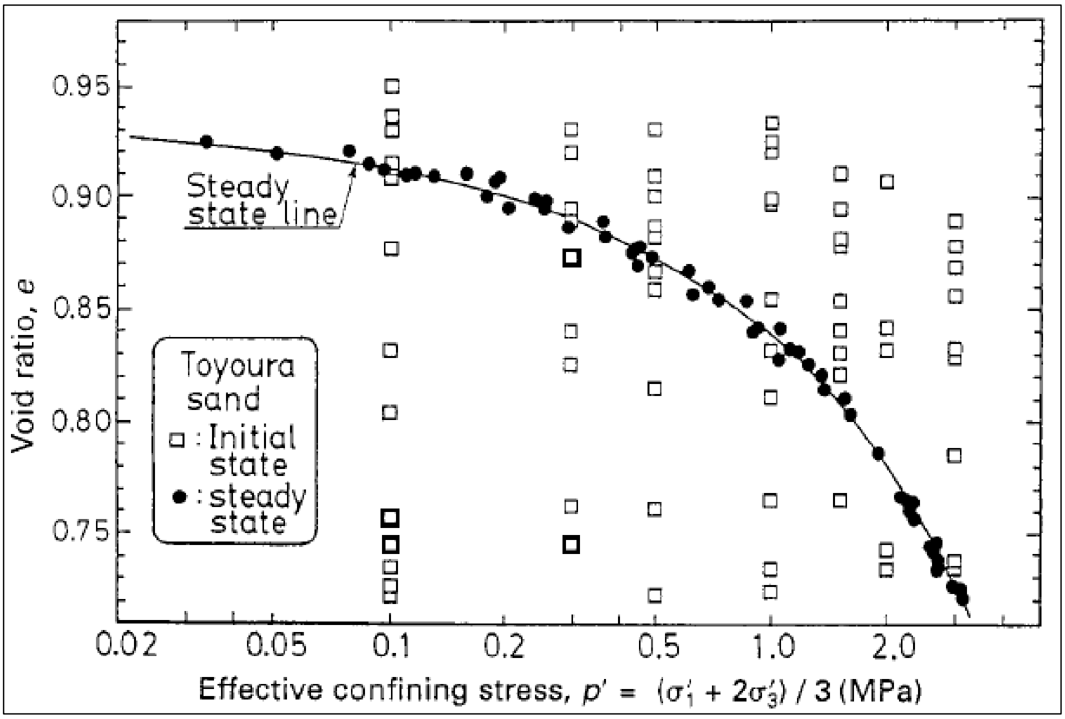

Figure 2.11. Steady state line of Toyoura sand (Ishihara, 1996)

Case 2:

Depending on the void ratio and confining stresses, after a peak in shear stress, sands show strain softening (contractive) behavior until a certain strain level, and at that point, minimum mean effective stress is obtained. After that point, contractive behavior turns into dilative behavior. This point is called phase transformation (Ishihara et al., 1975). In the q vs. p′ graphs, phase transformation is observed in an elbow shape, as shown in Figure 2.12, which shows the phase transformation of Toyoura sand (Ishihara, 1996). After phase transformation, sands show strain hardening behavior until reaching the ultimate steady-state.

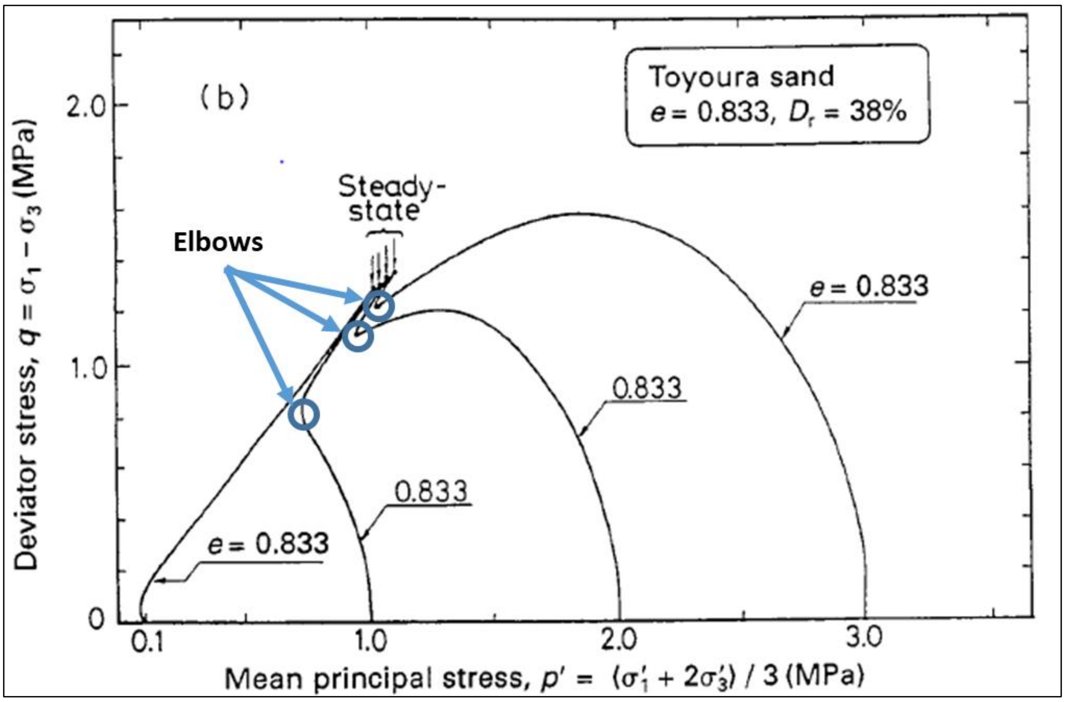

Figure 2.12. Phase transformation of Toyoura sand (Ishihara, 1996)

Case 3:

Similar to case 2, after a peak in shear stress, sands show strain-softening response until a certain strain level, and minimum mean effective stress is reached. Unlike case 2, deformation occurs under constant shear stress until a certain strain level. This state is called quasi steady state. After that certain strain level, if confining stress is not high enough to prevent dilative behavior, dilative behavior picks up again, and strain hardening behavior continues until reaching the ultimate steady state. The Quasi steady state, unlike the ultimate steady state, changes slightly depending on the initial confining stress. The higher the initial confining stress for the same void ratio, the higher the minimum strength (at quasi steady state). However, this difference is not significant, and therefore, a unique quasi steady state line can be drawn in the e-p′ plane by taking average mean effective stress for sand samples, as shown in Figure 2.13, which shows a quasi steady state line of Toyoura sand (Ishihara, 1996). On the other hand, unlike the steady state line, the quasi steady state line is severely affected by the initial fabric and structure. For this reason, the experiments should be performed with the same fabric and structure if quasi steady state line is to be determined (Verdugo and Ishihara, 1996).

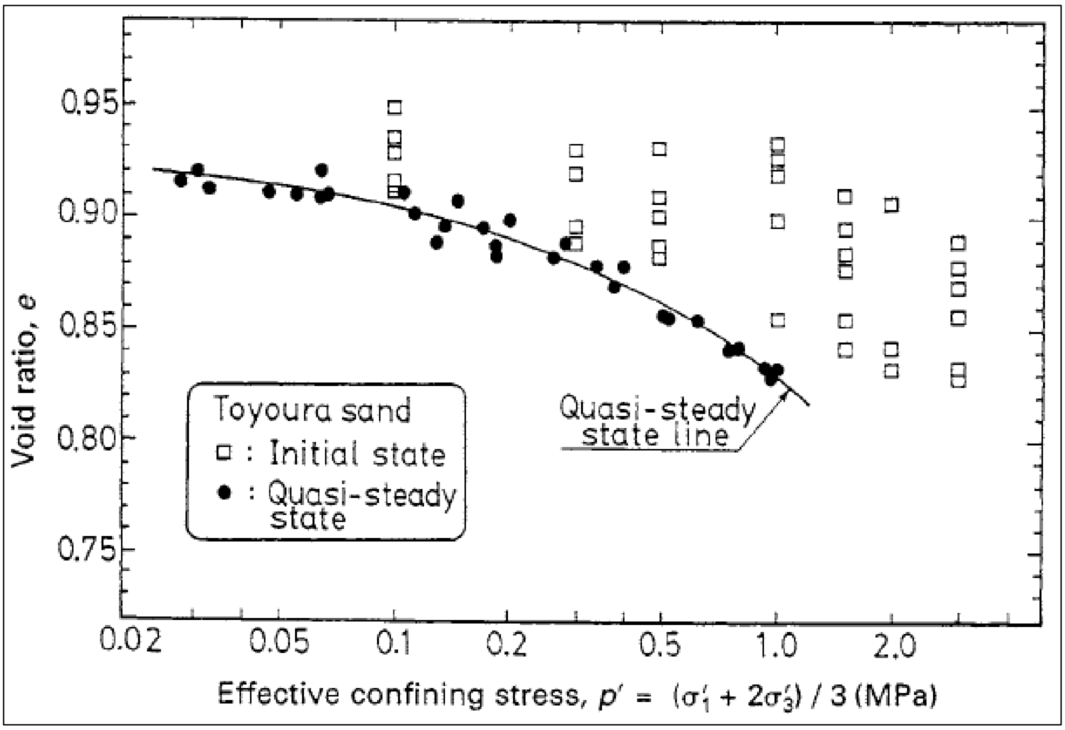

Figure 2.13. Quasi steady state line of Toyoura sand (Ishihara, 1996)

Case 4:

In this case, after reaching minimum strength, sands go directly to the ultimate steady state. The reason is that after reaching minimum strength, dilative behavior never shows up because of the very loose structure or relatively high confining pressure states. This is called critical steady state.

Ishihara (1996) points out a characteristic line called the initial dividing line (IDL) for sands as shown in Figure 2.14 for Toyoura sand. This line defines the boundary for initial conditions (a combination of initial void ratio and mean effective stress before shearing), where sands show strain hardening or strain-softening behavior. IDL shows (as reference to initial conditions) if samples show strain hardening (circles) or strain softening (dots) behavior, as shown in Figure 2.14.

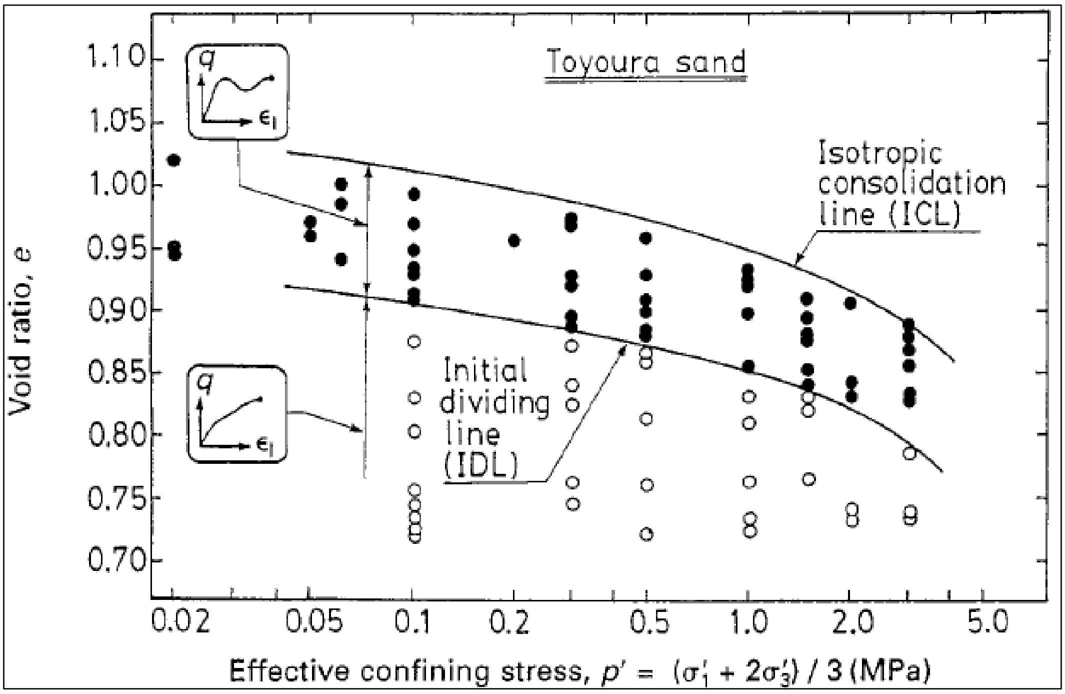

Figure 2.14. Initial Dividing Line for Toyoura Sand (Ishihara, 1996)

In the Figure 2.15, characteristic lines (isotropic consolidation lines for the loosest and the densest states (ICL), which are drawn with e vs. p′ data pairs under isotropic consolidation, such as initial dividing line (IDL), quasi steady state line (QSSL), and steady state line (SSL) for Toyoura sand are shown. With these characteristic lines, Toyoura sand’s behavior is well constrained based on their void ratio and mean effective stress states. With this, boundaries of behavior are known, and thus, information about the direction of behavior is obtained according to soil conditions.

A point to note here is that if the initial conditions are below the IDL, the QSSL does not have any significance since the sample goes into the steady state directly with increasing strain.

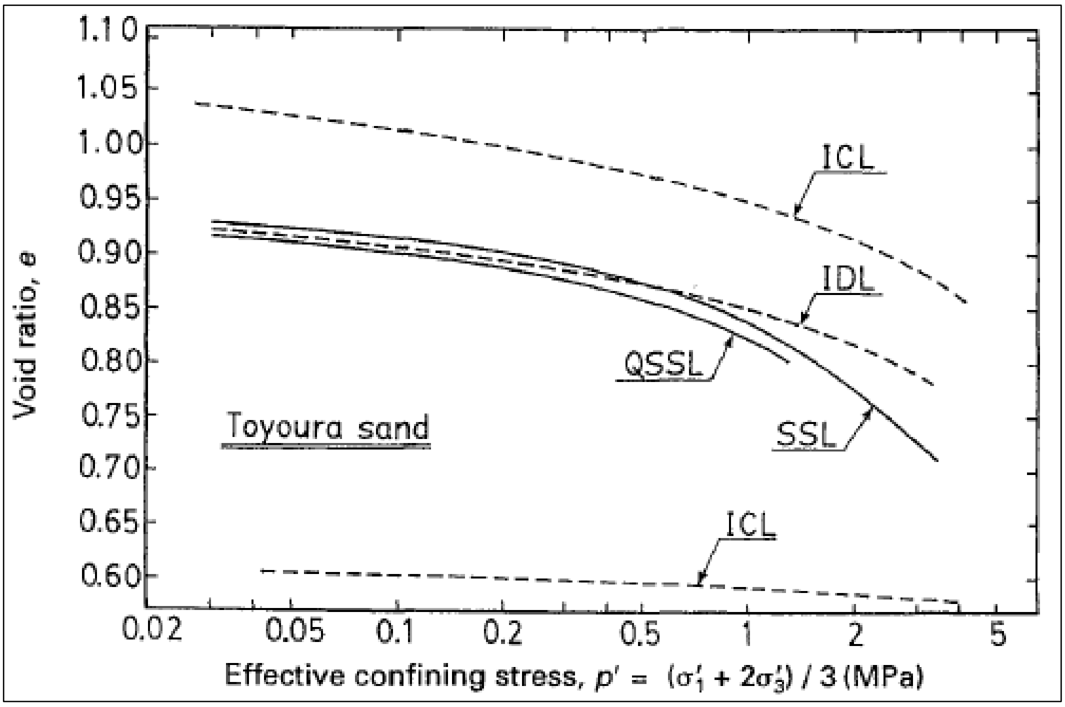

Figure 2.15. Characteristic Lines for Toyoura Sand (Ishihara, 1996)

2.2 One Dimensional Compression Behavior of Sands

Although stress levels in most of the geotechnical engineering works are not very high, in some areas of geotechnical engineering such as high earth dams, mine shafts, deep-driven pile foundation systems, and tunnels, sands may be subjected to very high pressures (Yamamuro et al., 1996). In these cases, understanding their one-dimensional compression behavior may be crucial for design purposes.

Under one dimensional loading, sands show particle rearrangement in three-ways: particle sliding, rolling, and crushing. Particle crushing is considered as the most critical factor in sand behavior under high stresses. Nakata et al. (2001) states that yield stress is a stress level at which rapid changes occur in the void ratio with effective vertical stress increments (in logarithmic scale). Yielding stress is mainly affected by the crushing behavior of particles. Therefore, sands’ one-dimensional behavior at high-stress levels, are mainly governed by the crushing behavior of particles.

Particle crushing or particle damage is quantified in three-levels. Level I damage can be considered as an abrasion of particle surface asperities. Level II damage can be considered as the crushing of particle edges and corners. Finally, level III damage can be considered as the splitting of the particle (Roberts & de Souza, 1958; Hendron 1963; Marsal 1967; Hardin 1985; Rahim 1989; Coop 1990; Pestana and Whittle 1995; Nakata et al. 2001; Chuhan et al. 2002, 2003). During one-dimensional loading, two mechanisms occur, locking (compression or rearrangement in more compact structure, leads to more stiff structure) and unlocking (particle damage, leads to less stiff structure) (Vesic & Clough 1968; Lambe & Whitman 1969). These locking and unlocking mechanisms take place simultaneously. A combination of these mechanisms determines the behavior of sand under one-dimensional loading. When locking behavior dominates unlocking behavior, constrained modulus ($M = \Delta\sigma'_v / \Delta\varepsilon_v$) increases with increasing vertical stress (Chuhan et al. 2002, 2003). When unlocking behavior dominates locking behavior, constrained modulus decreases with increasing vertical stress. In an equilibrium situation (locking and unlocking behavior takes place equally), constrained modulus remains constant with increasing vertical stress.

During one-dimensional loading, two types of compression occur: primary and secondary compression. Vertical loading increments cause the primary compression, while secondary compression continues under constant vertical stress (Mesri and Vardhanabhuti, 2009). Because of sands’ higher permeability, primary consolidation is completed in a short time after vertical loading application. Secondary compression, on the other hand, continues with time since all rearrangement mechanisms (sliding, rolling, and crushing) are time-dependent (Terzaghi and Peck 1948; Roberts and de Souza 1958; Lee and Farhoomand 1967; Mesri and Godlewski 1977; Lade et al. 1997).

There are different opinions to define yield stress in one-dimensional loading. Yield stress is determined as the vertical stress at the point where the e versus logσ'_v graph exhibits the maximum curvature $(\sigma'_v)_{MC}$ (Hagerty et al. 1993; McDowell et al. 1996; Nakata et al. 2001; McDowell 2002; Chuhan et al. 2003). Mesri and Vardhanabhuti (2009) states that yield stress is the vertical stress level at the maximum tangent-constrained modulus $(\sigma'_v)_{Mmax}$ in e versus logσ'_v domain. It is considered that the abrupt onset of level III particle damage starts at this stress level.

The crushing behavior of soils varies with different factors. Particle size, initial void ratio, particle shape (angularity), particle composition are the main factors that affect the crushing behavior of sands under one-dimensional loading. As a result of a comprehensive research study carried out by Nakata et al. (2001), the effects of particle size, initial void ratio, particle shape, and composition are defined as follows:

Effect of Particle Size

To define particle size's effect on the crushing behavior, three different silica samples with the same initial void ratio and different particle sizes, 1.550, 0.655, and 0.275 as D_{50} values, had been prepared. As can be seen from Figure 2.16, as the particle size decreases, the yield stress increases.

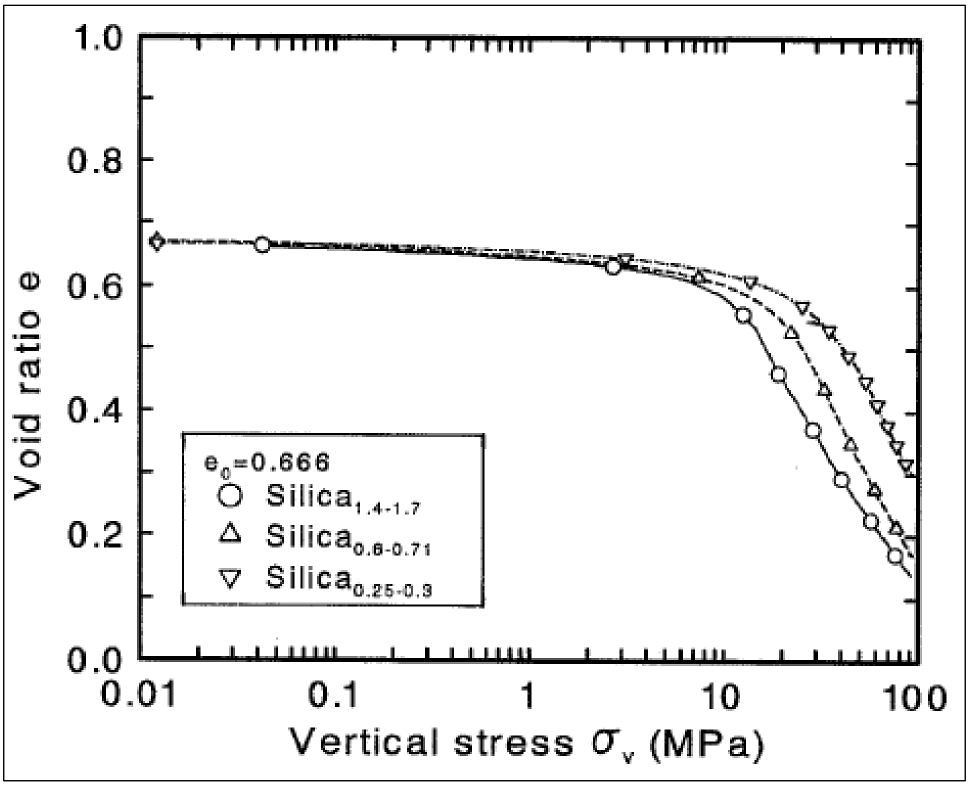

Figure 2.16. Effect of particle size on the compressibility behavior of Silica Sand under one dimensional compression

Effect of Initial Void Ratio

Three different Toyoura Sand samples had been prepared with different initial void ratios to define the initial void ratio’s effect. As can be seen on Figure 2.17, as the initial void ratio increases, the yield stress decreases, as stated before by Hagerty et al. (1993), Pestana and Whittle (1995).

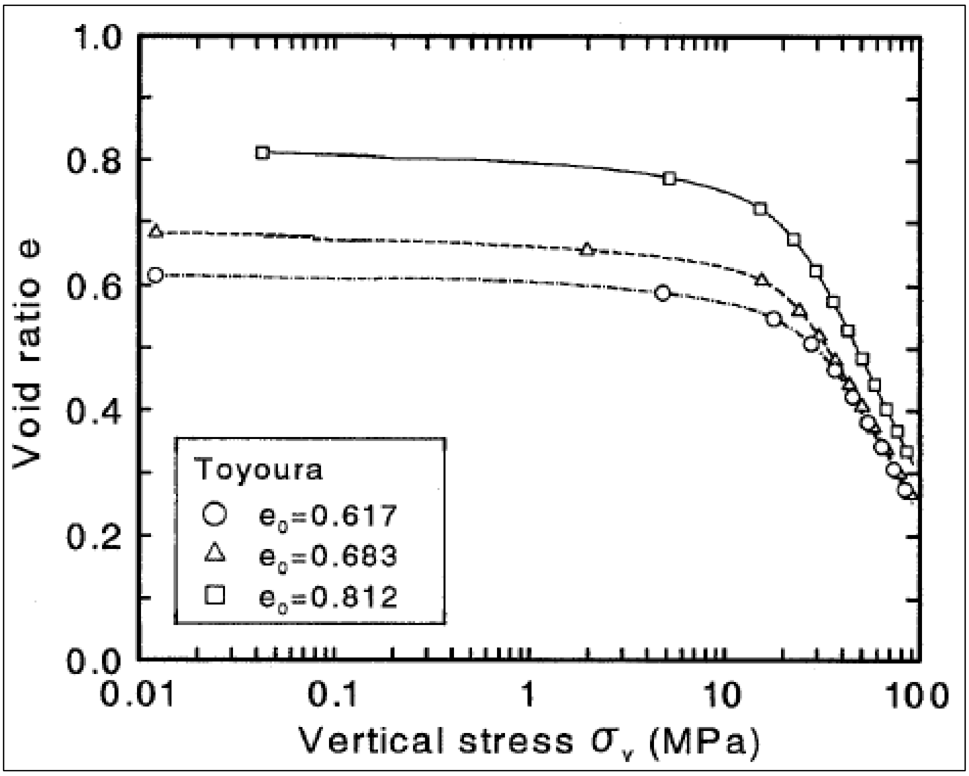

Figure 2.17. Effect of initial void ratio on the compressibility behavior of Toyoura Sand under one dimensional compression

Effect of Particle Angularity

To define the effect of particle angularity, two different samples: angular glass (AG) and glass ballotini (GB), had been prepared with almost the same initial relative density and particle sizes (0.85-1 mm). The results are shown in Figure 2.18. As can be seen from Figure 2.18, as the angularity increases, yield stress decreases mostly. Yield stress for AG sample is almost 6 MPa while 20 MPa for GB sample.

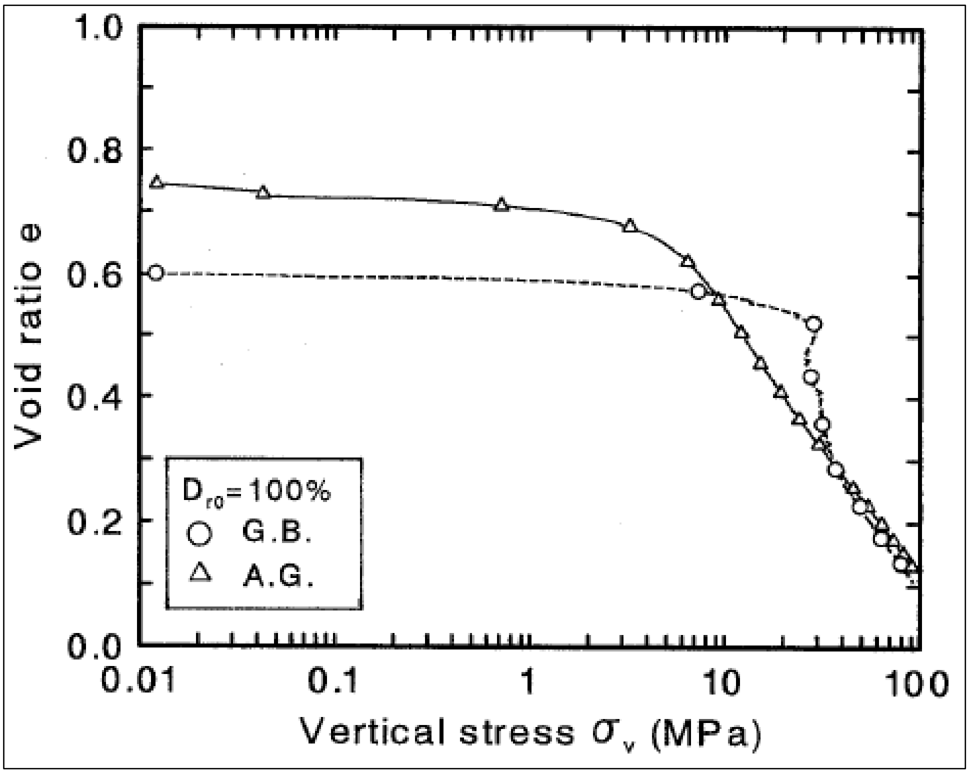

Figure 2.18. Effect of particle angularity on the compressibility behavior

Effect of Mineral Composition

To define the mineral composition effect, three different sand samples, Silica, Aio, and Masado, had been prepared at the same relative density with identical particle sizes, but angularity is different. Masado samples have more angular particles than others. Composition of samples:

Silica 100 % quartz

Aoi 70 % quartz and 30 % feldspar

Masado 30 % quartz, 40 % feldspar, and 30 % mixture (quartz and feldspar)

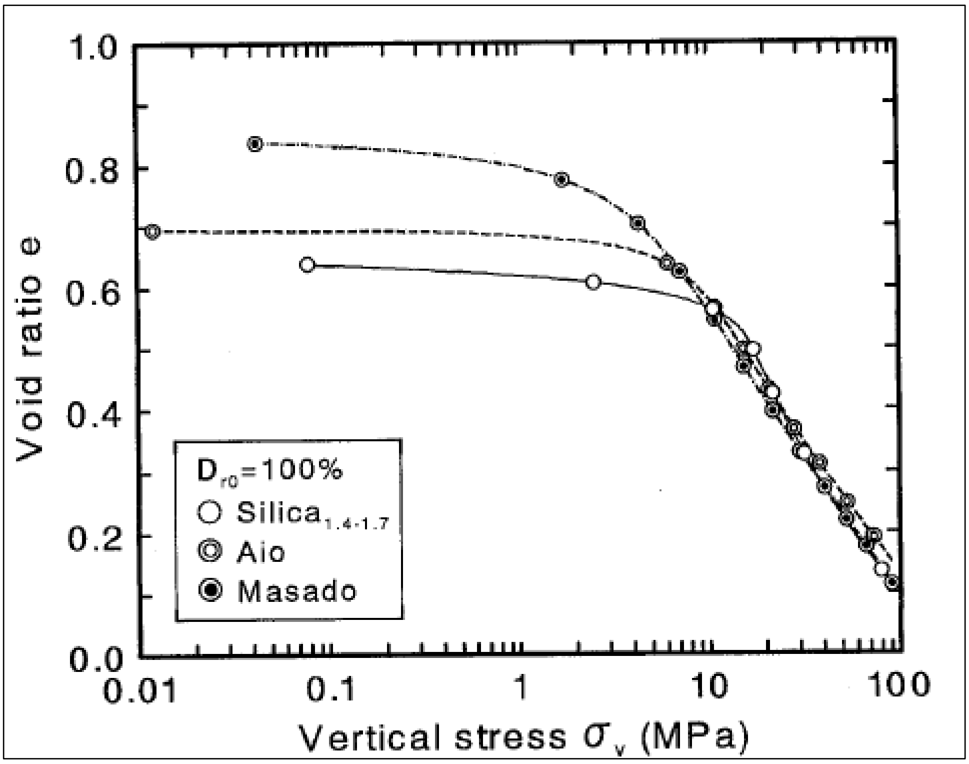

Figure 2.19. Effect of mineral composition on the compressibility behavior

On the basis of these test results, given in Figure 2.19, it can be concluded that the yield stress increases with increasing quartz mineral composition. However, since samples do not have the same angularity, this conclusion can not be fully validated.

CHAPTER 3

EXPERIMENTAL WORKS

Within the scope of the laboratory tests, sieve analysis, specific gravity, maximum and minimum void ratio determinations were carried out to characterize Çine sand. Triaxial and oedometer tests were performed to understand the shearand volumetric straining responses of Çine Sand, respectively.

3.1 Index Properties of Çine Sand

Based on the result of three sieve analysis test with reference to ASTM D6913/D6913M – 17, particle size distribution curves are shown in Figure 3.1, and D_{60}, D_{30} , D_{10}, coefficient of uniformity (C_u) and coefficient of curvature (C_c) values are shown in Table 3.1.

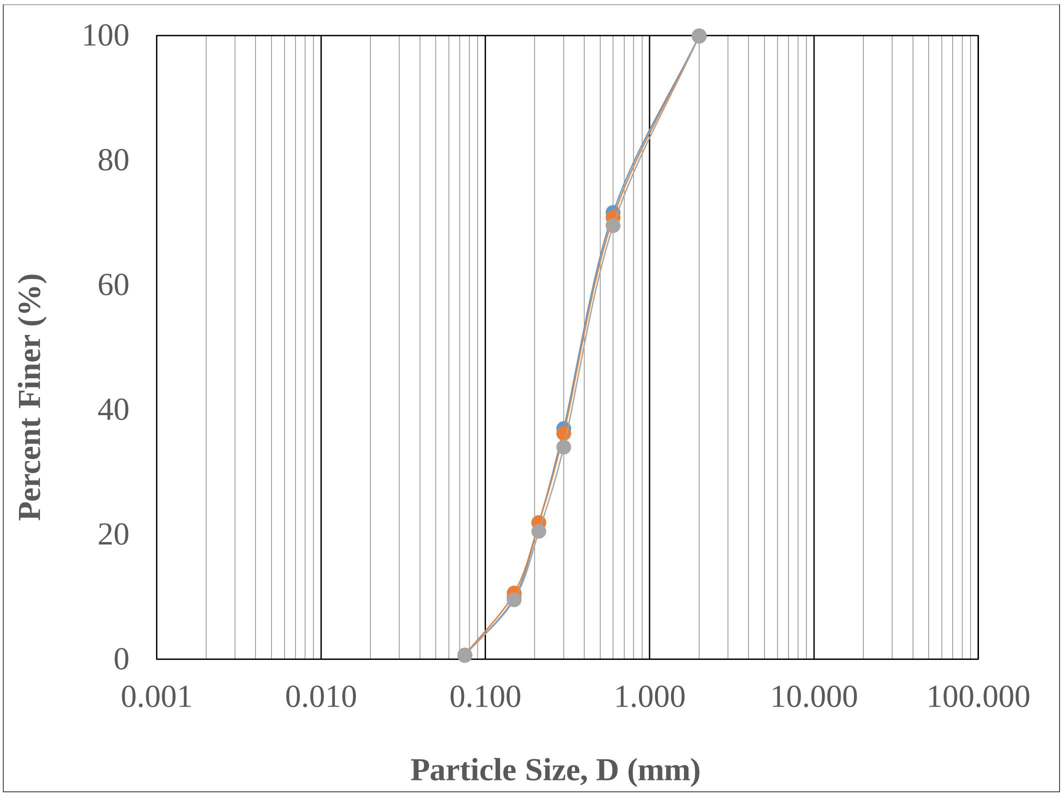

Figure 3.1. Particle size distribution curves of Çine sand

Table 3.1 D_{60}, D_{30}, D_{10}, C_c, and C_u values of Çine sand

D_{60} (mm)	0.50
D_{30} (mm)	0.26
D_{10} (mm)	0.15
C_c	0.89
C_u	3.30

On the basis of test results, more than 50 % of particles are observed to pass through 4.75 mm sieve openings. The coefficient of uniformity value is 3.3, and the coefficient of curvature value is 0.9. According to the Unified Soil Classification System (USCS), Çine sand is defined as a poorly graded sand (SP). Grain shapes of Çine sand is shown in Figure 3.2.

Figure 3.2. Grain shapes of Çine sand

Specific Gravity:

Four different specific gravity tests were performed to define the specific gravity of the Çine sand. As a result of tests, the specific gravity of Çine Sand was estimated as 2.66. Test results are shown in Appendix A.

Maximum and Minimum Void Ratio:

Maximum void ratios were estimated per ASTM D4254 – 16 – Method A. Minimum void ratio tests were performed with a vibrating machine. Test results are shown in Appendix B. As a result of these tests, maximum and minimum void ratios were estimated as 0.826 and 0.501, respectively.

3.2 Triaxial Testing System

3.2.1 System Components

To understand the shear straining response of Çine Sand, 20 isotropically consolidated undrained triaxial compression tests were performed. The VJ TECH automated triaxial test system used in this study, is shown in Figure 3.3.

Figure 3.3. VJ TECH automated triaxial test system

System components are:

- Load frame
- Cell and back pressure controllers
- Data logger (MPX3000 with ∓5V range and 16 bits resolution)
- Load cell

- Displacement transducer - LVDT
- PWP transducer
- Triaxial cell and specimen
- Water tank
- Valves
- Software – Clisp Studio

Apparatus used are shown in Figure 3.4.

Figure 3.4. Apparatus used in triaxial tests

- Split Mold – Used for specimen preparation in predefined dimensions.
- Cap and Base - The cap and base used to provide drainage should be compatible with the sample geometry. Since the top cape transmits vertical force to the sample, it should have enough stiffness.
- Porous Discs – To provide drainage.

- Rubber Membrane – Membranes are mainly used to separate the sample and fluid in the triaxial cell. They are usually made from latex rubber. Generally, their thickness is between 0.3 mm and 0.64 mm. Membrane thickness should not exceed 1% of the specimen diameter. (ASTM - D4767 - 11). Diameters of the membranes generally range from 35 mm to 150 mm. The membrane diameter to be used must be compatible with the sample diameter. Also, membrane length should be long enough to use o-rings in the top cape and base pedestal. Since the membranes transmit the pressure inside the cell to the sample, they should carry a minimum axial load, so their elasticity is significant. They should not resist axial deformation. In granular samples, membrane perforation can be observed at high pressures. Two thinner membranes can be used by applying silicon grease to prevent this situation rather than using a single thick membrane. Even if the inner membrane tears, the outer membrane will not tear, and the cell's fluid will not enter the sample.
- O-rings – It is used to adhere the membrane to the top cape & base to prevent specimens from the membrane. Also, they prevent air from entering into the sample.

Other apparatus are; funnel, pressure regulator, spoon, 0-ring expander, vaseline, CO_2 tube, tamper, cables, vacuum motor, balance, caliper.

3.2.2 Test Stages

Specimen Preparation

The diameters of the samples to be used in the triaxial tests vary between 37.7 - 38.1 mm, while the sample heights vary between 81 - 83 mm. H/D ratio for samples changes between 2.1 and 2.2. Since Çine sand is uniformly graded and the maximum particle size is 2 mm, the sample diameters fulfill the requirement that it should be selected as six times greater than the maximum particle size (as proposed by Marachi et al., 1972 and Wong et al., 1975).

The experiments were started on dense samples first. The four sets of samples, samples with 80^{+}, 70, 60, and 47 % relative density, were prepared with the tapped funnel deposition method. However, the loosest set could not be prepared with the tapped funnel deposition method. Therefore, the loosest set was prepared with undercompaction method.

Sample preparation with the tapped funnel deposition method (for 60 % RD) is explained below:

To find exact diameter and height of sand sample under a certain pressure (generally under 30 kPa vacuum), trial preparation is needed. Steps of trial sample preparation:

- For the 60 % RD sand sample, the sample's weight is defined for trial height and diameter, 82 and 38 mm, respectively.
    - $G_s = 2.66$
    - $e_{min} = 0.501$
    - $e_{max} = 0.826$
    - Required weight of sample = 151.4 g
- After defining the sample's weight, preparation is completed with the tapped funnel deposition method, as explained in the literature review part. 81.9 mm height and 37.8 mm diameter are measured under a 30 kPa vacuum. Exact height and diameter are found under a 30 kPa vacuum. With these exact values, the required weight of sand is defined again.
- For the 60 % RD sand sample, weight of the sample is defined for exact height and diameter, 81.9 & 37.8 mm, respectively.
    - $Gs = 2.66$
    - $e_{min} = 0.501$
    - $e_{max} = 0.826$
    - Required weight of sample = 149.6 g

After defining exact values of weight, diameter, and height, sample preparation is completed with tapped funnel deposition method as shown in Figure 3.5.

Figure 3.5. Tapped funnel deposition method

After specimen preparation, a 30 kPa vacuum is applied to the sample, which has reached the predetermined height, and then the mold is removed. Then dimensions are measured once again for checking predetermined height and diameter as shown in Figure 3.6.

Figure 3.6. Measuring diameter and height

Then the specimen is placed into the cell, and the cell is filled with water to create cell pressure, as shown in Figure 3.7. Cell pressure is adjusted to 30 kPa. The increase in cell pressure and the decrease in the vacuum applied inside the sample are kept at the same rate to keep effective stress constant.

Figure 3.7. Filling the cell with water

For the loosest set (21-26 % relative densities), samples were prepared by the undercompaction method proposed by Ladd (1978). An example preparation method for 21.4 % relative density is described below:

- The required specimen diameter, height, and the sand amount to be used are determined for the relative density planned to be obtained (diameter = 38.1 mm, height = 81 mm, and weight of sand = 139.6 g for 21.4 % relative density).
- The specimen is brought to a certain water content (w = 25 % or 34.9 g water in this preparation).

- The number of layers is selected (8 layers for this preparation).
- Total wet specimen is calculated (139.6 + 34.9 = 174.5 g). Then the amount of wet specimen for each layer is calculated (174.5 / 8 = 21.8125 g for each layer).
- A value of U_{ni} is selected (0.15 selected for this preparation). Then required height of the n^{th} layer is calculated with given formula.

$$h_n = \frac{h_t}{n_t} \times \left((n-1) + (1 + \frac{U_n}{100})\right) \qquad \text{Eqn. 3.1}$$

where

$$U_n = U_{ni} - \left(\frac{(U_{ni} - U_{nt})}{n_t - 1} \times (n-1)\right) \qquad \text{Eqn. 3.2}$$

U_{ni}: percent undercompaction selected for first layer

U_{nt}: percent undercompaction selected for final layer (usually zero)

U_n: percent undercompaction for layer being considered

n: number of layer being considered

n_t: total number of layers

h_t = total height of the specimen

- Each layer is compacted to its pre-defined height.
- And finally, dimesions are measured under a 30 kPa vacuum.

Saturation Stage

The saturation process is started by passing CO_2 through the sample, as shown in Figure 3.8. Not to change effective stresses and void ratios in the sample locally, the CO_2 percolation is made at a slow rate (3 bubble per second).

Figure 3.8. Passing CO_2 through the sample

After about 1 hour of CO_2 passing, de-aerated water is passed through the sample, as shown in Figure 3.9. The water percolation process is completed with the end of the air bubbles coming out of the sample. Then back pressure application is started, and step by step B-value check is made. After the degree of saturation is reached a B value of 93-95%, the saturation phase is completed.

Figure 3.9. Percolation of de-aerated water

Consolidation Stage

Within the scope of this research, four different consolidation pressures were conducted for each relative density. These pressures were 50, 100, 200, and 400 kPa. Samples were consolidated isotropically. In other words, all principal stresses (σ_1 - σ_2 - σ_3) were equal during the consolidation stage. After consolidation processes, as explained in the literature system review, dimensions were corrected. Because of the isotopic consolidation, volume reduction was the same in three axes. The procedure to calculate new dimensions is explained as below:

- The volume of water released after consolidation is found.
- Then volumetric strain (ε_v) is calculated as:

$$\varepsilon_v = \frac{The\ volume\ of\ water\ released\ after\ consolidation}{Total\ volume\ of\ sample} \qquad \text{Eqn. 3.3}$$

- Then axial strain (ε_a), new height, and new diameter are calculated as follows:

$$\varepsilon_a = \frac{\varepsilon_v}{3} \qquad \text{Eqn. 3.4}$$

$$H_c = H_0 - (H_0 \times \varepsilon_a) \qquad \text{Eqn. 3.5}$$

$$D_c = D_0 - (D_0 \times 2 \times \varepsilon_a) \qquad \text{Eqn. 3.6}$$

H_0: initial height

H_c: height after consolidation

D_0: initial diameter

D_c: diameter after consolidation

Shear Stage

After the consolidation phase was over, the shear stage was started. Since the experiments to be carried out were undrained, all drainage channels were closed when the shearing stage starts. The experiments were continued up to 15 - 25% strain levels.

Throughout the shear stage, axial load, pore pressure, and axial deformation were recorded as raw data. Then these data were made suitable for engineering studies. Some conversions were made with these raw data to determine Çine sand's behavior, as shown below.

$$\varepsilon_a = \frac{\Delta h}{H_c} \qquad \text{Eqn. 3.7}$$

ε_a: axial strain

Δh: axial deformation

H_c: height after consolidation

$$\sigma_d = \frac{F_c}{A *_c} \qquad \text{Eqn. 3.8}$$

σ_d: deviatoric stress (without membrane correction)

F_c: corrected vertical load

$A*_c$: corrected area

During the shear stage, the area of the specimen changes with the axial strain, and therefore it should be corrected. Area correction for each strain increment is made as follow:

$$A *_c = \frac{A_c}{1 - \varepsilon_a} \qquad \text{Eqn. 3.9}$$

A_c: area after consolidation

Axial load corrections are caused by piston uplift, piston friction, and membrane. Piston uplift is sourced by the cell pressure, which tends to lift the piston. Piston friction is created by the friction between the piston and the bushing. If the piston and the top cap are not connected, there is no need for piston uplift and piston friction corrections. The first reading of total vertical load in the shear stage includes the piston uplift and piston friction. Therefore, by zeroing this value, piston uplift and piston friction are eliminated.

Membranes carry a certain amount of vertical load depending on their elasticity, and therefore a correction is required. Duncan & Seed (1967) suggest the following equation for axial and radial membrane corrections for large and small strains.

$$\Delta\sigma_{dcorr} = -\frac{2}{3} \times E_m \times \left[2 \times \varepsilon_a + 1 - \sqrt{\frac{1 - \varepsilon_v}{1 - \varepsilon_a}}\right] \times \frac{4 \times t_0}{D_c \times (1 - \varepsilon_v)} \qquad \text{Eqn. 3.10}$$

$\Delta\sigma_{dcorr}$: deviatoric stress membrane correction

E_m: modulus of elasticity of the rubber membrane

ε_v= volumetric strain of the specimen (since no volumetric strain in the shear stage of undrained tests, ε_v will be found at the end of the consolidation stage)

t_0= initial thickness of the rubber membrane

D_c = diameter of the specimen after consolidation

$$\Delta\sigma_{rcorr} = -\frac{2}{3} \times E_m \times \left[\varepsilon_a + 2 - 2 \times \sqrt{\frac{1 - \varepsilon_v}{1 - \varepsilon_a}}\right] \times \frac{2 \times t_0}{D_c \times (1 - \varepsilon_v)} \quad \text{Eqn. 3.11}$$

$\Delta\sigma_{rcorr}$: radial stress membrane correction

$$\sigma_{dcorr} = \sigma_d + \Delta\sigma_{dcorr} \quad \text{Eqn. 3.12}$$

σ_{dcorr}: corrected deviatoric stress (after membrane correction)

Principal stresses are calculated as the following formulas:

$$\sigma_1 = \sigma_3 + \sigma_{dcorr} \quad \text{Eqn. 3.13}$$

σ_1: major principal stress

σ_3 ($\approx \sigma_{cell}$): minor principal stress or cell pressure

$$\sigma'_1 = \sigma_1 - u \quad \text{Eqn. 3.14}$$

σ'_1: effective major principal stress

u: pore pressure

$$\sigma'_3 = \sigma_3 - u \quad \text{Eqn. 3.15}$$

σ'_3: effective minor principal stress

MIT p-q terms are defined as the following formulas:

$$q = (\sigma'_1 - \sigma'_3) / 2 \qquad \text{Eqn. 3.16}$$

$$p' = (\sigma'_1 - \sigma'_3) / 2 \qquad \text{Eqn. 3.17}$$

q: half of the deviatoric stress

p′: mean effective stress

After these conversions, the behavior of Çine sand will be shown with four-way plots and mohr circles in chapter 4. The benefit of the four-way plot is that it enables us to see the stress state and pore pressure values at the point where the sample fails or yields. A sample for-way plot is shown in Figure 3.10.

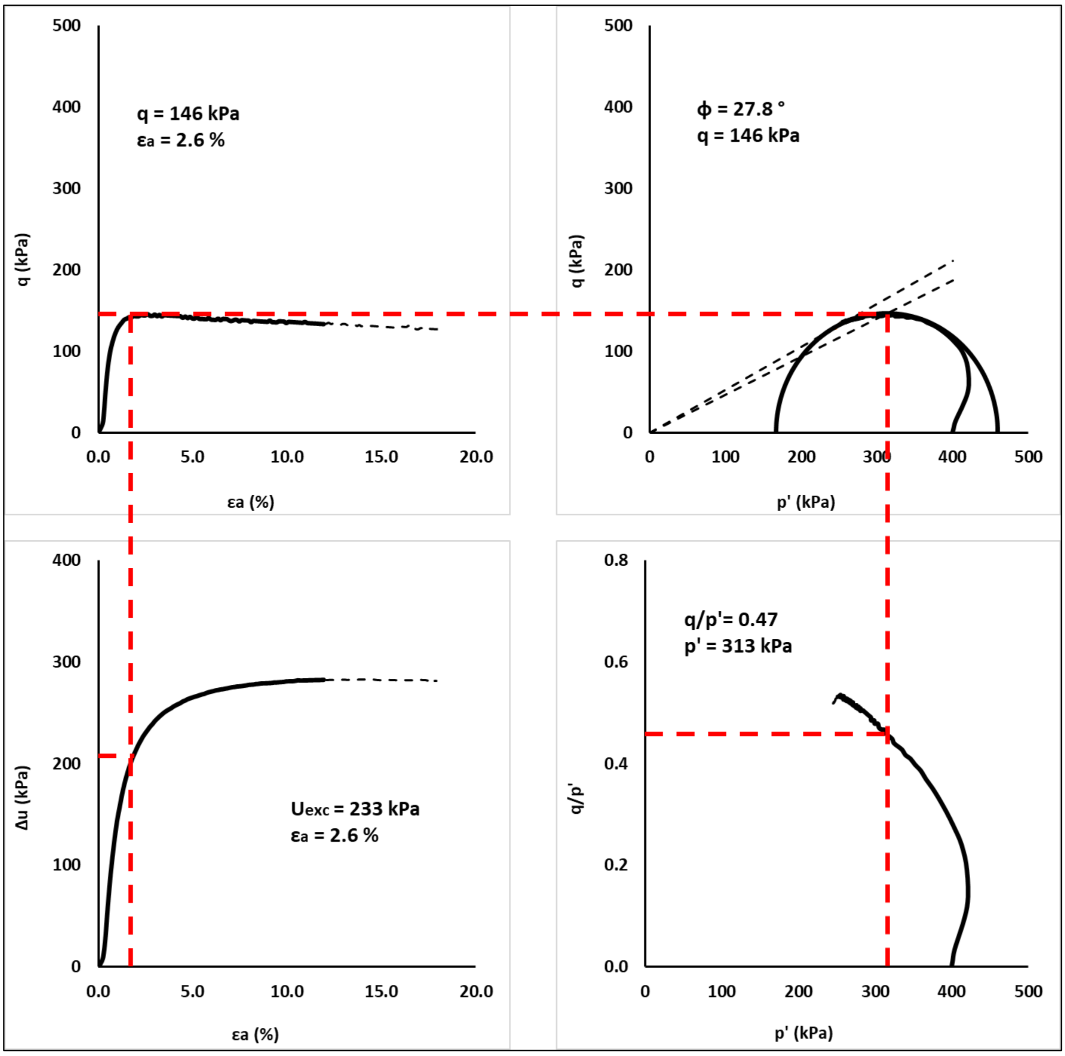

Figure 3.10. An example four-way plot (25 % Relative density – 400 kPa consolidation pressure)

3.3 Oedometer Testing System

The odometer test system is one of the most common test systems used to determine the soils' one-dimensional compression behavior. Although it is generally used for cohesive soils, it can also be used to investigate the one-dimensional compression behavior of cohesionless soils. The odometer test setup and apparatus to be used in this research are shown in Figure 3.11.

Figure 3.11. Oedometer test setup and apparatus

During the tests, dry Çine sand samples were prepared with tapped funnel method in the metal ring. The samples were covered with stiff metal plates to apply a uniform load on the specimen. In general, in odometer experiments with cohesive samples, the load is doubled for each loading, and each loading takes 24 hours. However, for Çine sand to accelerate the completion of loading phases, the load was not doubled for each loading and hence, loading times were shorter than those of clays. There are two different load arms in the test system, as shown in Figure 3.12. With one loading arm, 1:40 load amplification could be made, while 1:10 load amplification for another loading arm. In this way, almost 30 MPa stress could be applied to the samples.

Figure 3.12. Load arms of the test system

For this research, seven oedometer tests were performed with different initial void ratios. 85, 70, 60, 50, 35, and 25 % relative density samples were tested. Sixteen different weights were used, as shown in Figure 3.13.

Figure 3.13. Weights used for oedometer tests

Loadings were done manually. With these weights, total stress of 29 MPa was applied to the samples. During the test, deformations were measured with the help of LVDT, and values were recorded automatically.

To define machine deflection for each loading, three tests were performed without a sample. As a resul of the tests, machine deflections for each loading cycle are shown in Table 3.2. In calculating height changes, machine deflections were subtracted for loading and added for unloadings.

Table 3.2 Machine deflections for vertical stresses

σ'$_v$ (kPa)	MD (mm)	σ'$_v$ (kPa)	MD (mm)
23	0.009	6520	0.255
74	0.020	9743	0.281
174	0.032	12727	0.302
376	0.067	15945	0.323
879	0.116	19163	0.345
1685	0.163	22487	0.363
2491	0.189	25710	0.381
3297	0.208	28933	0.398

After getting data from tests, necessary terms and calculations were defined as follows:

$$\Delta e_1 = (e_0 + 1) \times \left(\frac{\Delta H_1}{H_0}\right) \qquad \text{Eqn. 3.18}$$

$$e_1 = e_0 - \Delta e_1 \qquad \text{Eqn. 3.19}$$

Δe_1: void ratio change after primary consolidation

H_0: initial height of the sample

e_0: initial void ratio of the sample

ΔH_1: change in height after primary consolidation

e_1: void ratio after primary consolidation

$$\Delta e_f = (e_0 + 1) \times \left(\frac{\Delta H_f}{H_0}\right) \qquad \text{Eqn. 3.20}$$

$$e_f = e_0 - \Delta e_f \qquad \text{Eqn. 3.21}$$

Δe_f: void ratio change after primary + secondary consolidation

ΔH_f: change in height after primary + secondary consolidation

e_f: void ratio after primary + secondary consolidation

$$\varepsilon_1 = \frac{\Delta H_1}{H_0} \qquad \text{Eqn. 3.22}$$

ε_1: vertical strain after primary consolidation

$$\varepsilon_f = \frac{\Delta H_f}{H_0} \qquad \text{Eqn. 3.23}$$

ε_f: vertical strain after primary + secondary consolidation

$$\sigma_v = \frac{F_v}{A} \qquad \text{Eqn. 3.24}$$

σ_v: vertical stress

F_v: total vertical force

A: area of the sample

$$C_c, C_r = \frac{\Delta e_1}{\Delta log\sigma_v} \qquad \text{Eqn. 3.25}$$

C_c: compression index

C_r: re-compression index

$$M = \frac{\Delta\sigma_v}{\Delta\varepsilon_1} \qquad \text{Eqn. 3.26}$$

M: constrained modulus

$$C_\alpha = \frac{\left(\frac{\Delta H_f - \Delta H_1}{H_0}\right) \times (e_0 + 1)}{logt_f - logt_1} \qquad \text{Eqn. 3.27}$$

C_α: secondary compression index

t_1: time of primary compression

t_f: time of primary + secondary compression

CHAPTER 4

TEST RESULTS AND INTERPRETATIONS

4.1 Results of Triaxial Tests

20 consolidated undrained monotonic compression triaxial tests were performed. Tabulated results are shown in Table 4.1. In the table, initial relative density, consolidation pressure, initial void ratio, void ratio after consolidation, failure strain, and angle of friction values for each test are shown.

Table 4.1 Results of isotropically consolidated undrained tests

Test ID	D_R (%)	σ'_c (kPa)	e_0	e_c	ε_f (%)	ϕ (°)
ICU-1	21	50	0.756	0.753	1.1	27.2
ICU-2	24	100	0.749	0.735	0.8	20.5
ICU-3	21	200	0.756	0.727	1.5	24.2
ICU-4	26	400	0.742	0.689	2.6	27.8
ICU-5	47	50	0.673	0.670	3.0	36.6
ICU-6	47	100	0.673	0.663	5.7	33.7
ICU-7	47	200	0.673	0.654	5.7	33.7
ICU-8	47	400	0.673	0.637	4.0	35.2
ICU-9	60	50	0.631	0.628	3.3	36.6
ICU-10	60	100	0.631	0.624	3.3	35.9
ICU-11	60	200	0.631	0.611	6.2	33.7
ICU-12	60	400	0.631	0.601	4.9	34.4
ICU-13	70	50	0.598	0.596	4.0	35.9
ICU-14	70	100	0.598	0.590	4.0	35.3
ICU-15	70	200	0.598	0.580	4.5	35.1
ICU-16	70	400	0.602	0.572	5.0	33.1
ICU-17	84	50	0.551	0.549	2.7	38.0
ICU-18	88	100	0.541	0.533	2.6	39.5
ICU-19	84	200	0.554	0.539	2.9	37.3
ICU-20	83	400	0.555	0.530	4.5	35.2

Four-way plots of all triaxial tests are shown in Figure 4.1 through 4.20. In these plots, red dashed lines show values at failure. Failure stresses were taken as maximum deviatoric stress for samples showing strain-softening behavior (loose samples). For samples showing strain hardening behavior (dense samples), on the other hand, the obliquity concept was used to determine failure strain and stresses. According to the obliquity concept, failure starts at the strain level, where the effective stress ratio is maximum $(q/p')_{max}$. In this case, the point to be considered is that as strain levels increase in triaxial experiments, the sample area's change is not precisely equal to the corrected area due to localizations. Therefore, it is observed in the results that the (q/p') values increase slightly after a certain strain level. For each experiment, $(q/p')_{max}$ values were taken at points where the (q/p') values are close to the maximum value, and change with axial strain is very little. In the plots, half of the deviatoric stress (q), mean effective stress (p′), excess pore water pressure (Δu), axial strain (ε_a), angle of friction (φ), stress ratio (q/p') values are shown at failure.

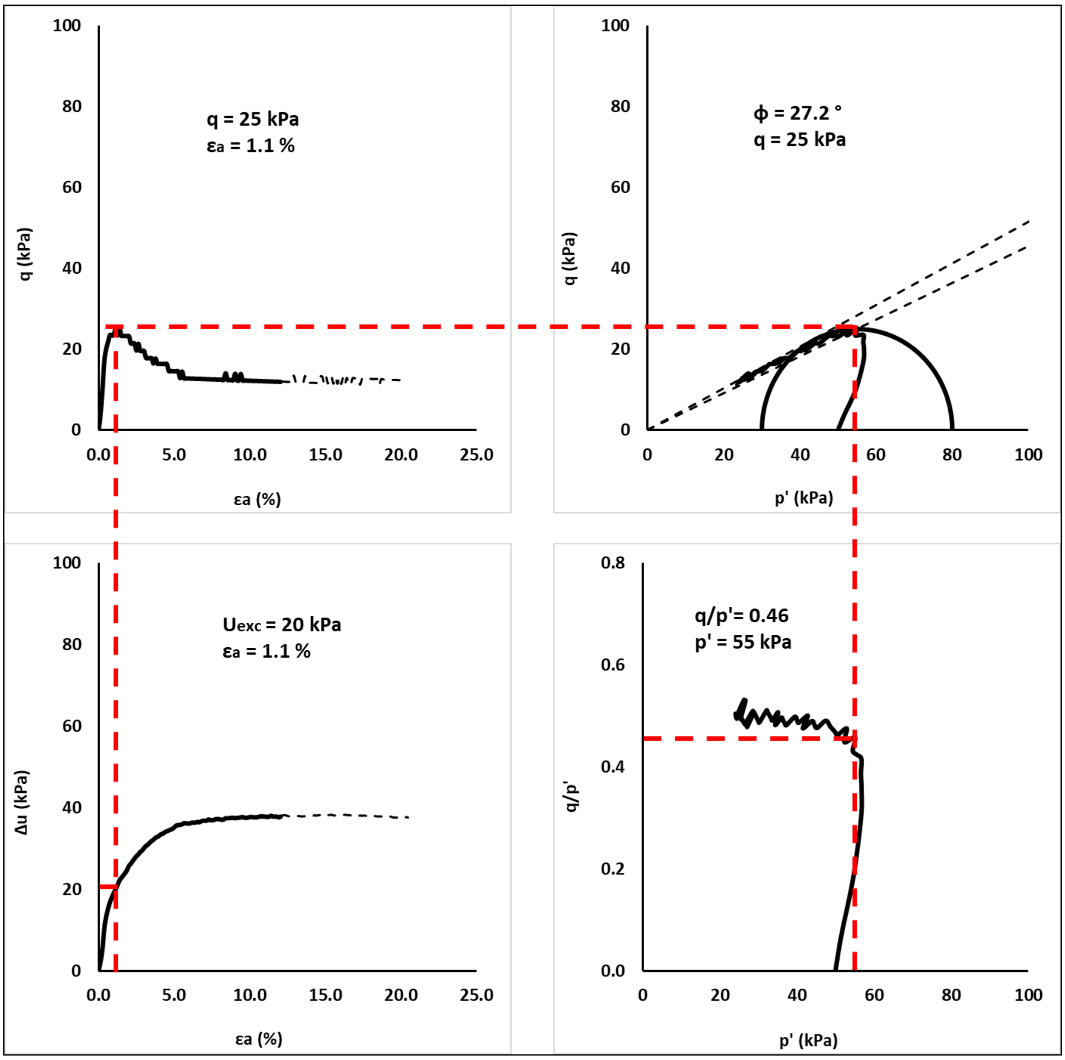

Figure 4.1. Four-way plot of ICU-1

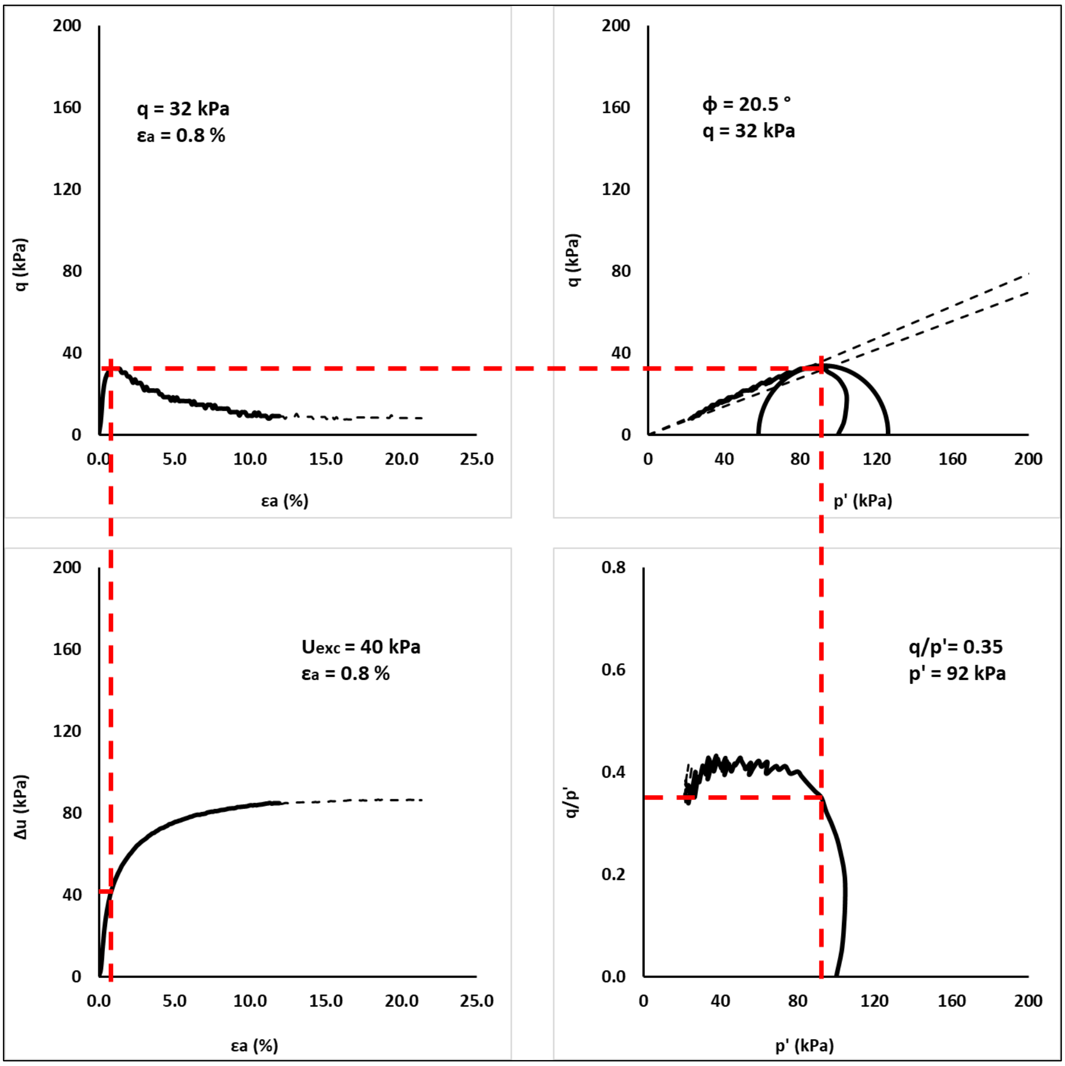

Figure 4.2. Four-way plot of ICU-2

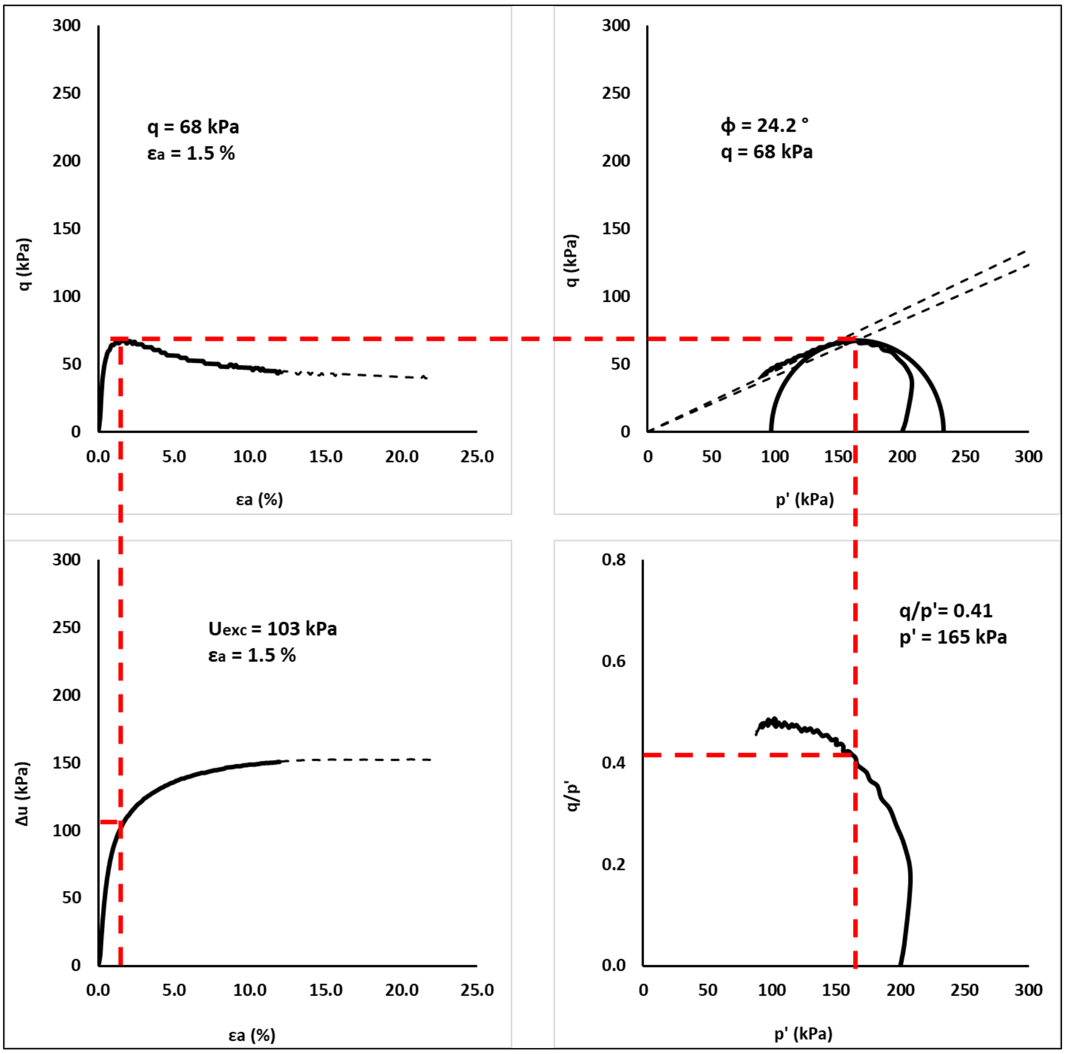

Figure 4.3. Four-way plot of ICU-3

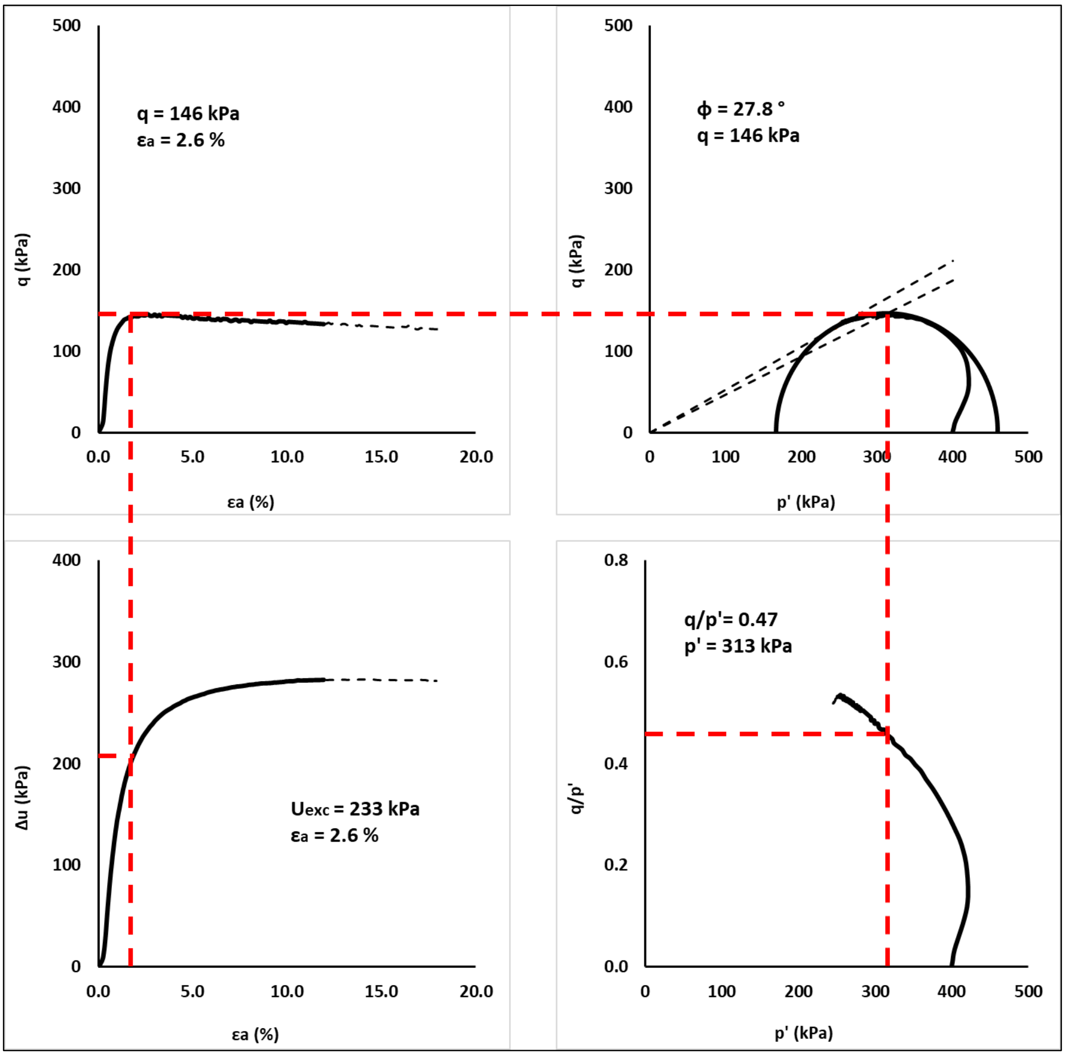

Figure 4.4. Four-way plot of ICU-4

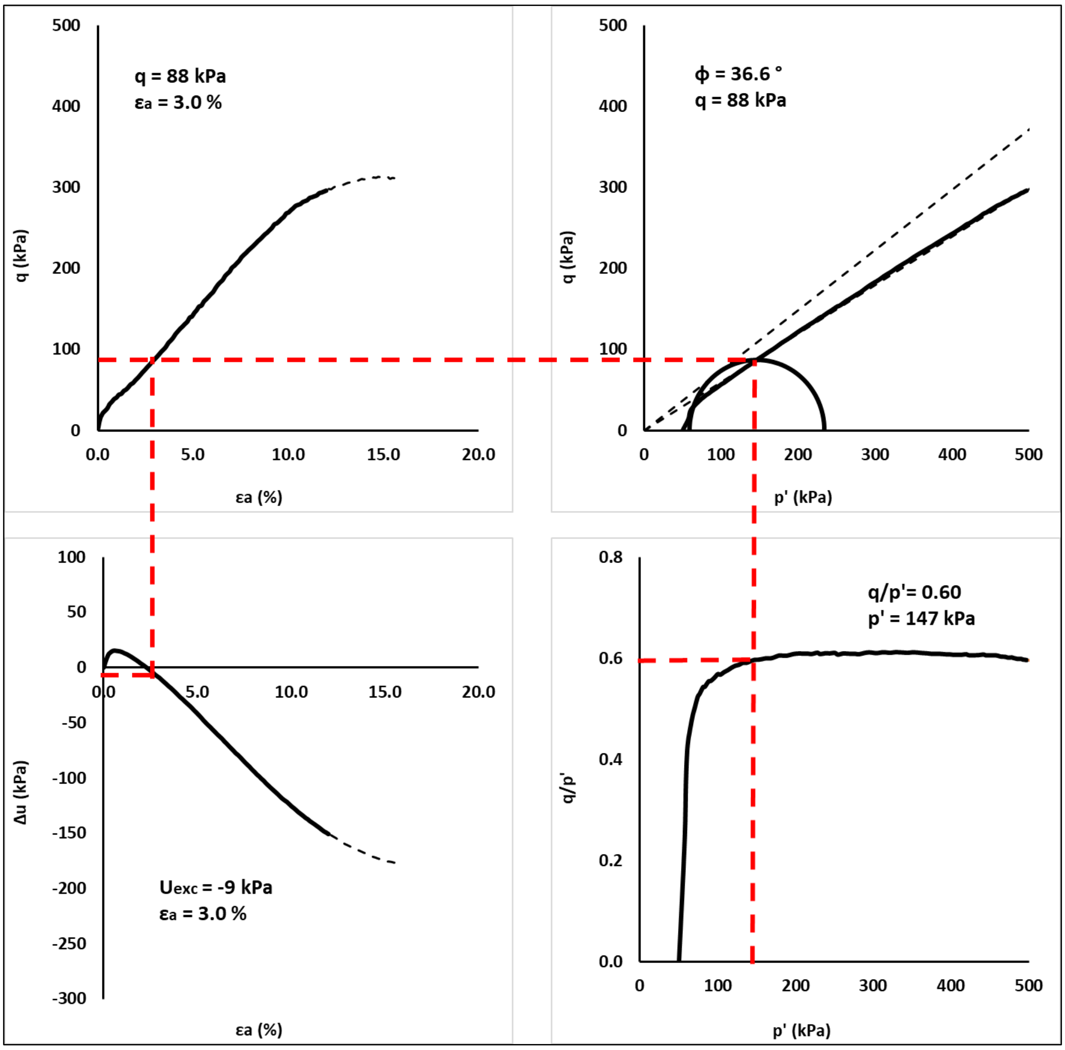

Figure 4.5. Four-way plot of ICU-5

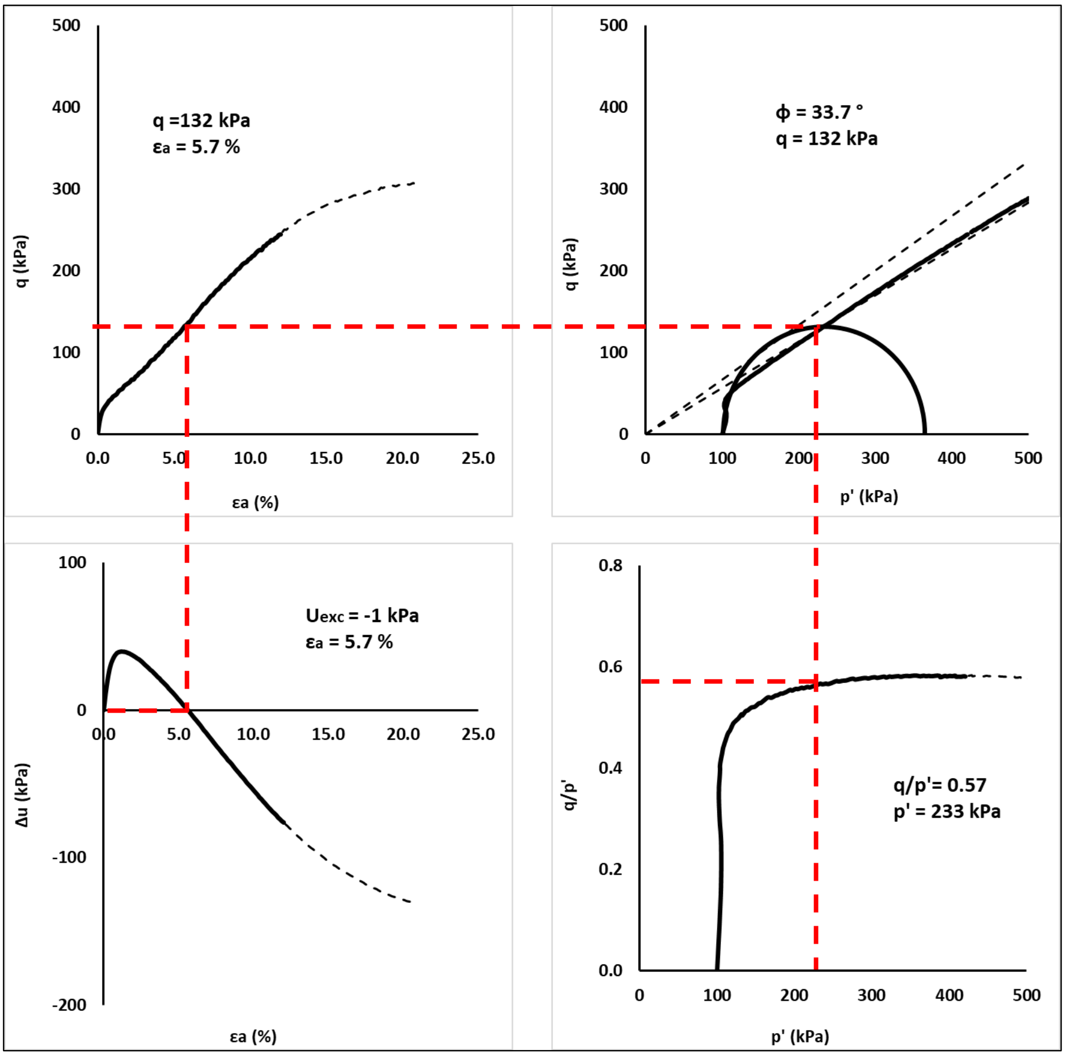

Figure 4.6. Four-way plot of ICU-6

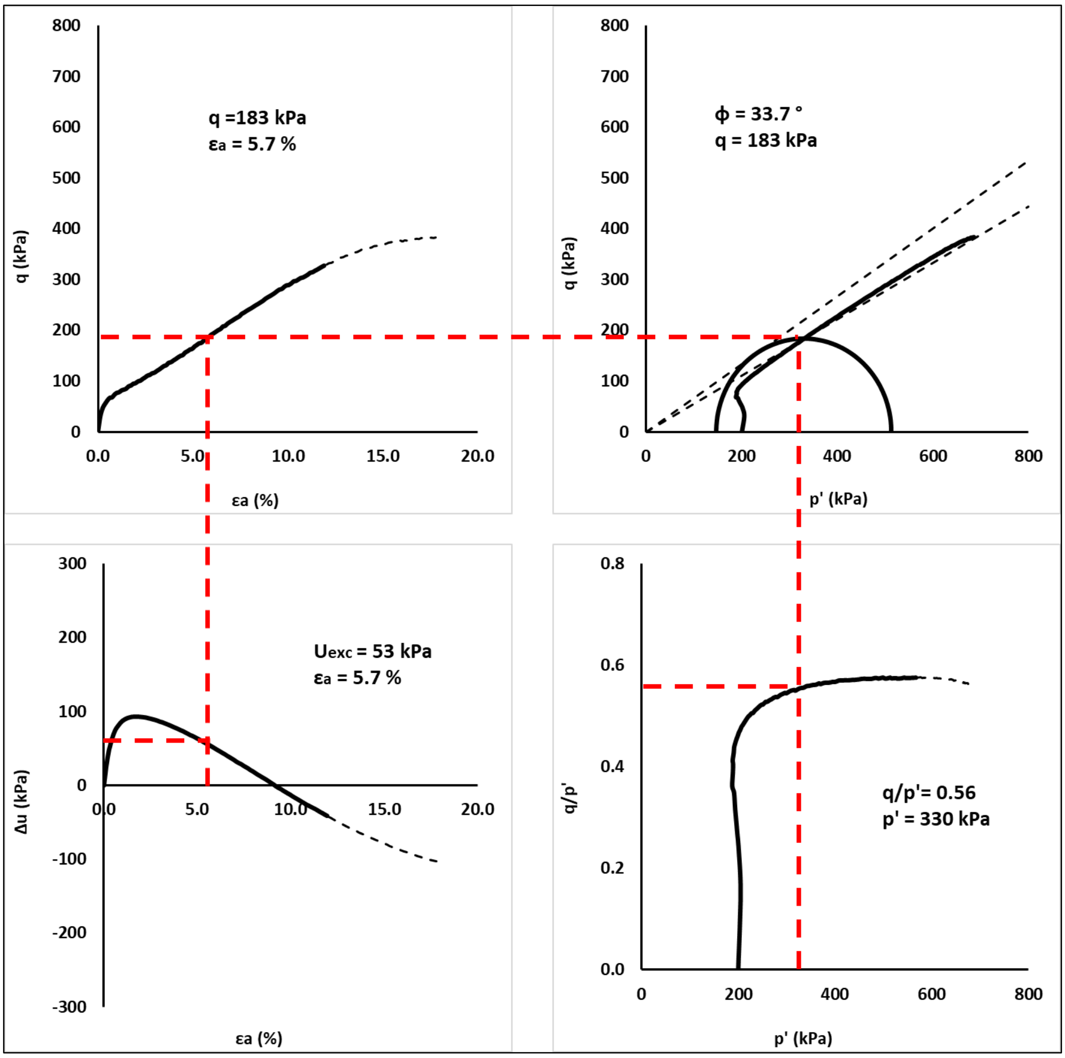

Figure 4.7. Four-way plot of ICU-7

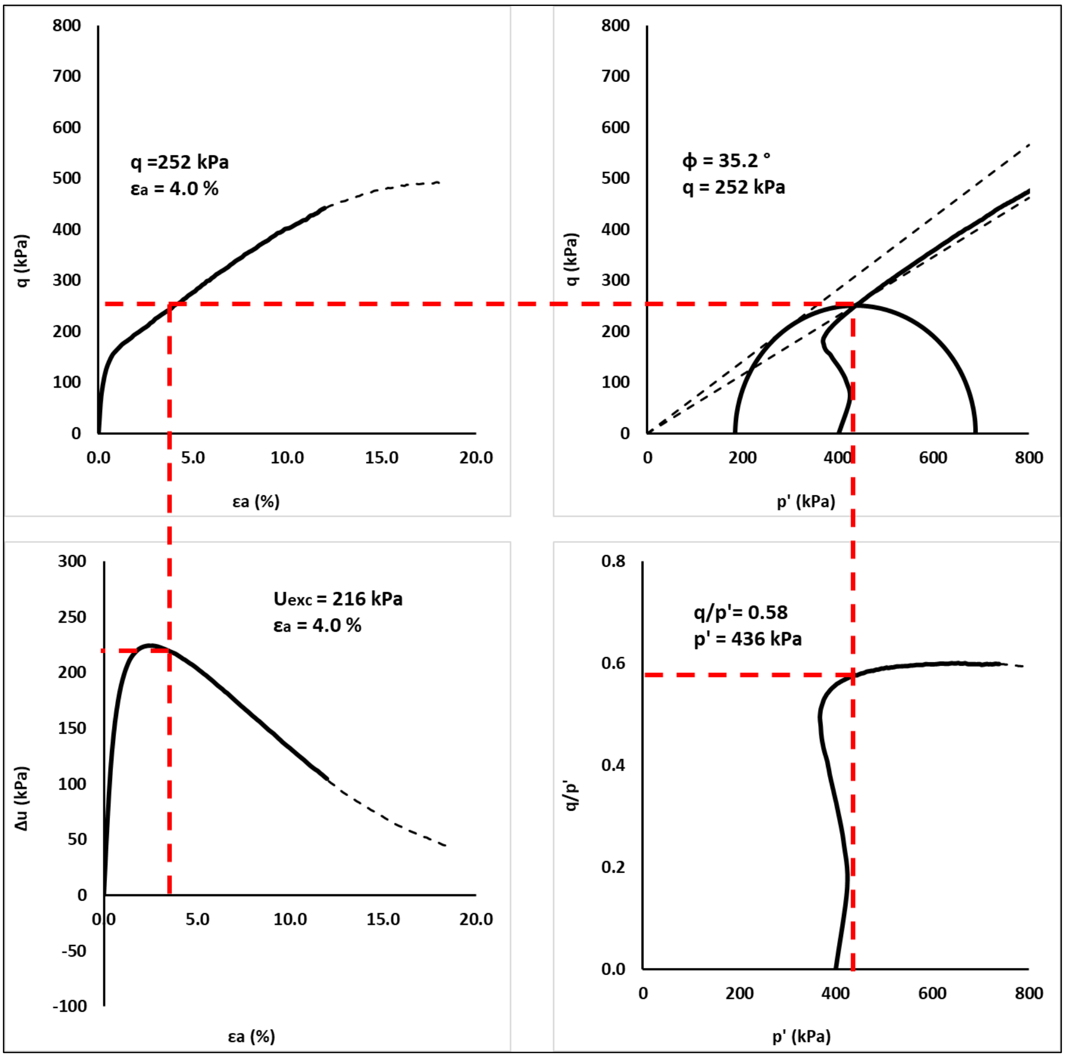

Figure 4.8. Four-way plot of ICU-8

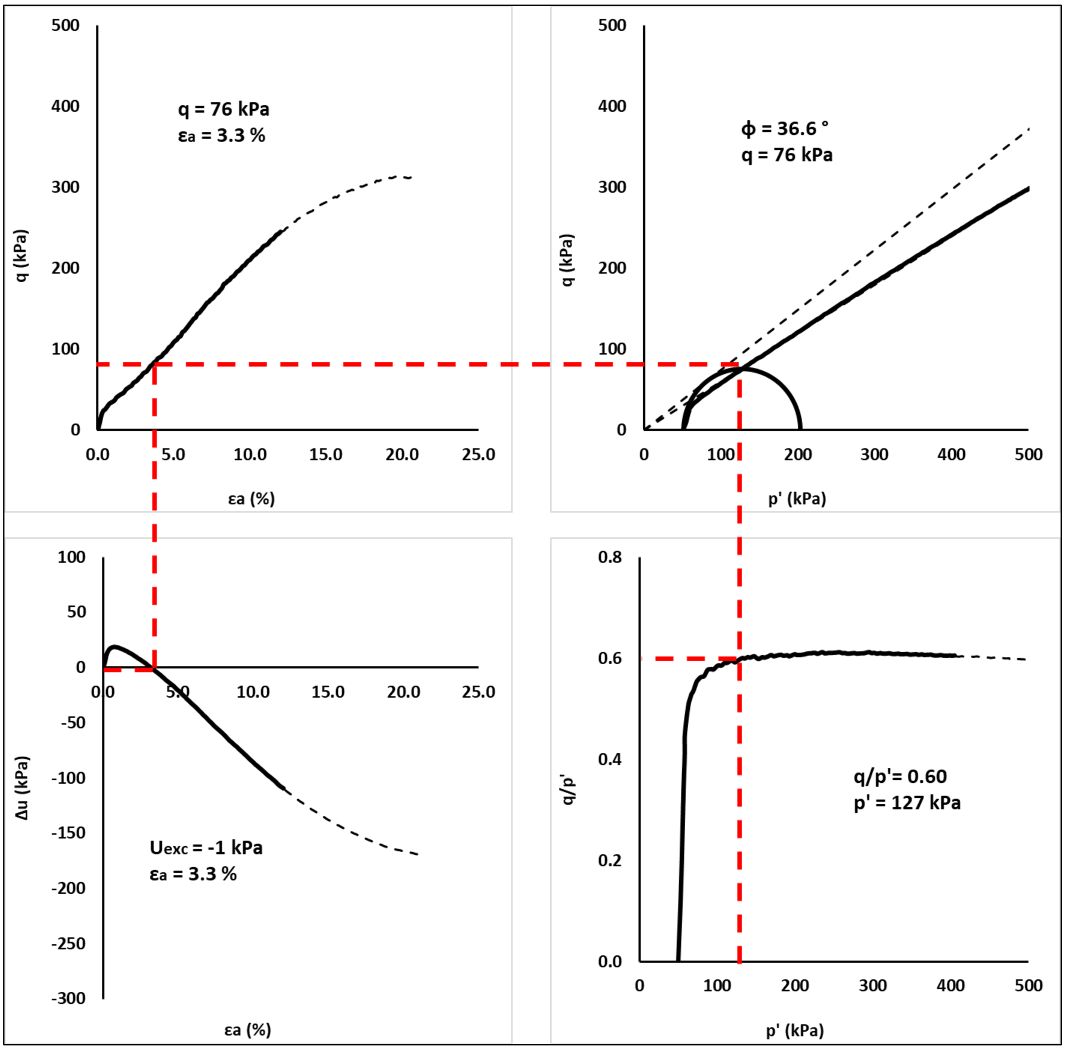

Figure 4.9. Four-way plot of ICU-9

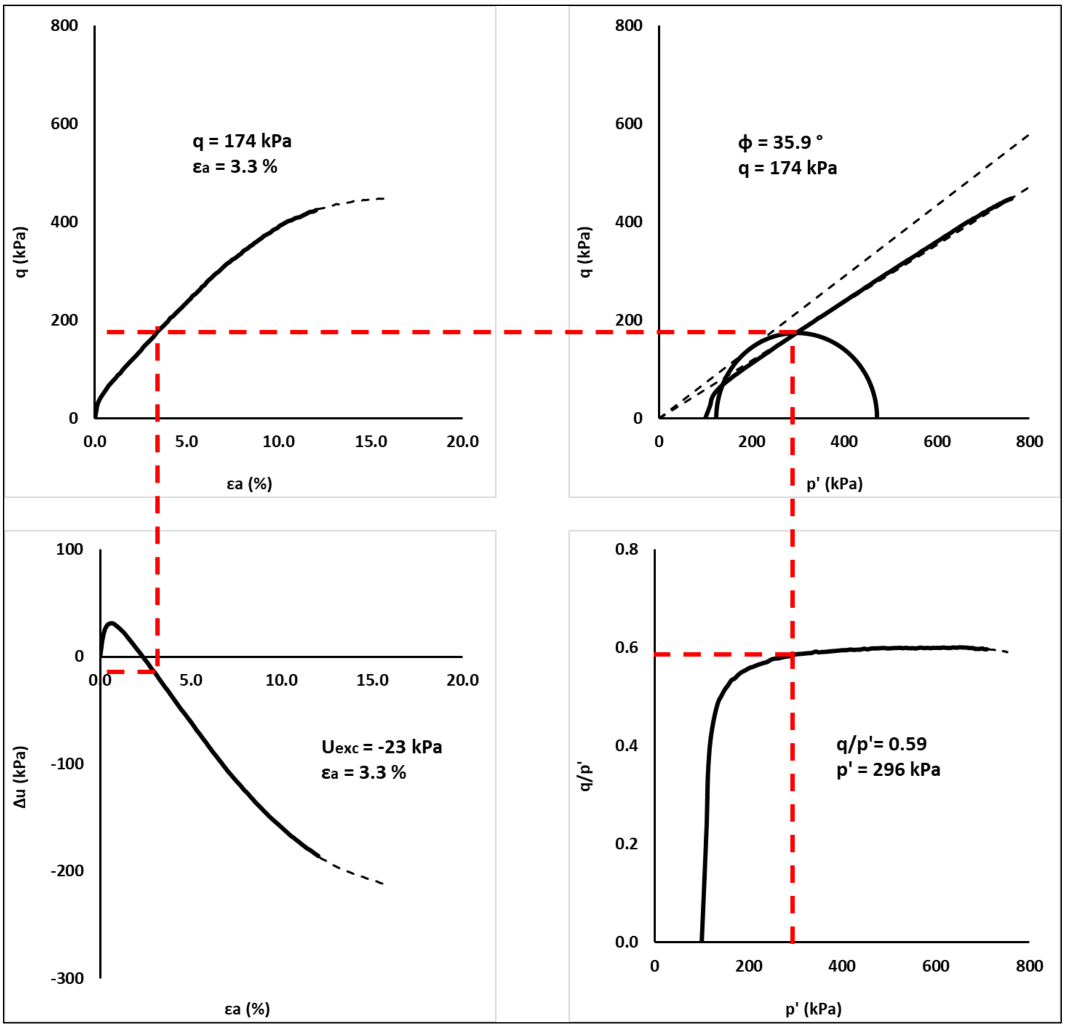

Figure 4.10. Four-way plot of ICU-10

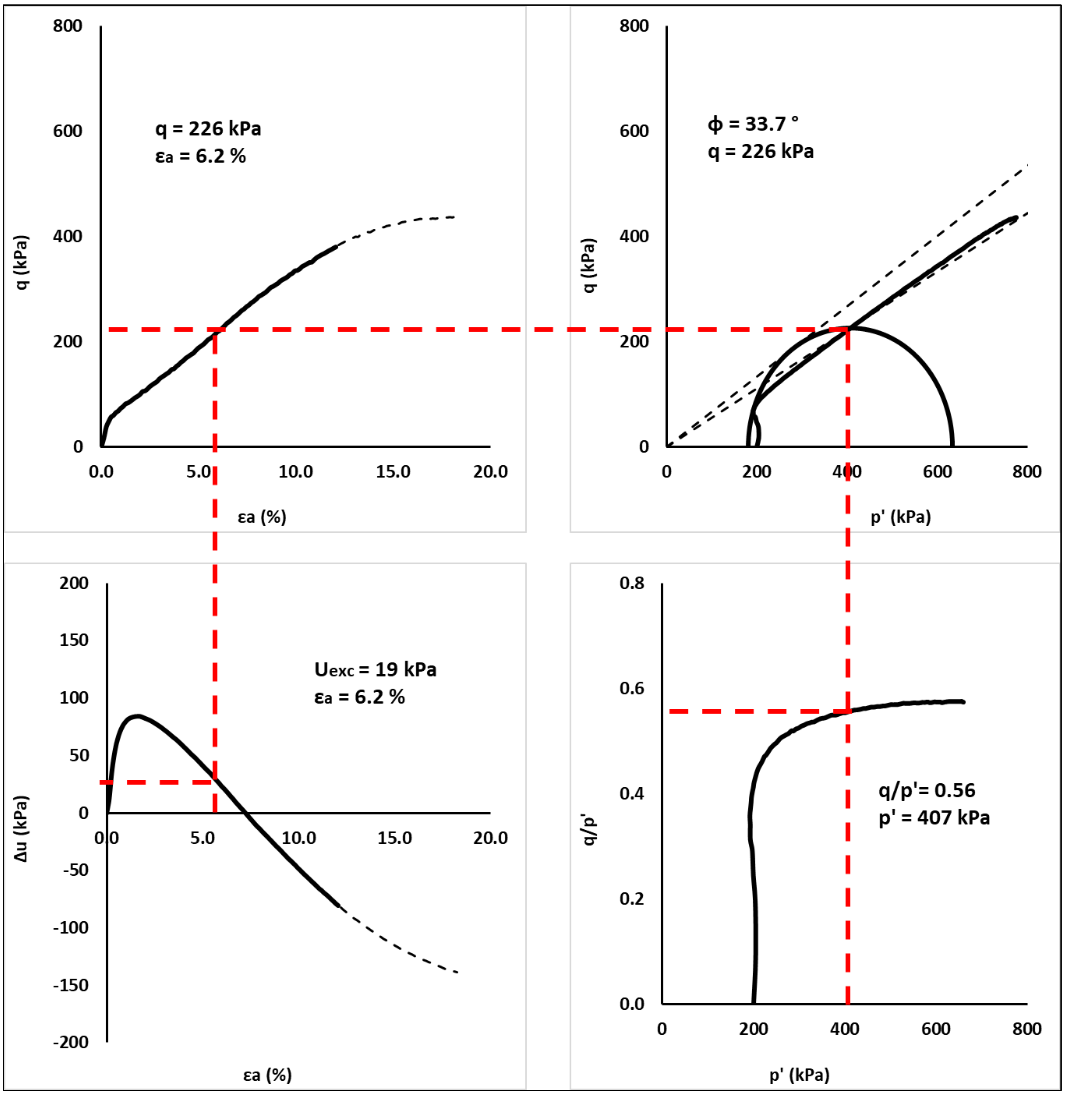

Figure 4.11. Four-way plot of ICU-11

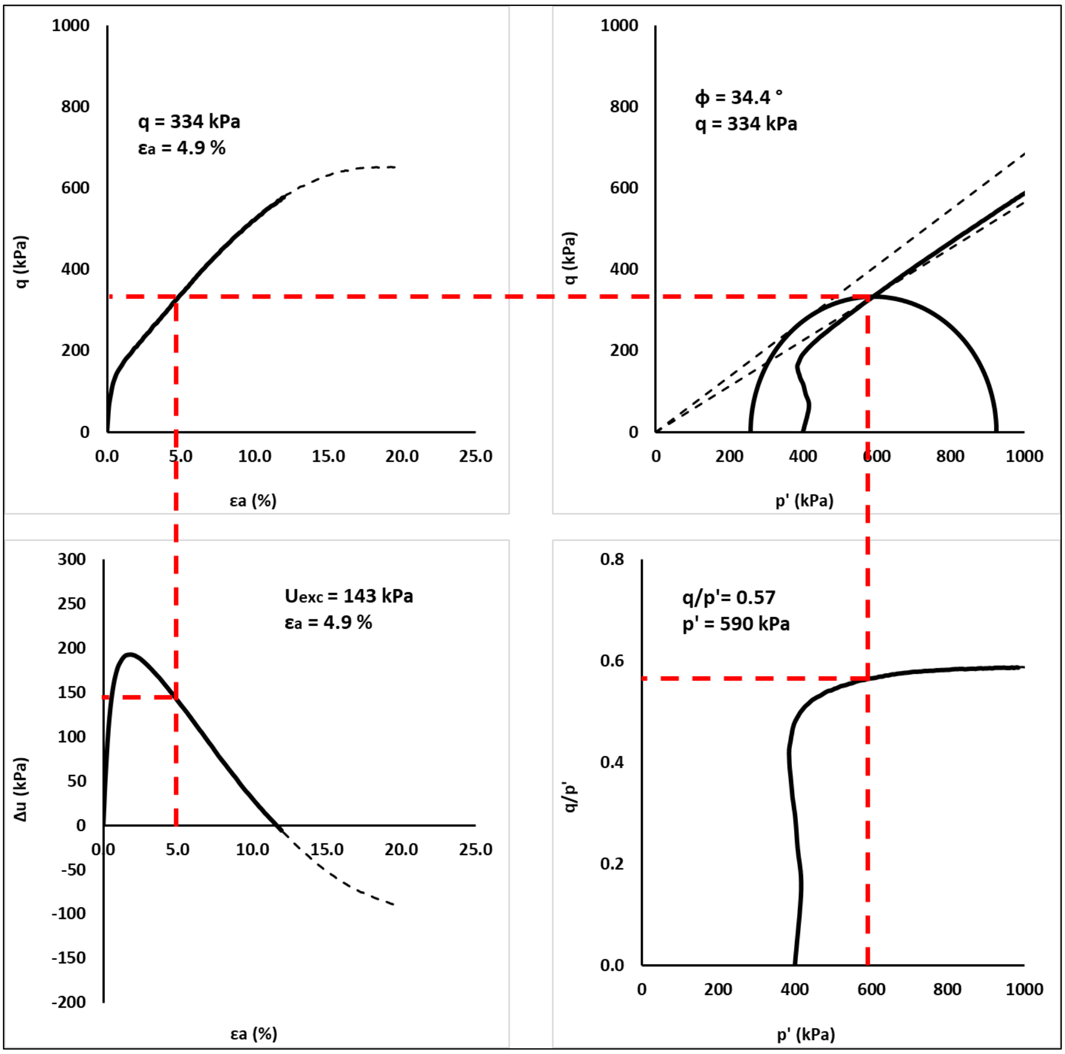

Figure 4.12. Four-way plot of ICU-12

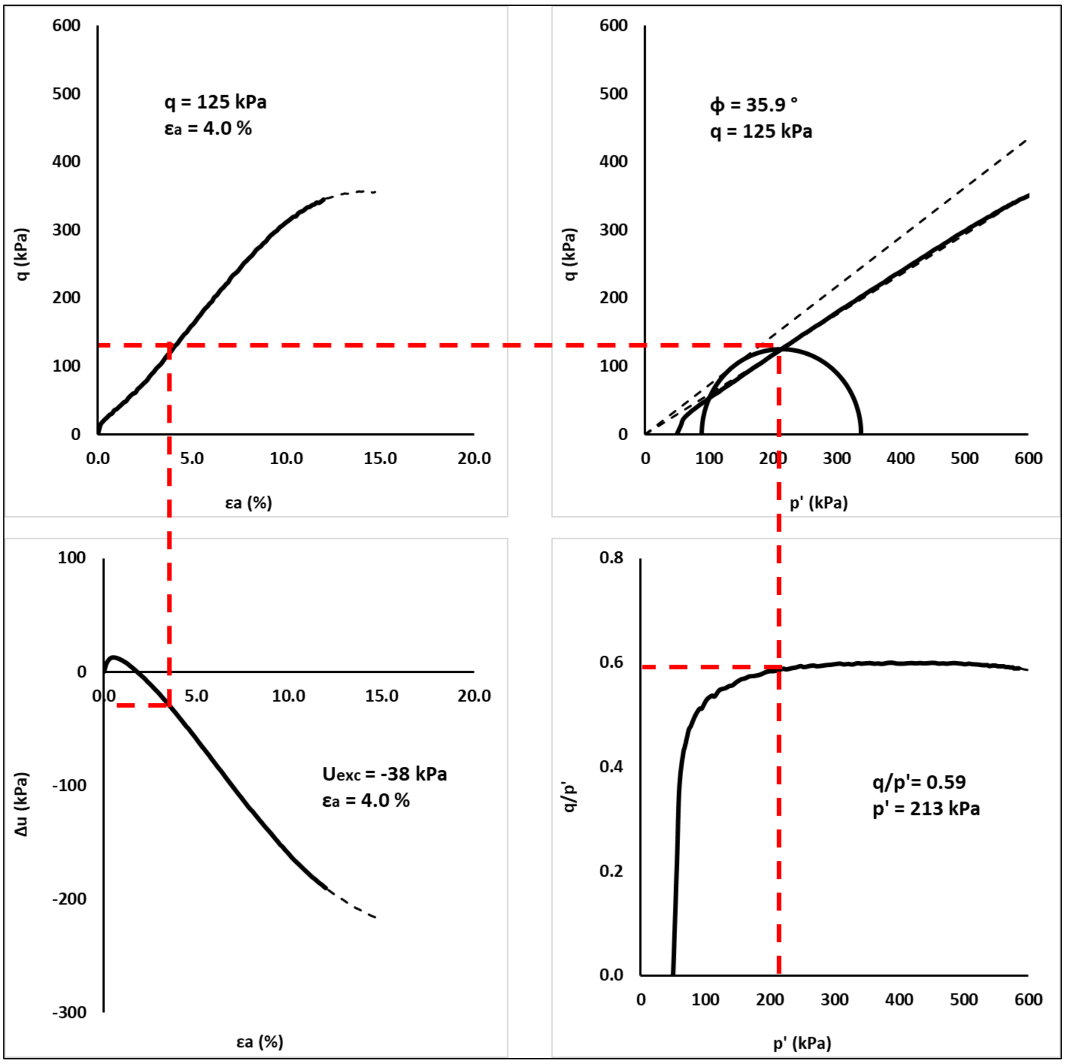

Figure 4.13. Four-way plot of ICU-13

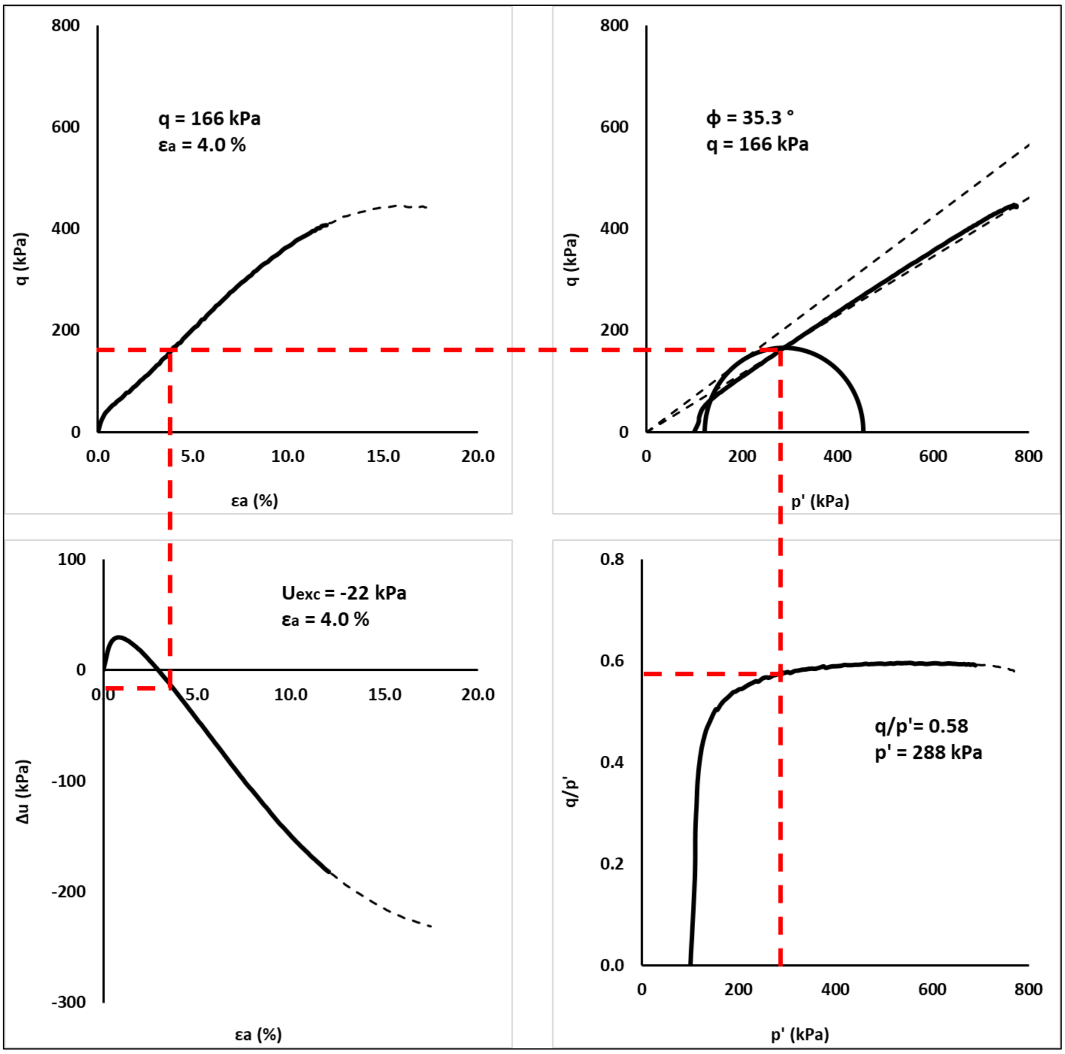

Figure 4.14. Four-way plot of ICU-14

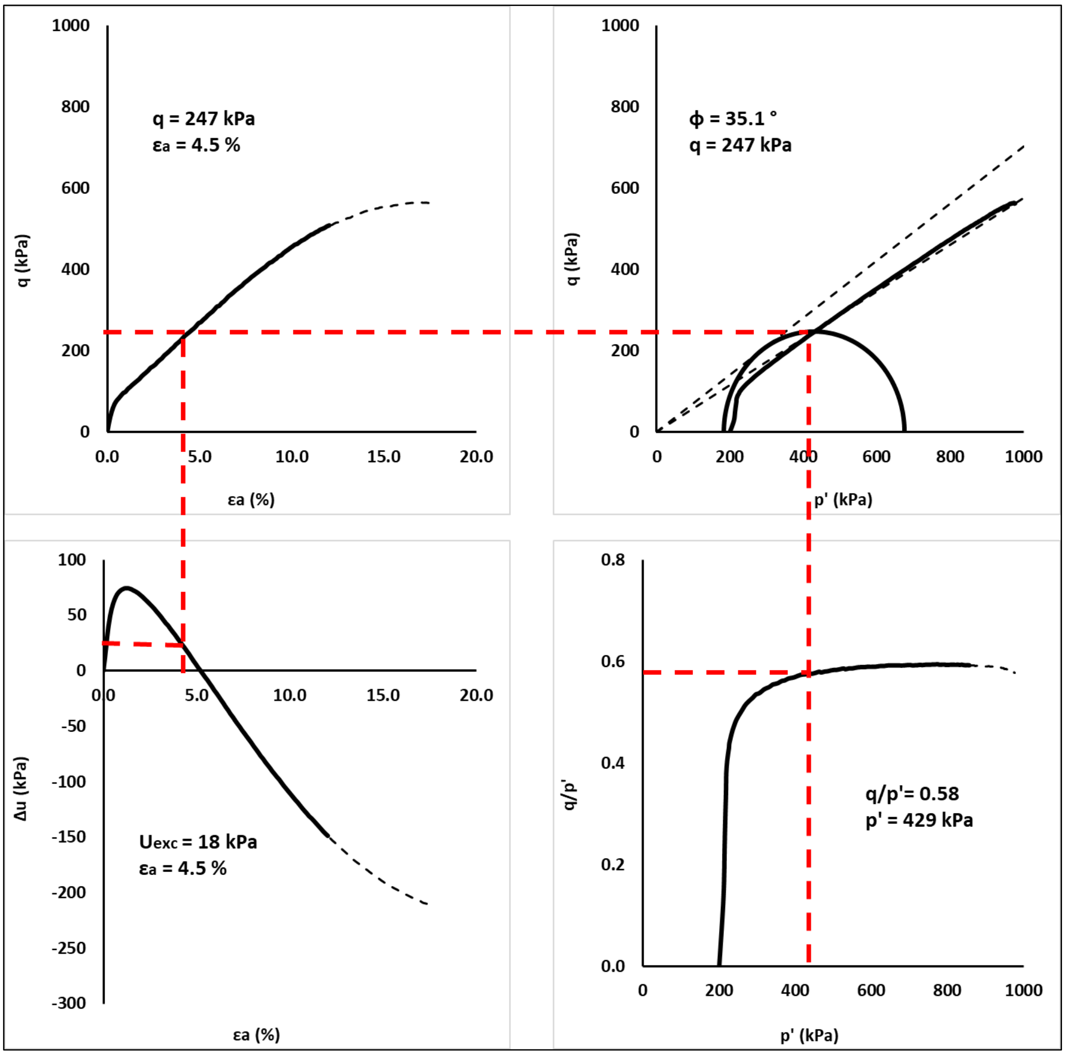

Figure 4.15. Four-way plot of ICU-15

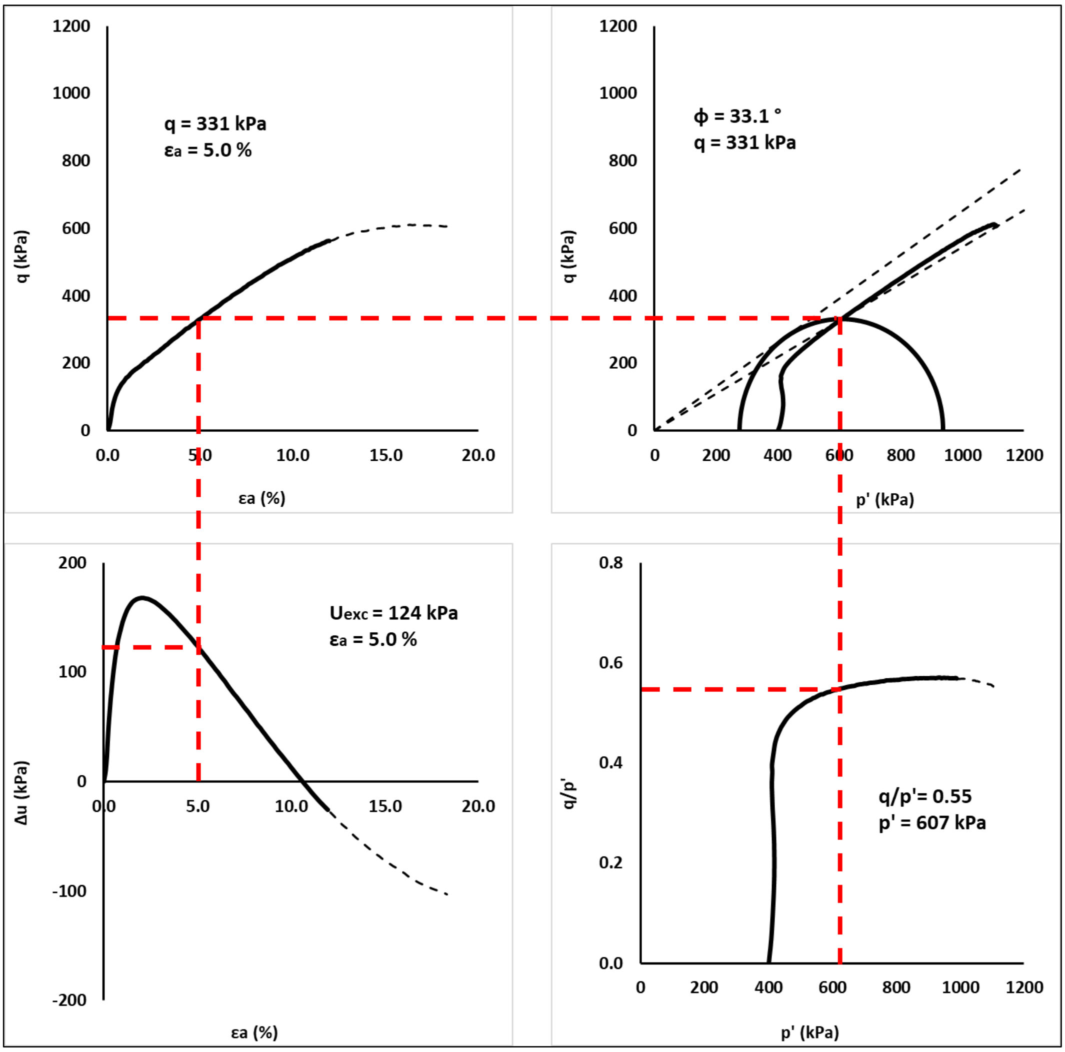

Figure 4.16. Four-way plot of ICU-16

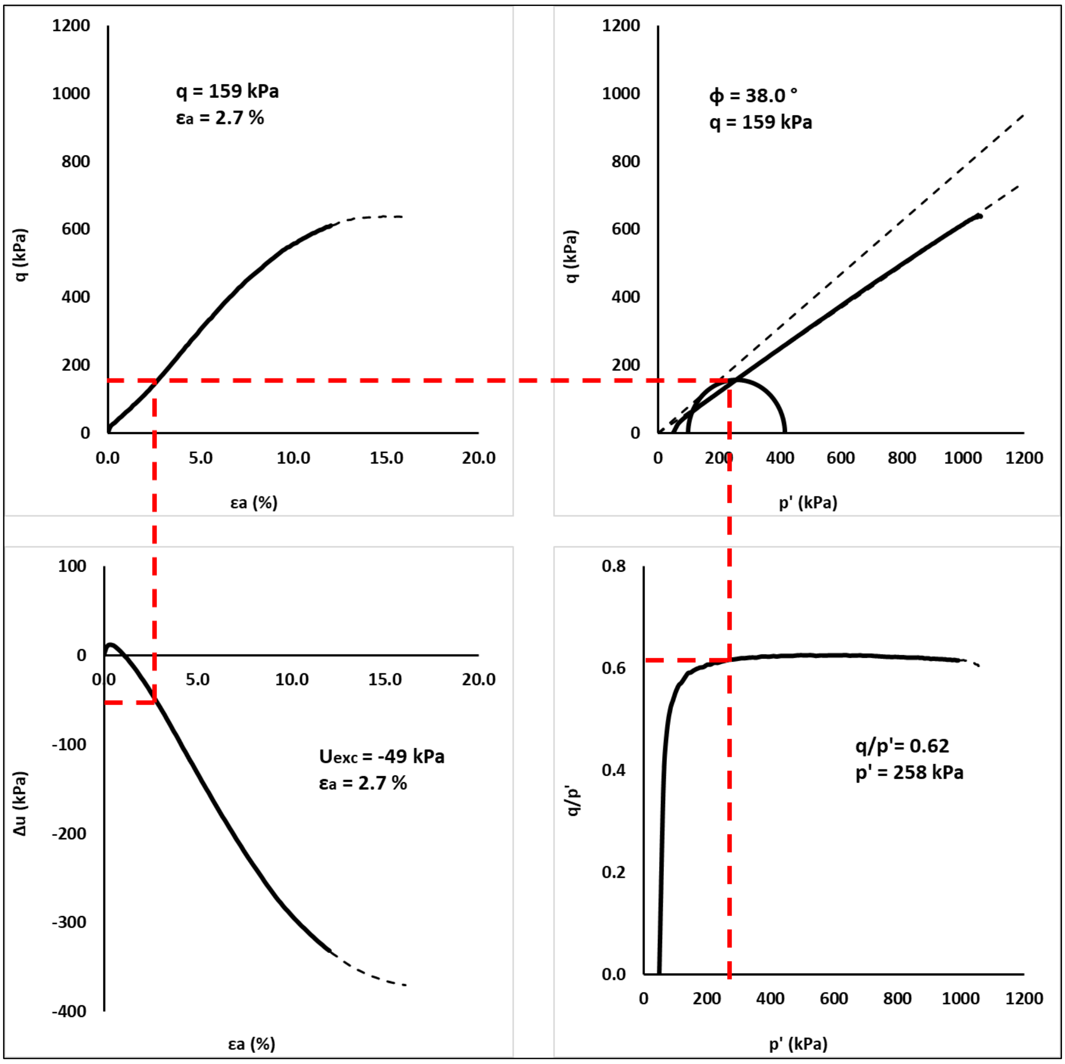

Figure 4.17. Four-way plot of ICU-17

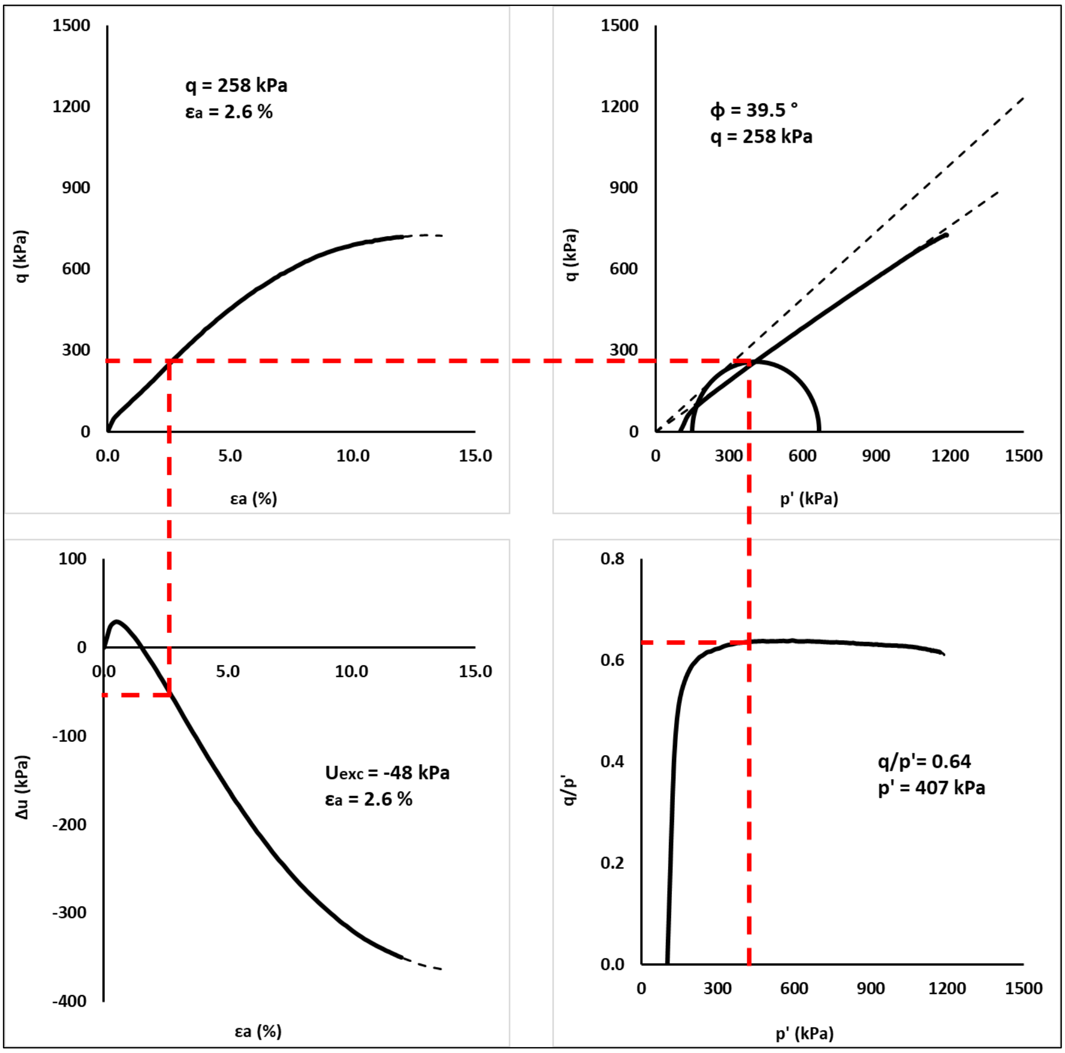

Figure 4.18. Four-way plot of ICU-18

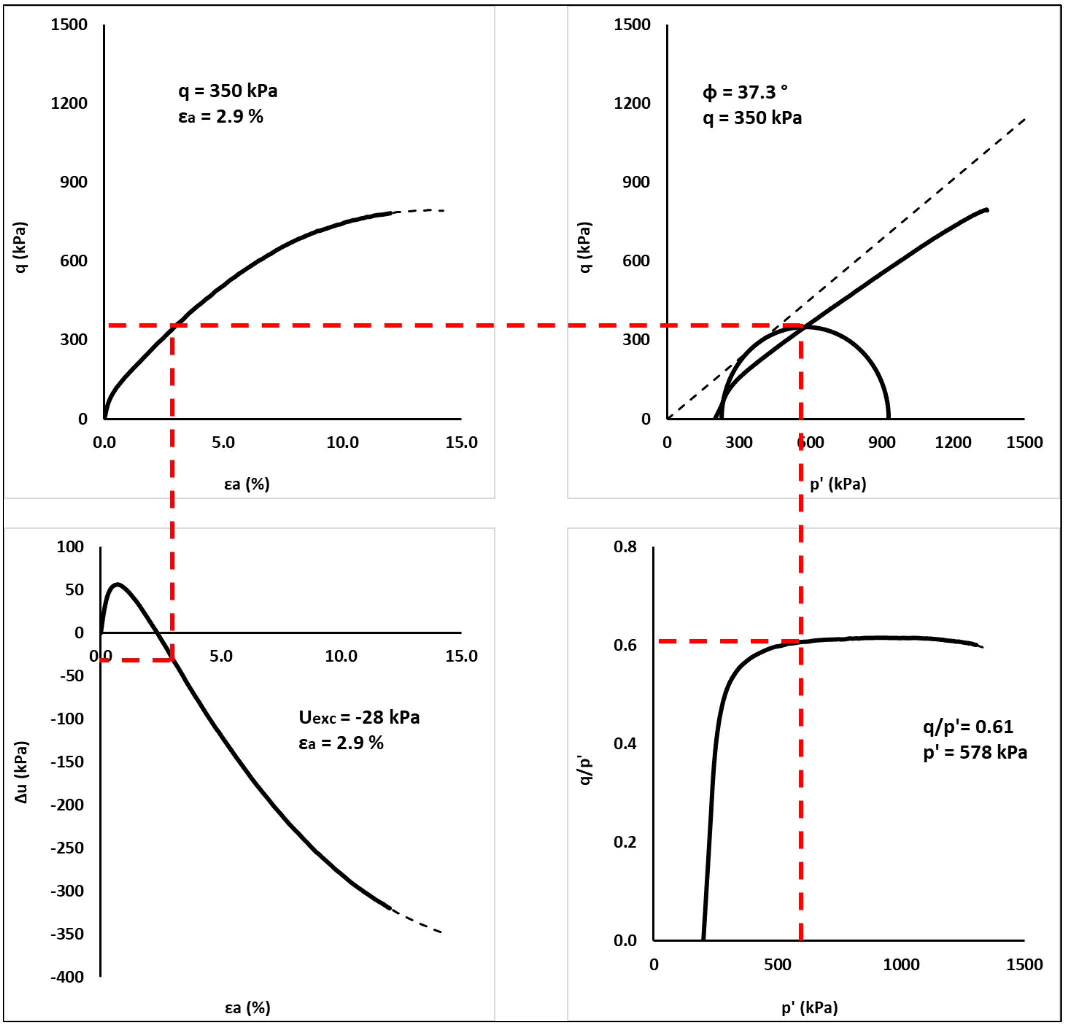

Figure 4.19. Four-way plot of ICU-19

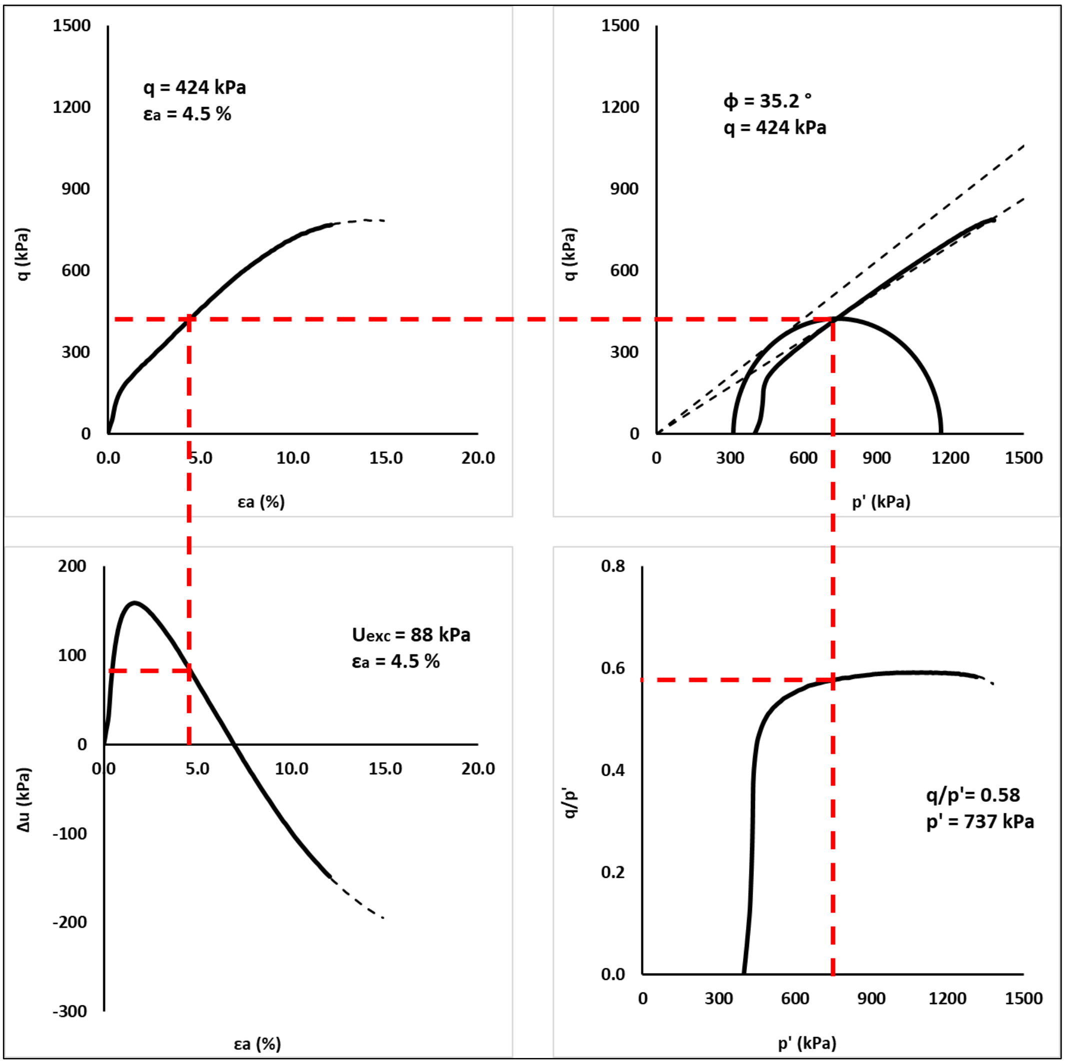

Figure 4.20. Four-way plot of ICU-20

4.2 Interpretation of Triaxial Test Results

Test results with different void ratios but consolidated to the same stress state is shown in Figure 4.21 to 4.28. Firstly, the graphs of q vs. ε_a and Δu vs. ε_a are compared in Figure 4.21 to 4.24. Then mohr circles are examined in Figures 4.25 to 4.28. The same procedure is repeated, this time the void ratio is identical but confining stress different, to assess the effect of stress state as shown in Figure 4.29 to 4.38.

As explained in the literature review chapter, as the void ratio decreases, dilative behavior is expected, resulting in a strain hardening overall response. Under the same consolidation pressures, the angle of friction is higher for lower void ratio samples. Also, as the consolidation pressure increases, contractive behavior is expected, resulting in a strain-softening overall response. Under the same void ratio, the angle of friction is higher for the samples consolidated to lower pressures.

Some fluctuations may be seen in the results due to the test system's and soil sample's variability. The test system consists of 4 main stages, and there may be some differences in each stage, and samples are not the same exactly for each test. Therefore, it is normal to be seen some fluctuations in results.

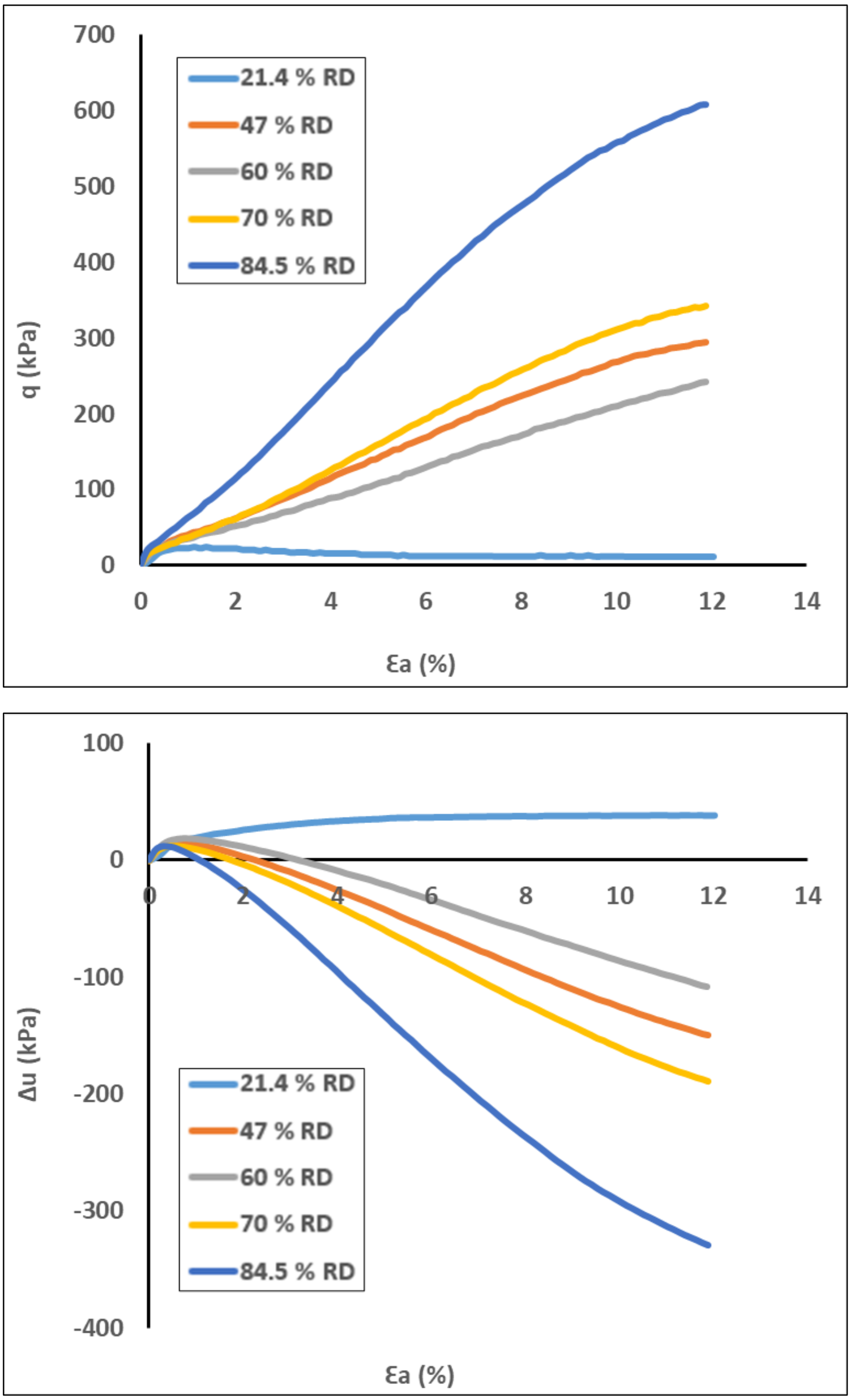

Figure 4.21. Effect of void ratio on the behavior of Çine sand under 50 kPa consolidation pressure

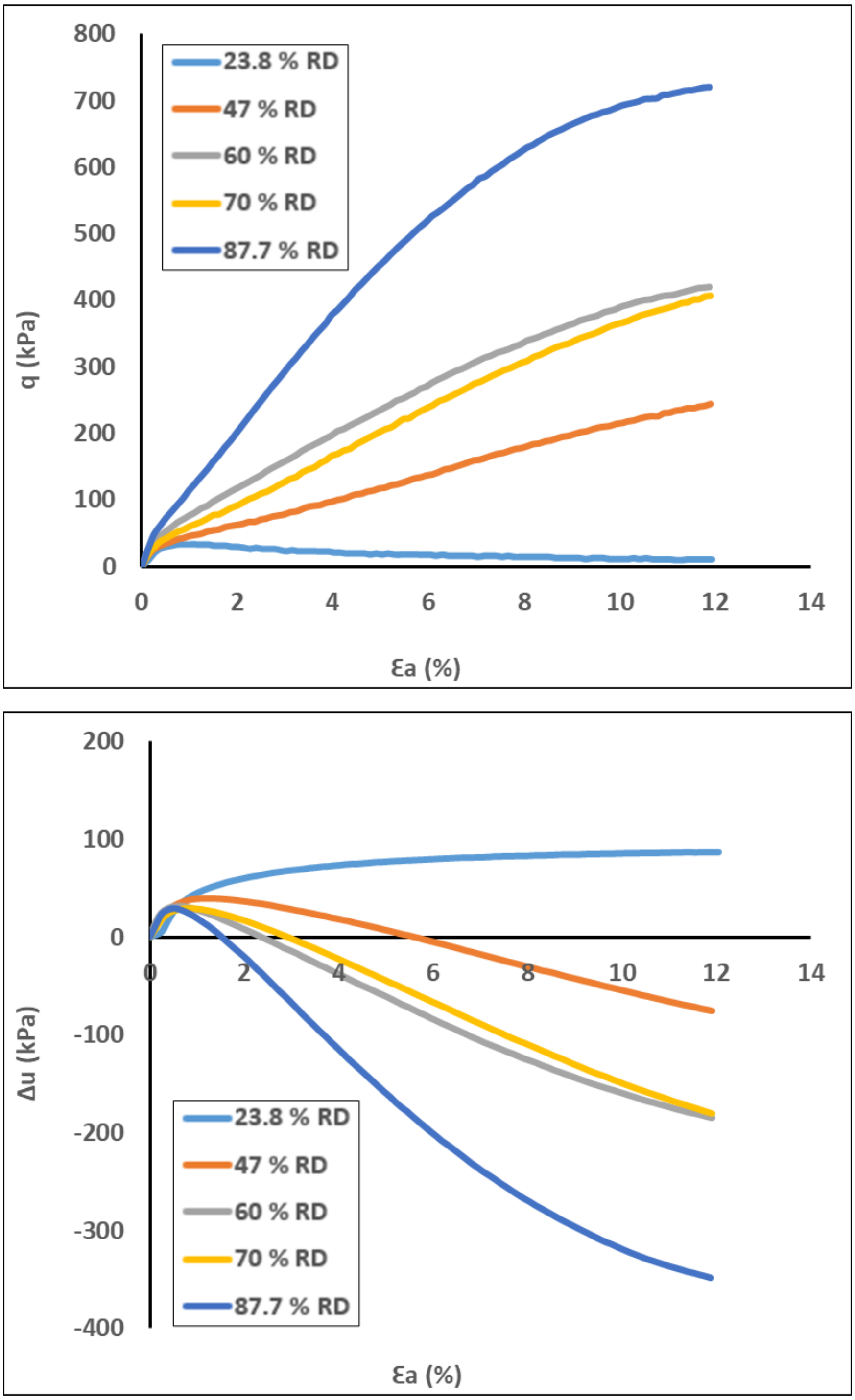

Figure 4.22. Effect of void ratio on the behavior of Çine sand under 100 kPa consolidation pressure

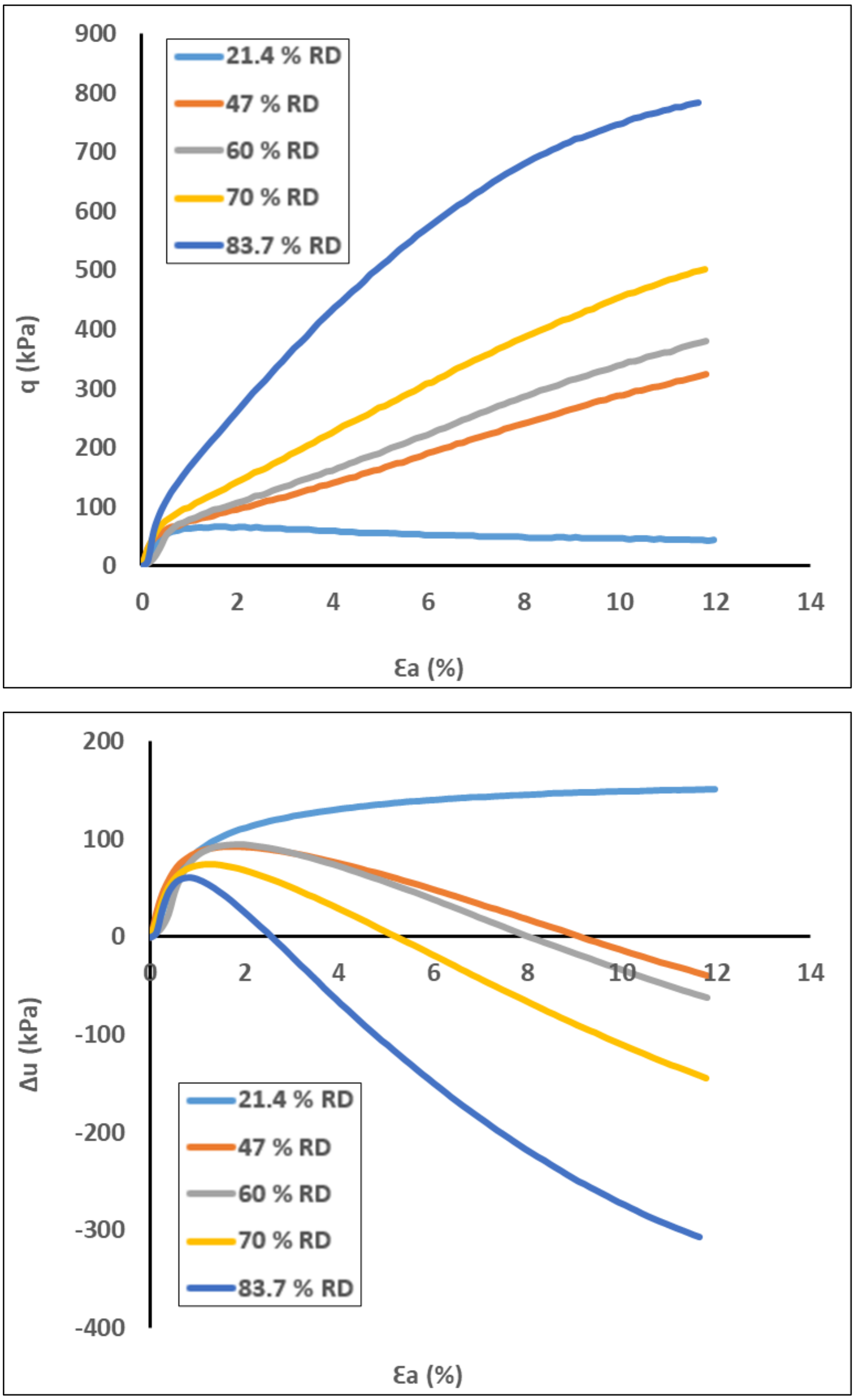

Figure 4.23. Effect of void ratio on the behavior of Çine sand under 200 kPa consolidation pressure

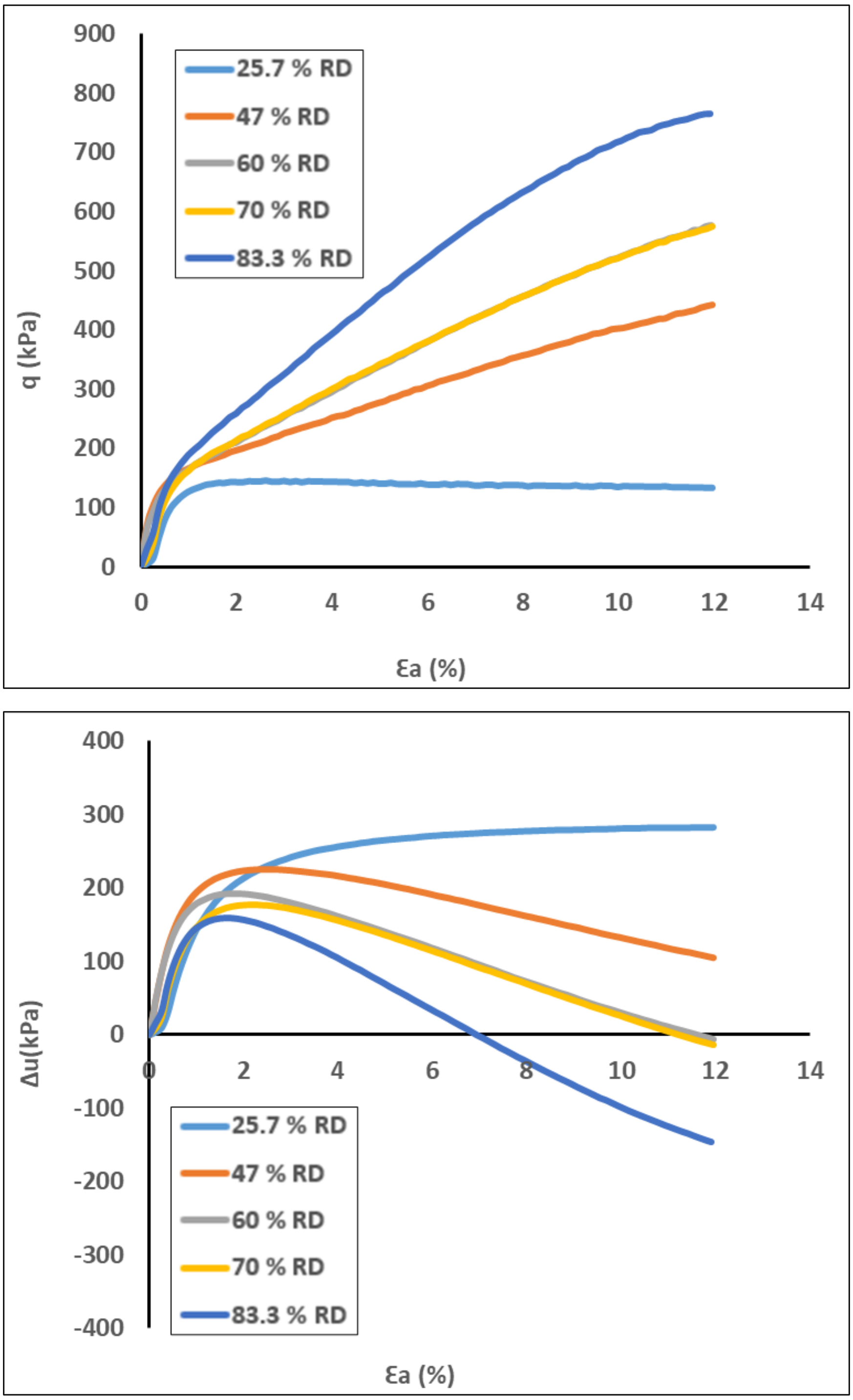

Figure 4.24. Effect of void ratio on the behavior of Çine sand under 400 kPa consolidation pressure

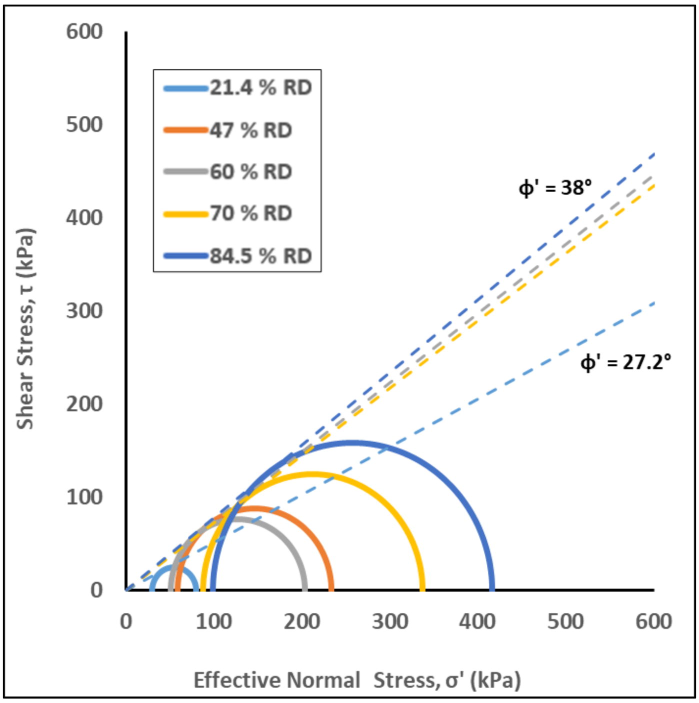

Figure 4.25. Mohr circles and failure envelopes for varying relative density samples subjected to 50 kPa consolidation pressure

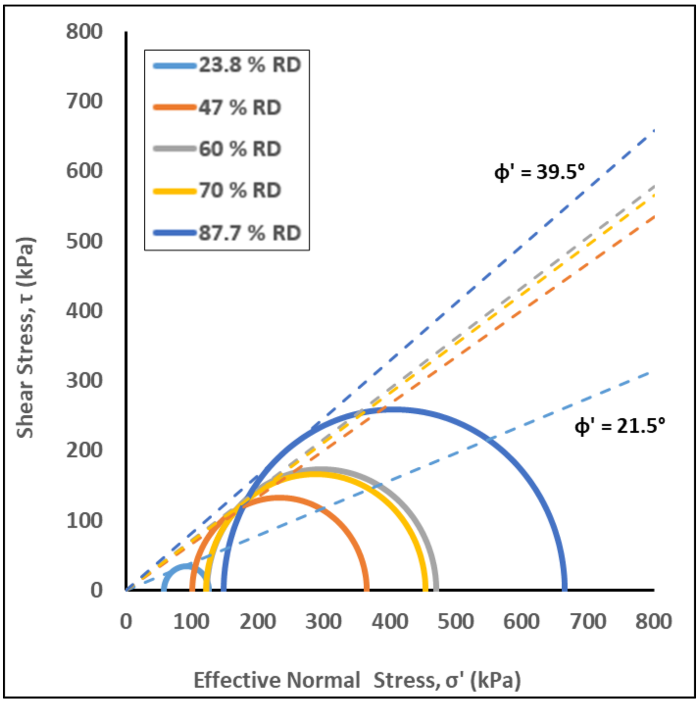

Figure 4.26. Mohr circles and failure envelopes for varying relative density samples subjected to 100 kPa consolidation pressure

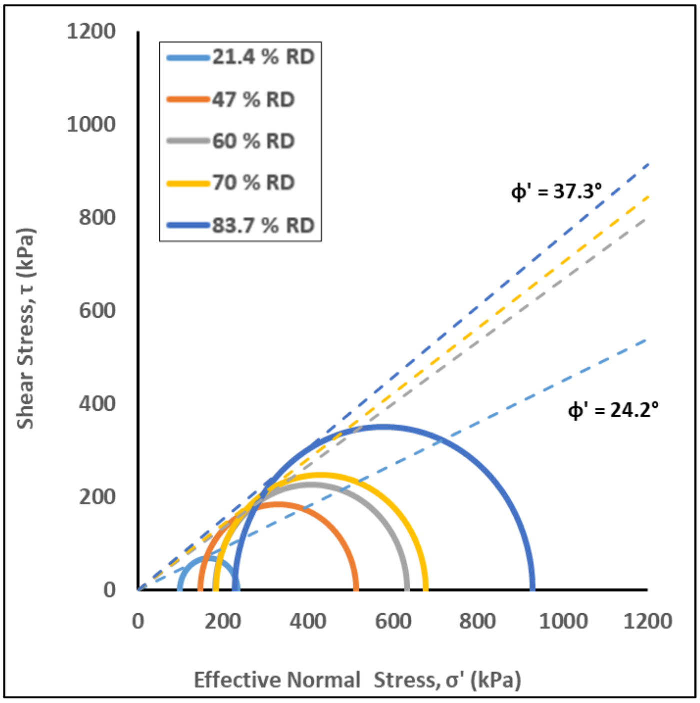

Figure 4.27. Mohr circles and failure envelopes for varying relative density samples subjected to 200 kPa consolidation pressure

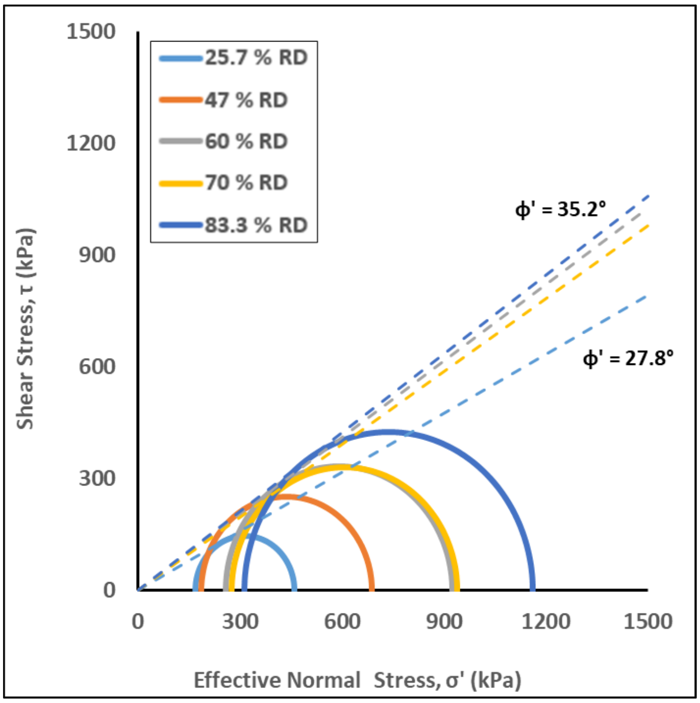

Figure 4.28. Mohr circles and failure envelopes for varying relative density samples subjected to 400 kPa consolidation pressure

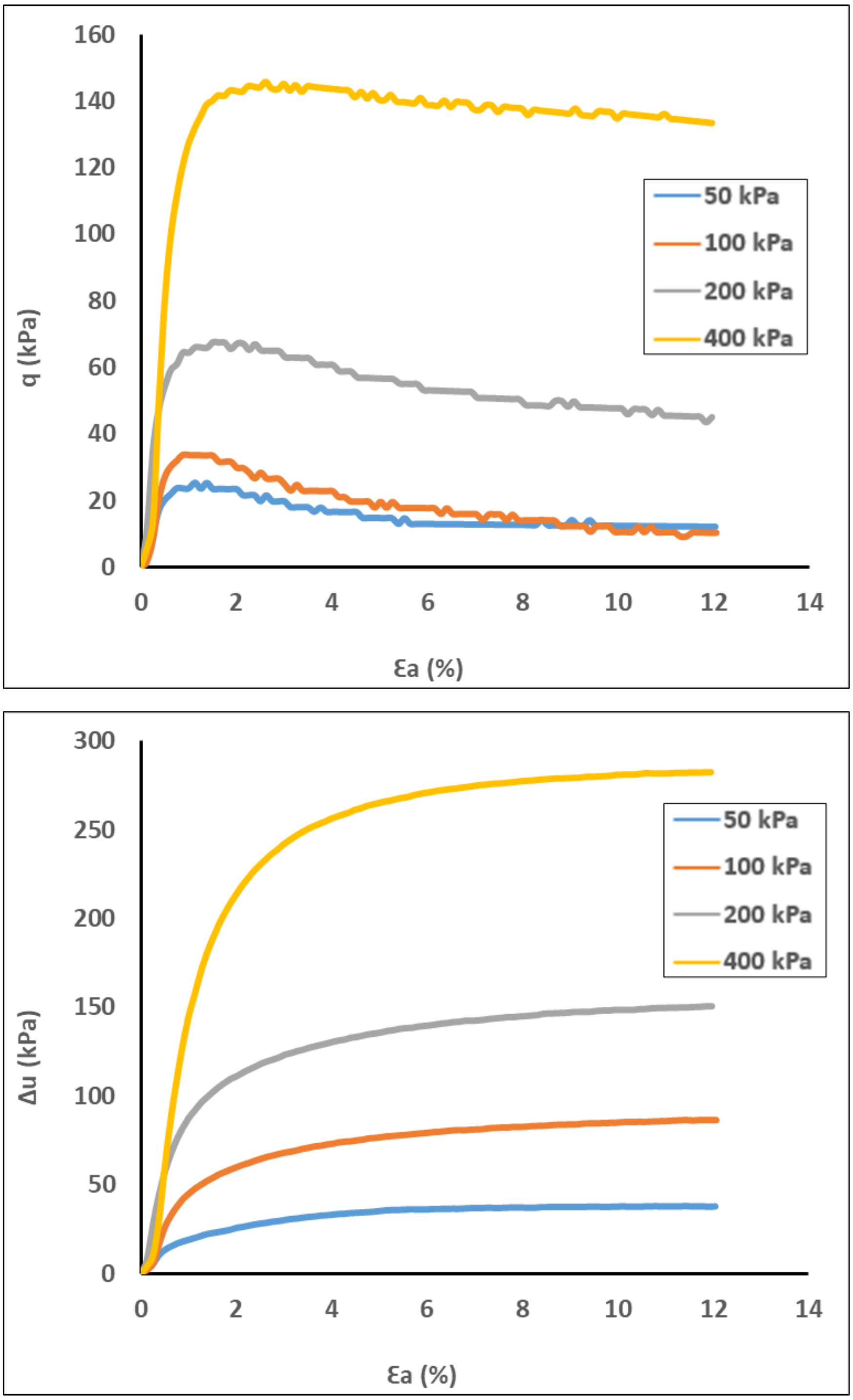

Figure 4.29. Effect of stress state on the behavior of Çine sand with 21 – 26 % relative density

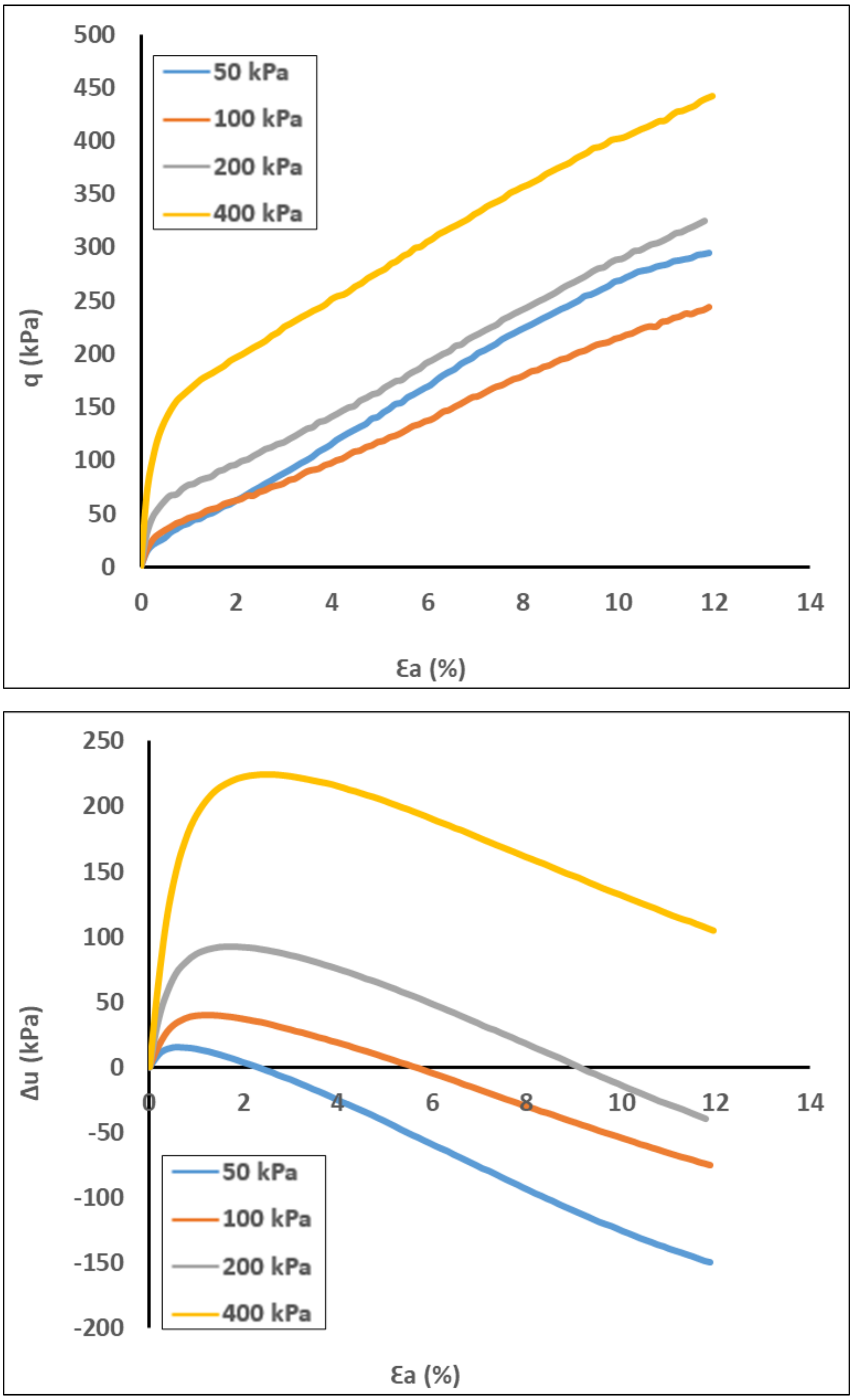

Figure 4.30. Effect of stress state on the behavior of Çine sand with 47 % relative density

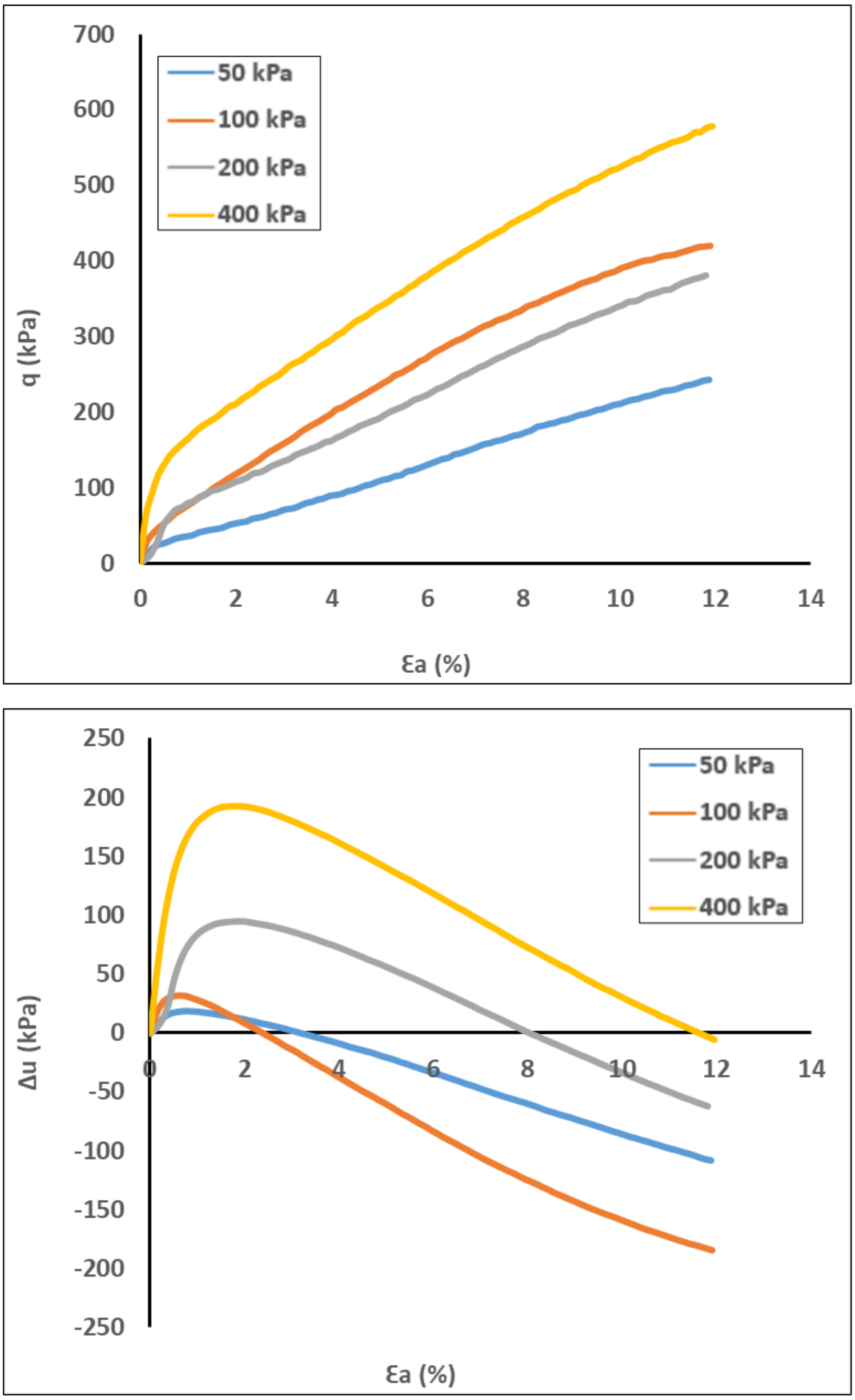

Figure 4.31. Effect of stress state on the behavior of Çine sand with 60 % relative density

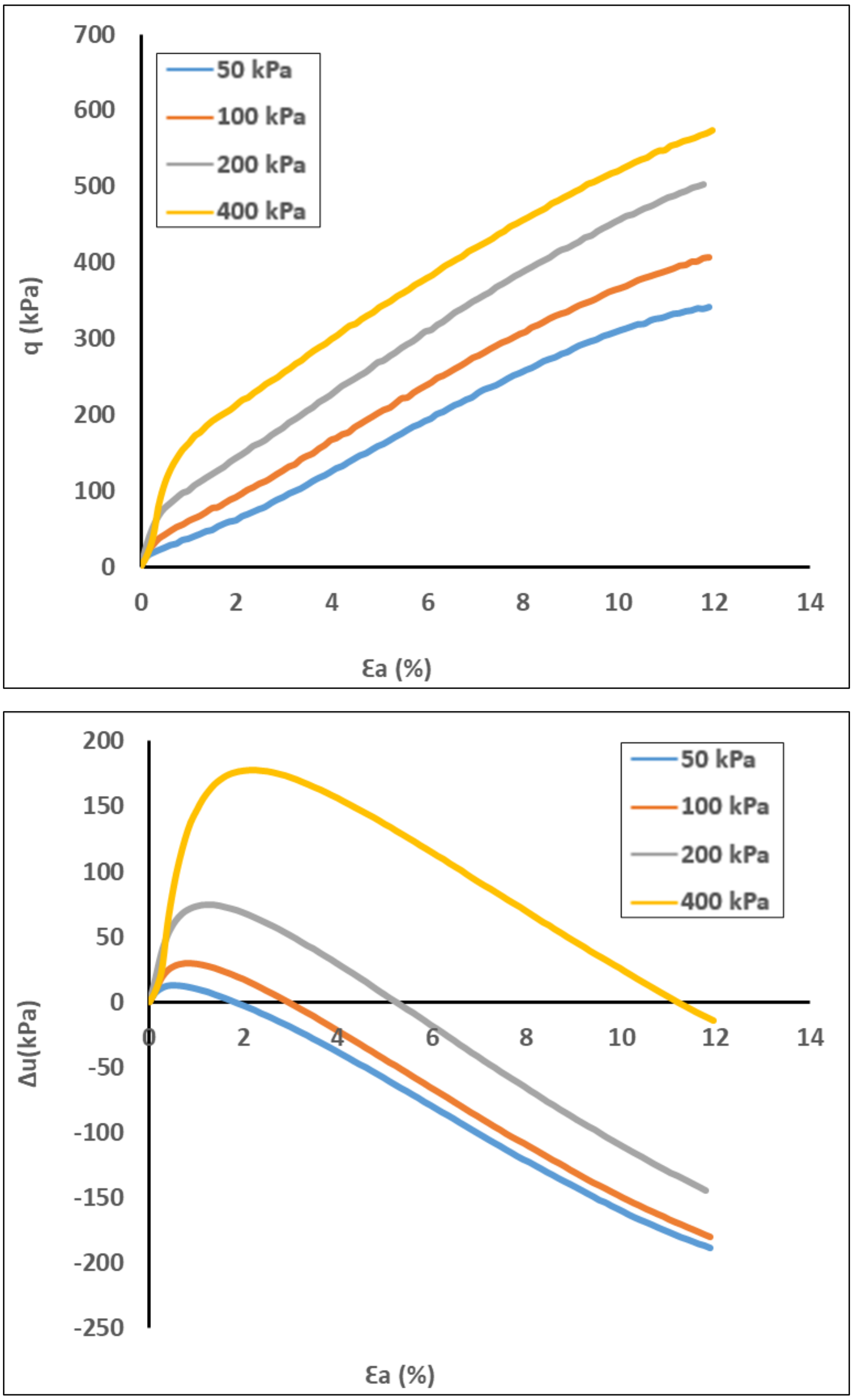

Figure 4.32. Effect of stress state on the behavior of Çine sand with 70 % relative density

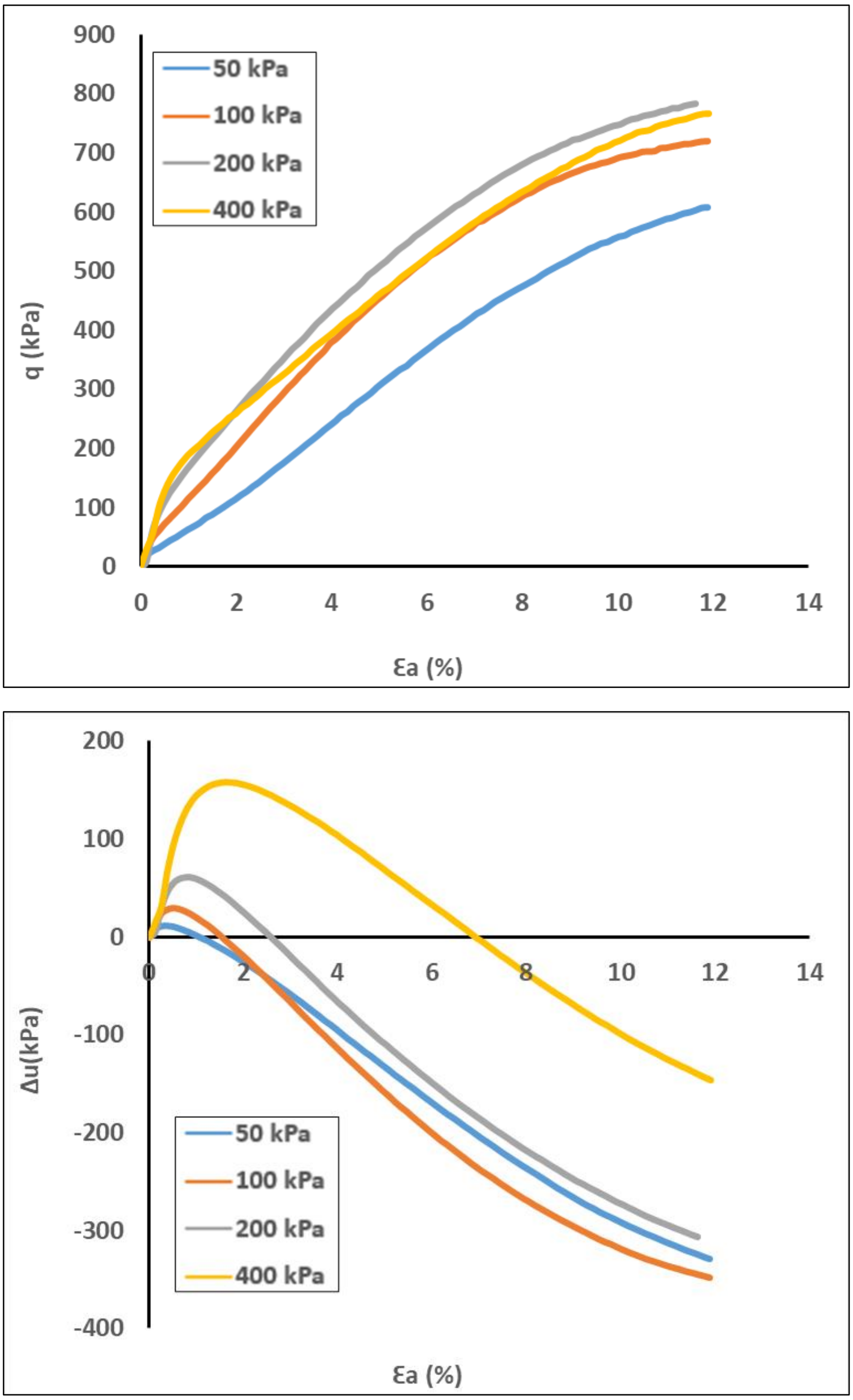

Figure 4.33. Effect of stress state on the behavior of Çine sand with 83 – 88 % relative density

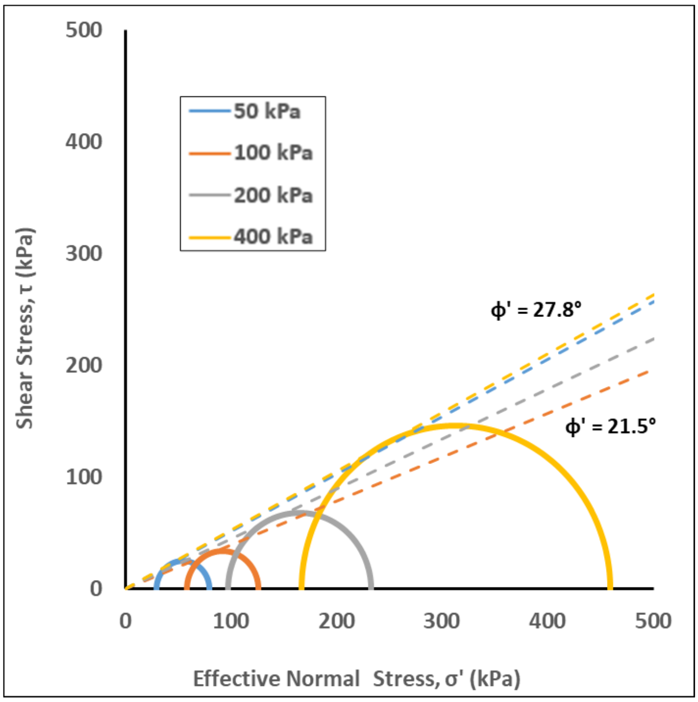

Figure 4.34. Mohr circles and failure envelopes for 21-26 % RD samples subjected to varying consolidation pressures

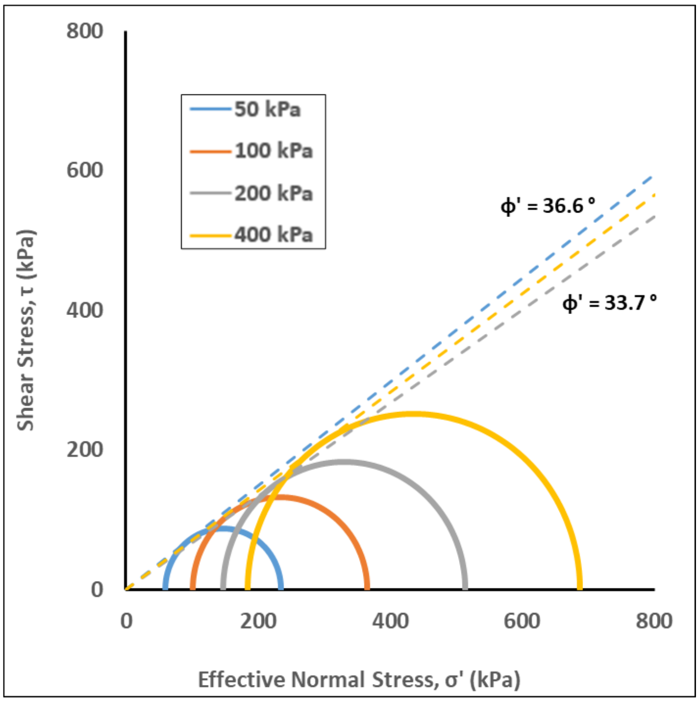

Figure 4.35. Mohr circles and failure envelopes for 47 % RD samples subjected to varying consolidation pressures

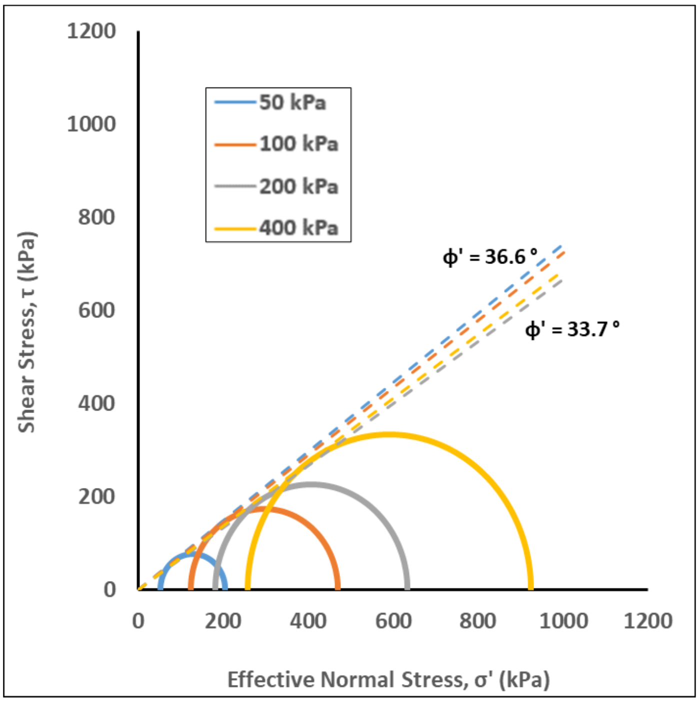

Figure 4.36. Mohr circles and failure envelopes for 60 % RD samples subjected to varying consolidation pressures

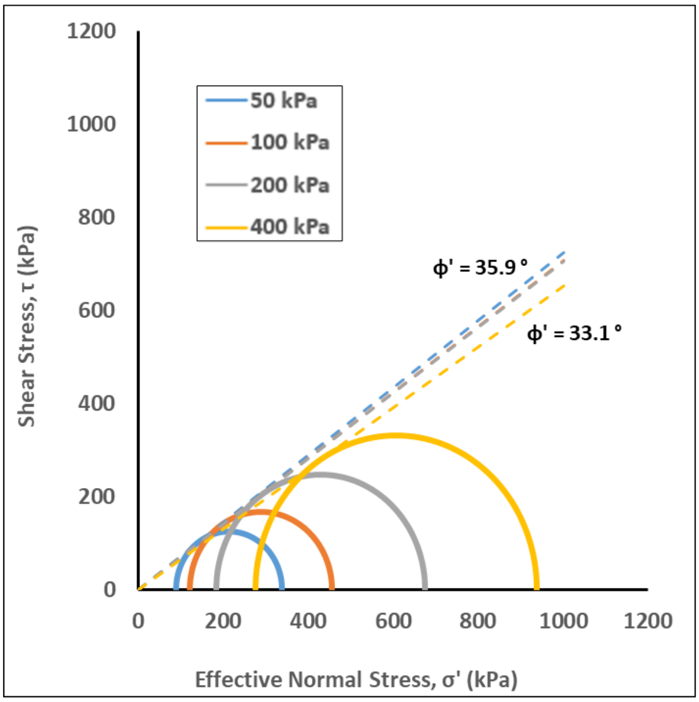

Figure 4.37. Mohr circles and failure envelopes for 70 % RD samples subjected to varying consolidation pressures

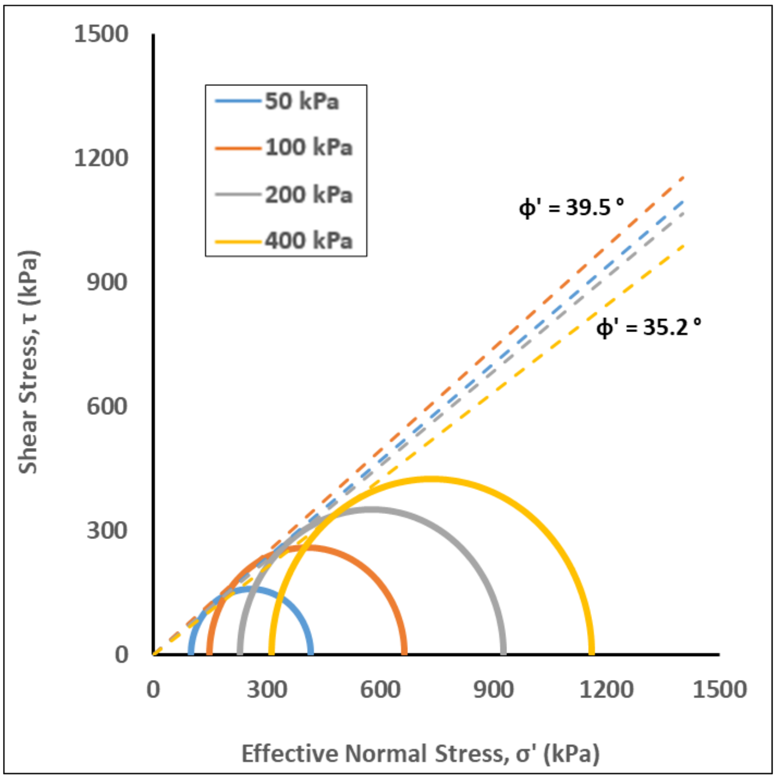

Figure 4.38. Mohr circles and failure envelopes for 83-88 % RD samples subjected to varying consolidation pressures

16 out of 20 samples showed strain hardening behavior, while 4 samples showed strain softening behavior. Due to the limited number of tests and the preparation of the loosest set with a different method (moist tamping), a precise initial dividing line could not be created. Therefore, the range of initial dividing line is shown in Figure 4.39.

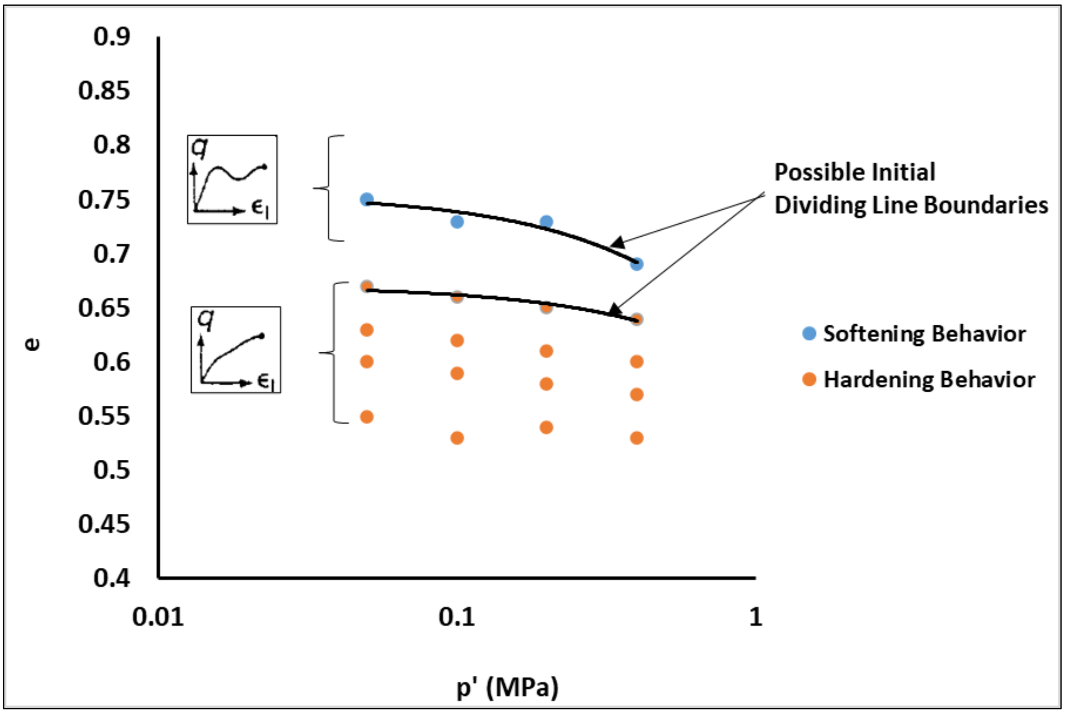

Figure 4.39. Possible initial dividing line boundaries of Çine sand

With triaxial test results, the steady state line was determined after plotting the steady state points in the e vs. p′ plane, as shown in Figure 4.40. The data in the p′ vs. q plane were combined, as shown in Figure 4.41.

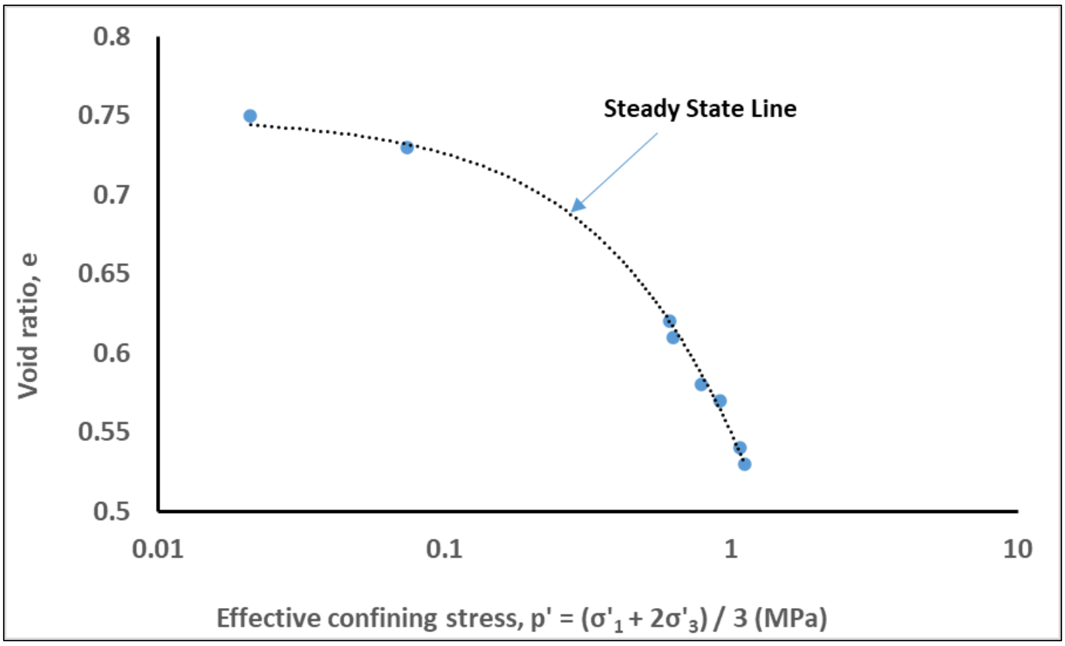

Figure 4.40. Steady state line of Çine sand

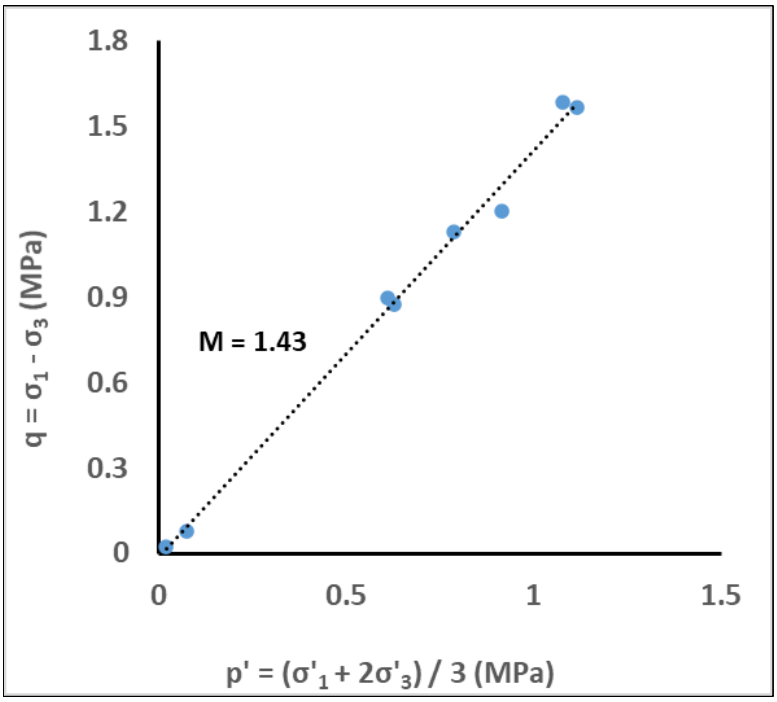

Figure 4.41. Steady state response in deviatoric stress vs. mean effective stress domain

4.3 Results of Oedometer Tests

Six oedometer tests were performed with different relative densities. Tabulated results are shown in Table 4.2. In the table, initial void ratio, relative density, and yielding stress of tests are shown.

Table 4.2 Results of Oedometer Tests

Test ID	e_0	D_R (%)	σ'_y (MPa)
OED-1	0.745	25	1.3
OED-2	0.712	35	1.5
OED-3	0.664	50	2.2
OED-4	0.631	60	2.3
OED-5	0.599	70	2.9
OED-6	0.550	85	3.1

With oedometer test results, void ratio versus the logarithm of effective vertical stress (e vs. $\log\sigma'_v$), effective vertical stress versus vertical strain (σ'_v vs. ε_v), and void ratio versus effective vertical stress (e vs. σ'_v) are shown in Figure 4.42 to 4.47.

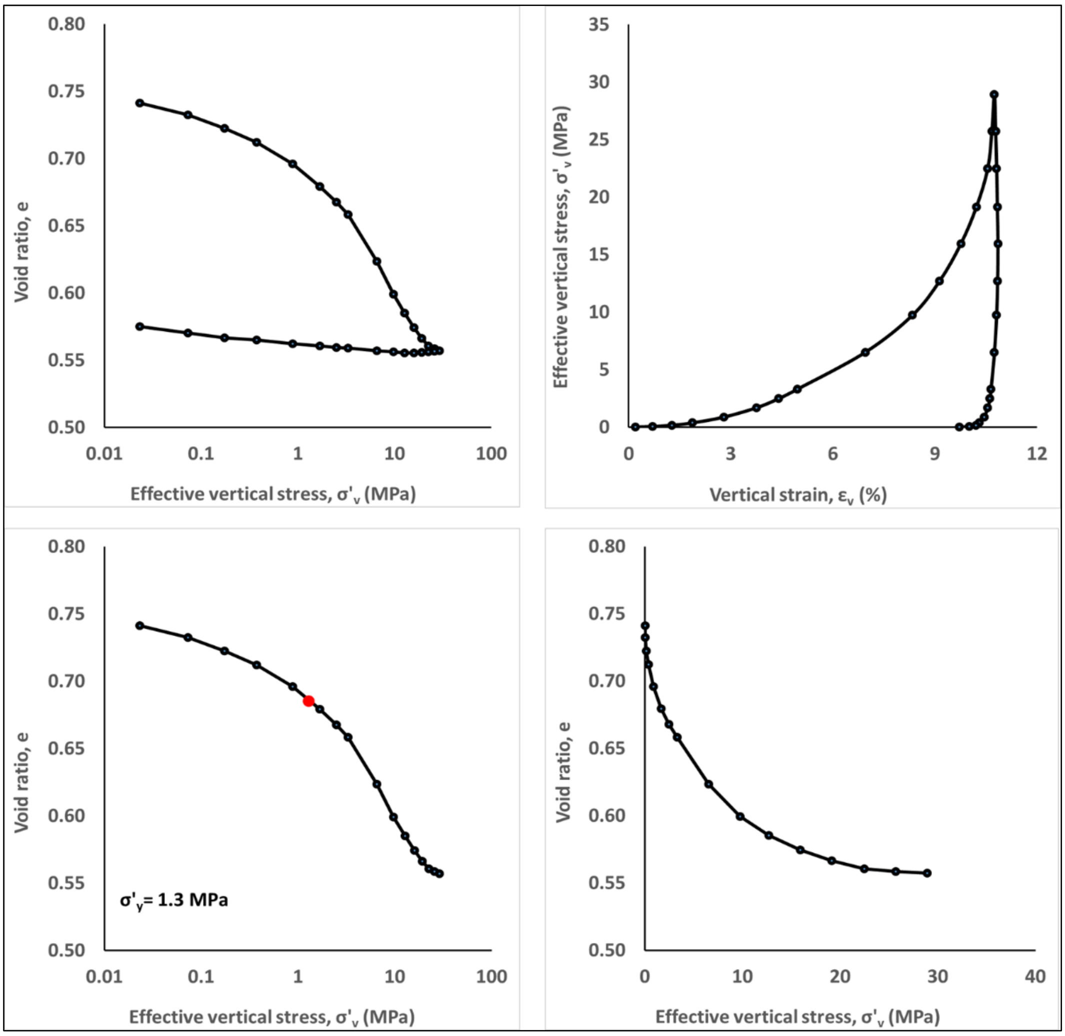

Figure 4.42. Oedometer test results of 25 % relative density sample

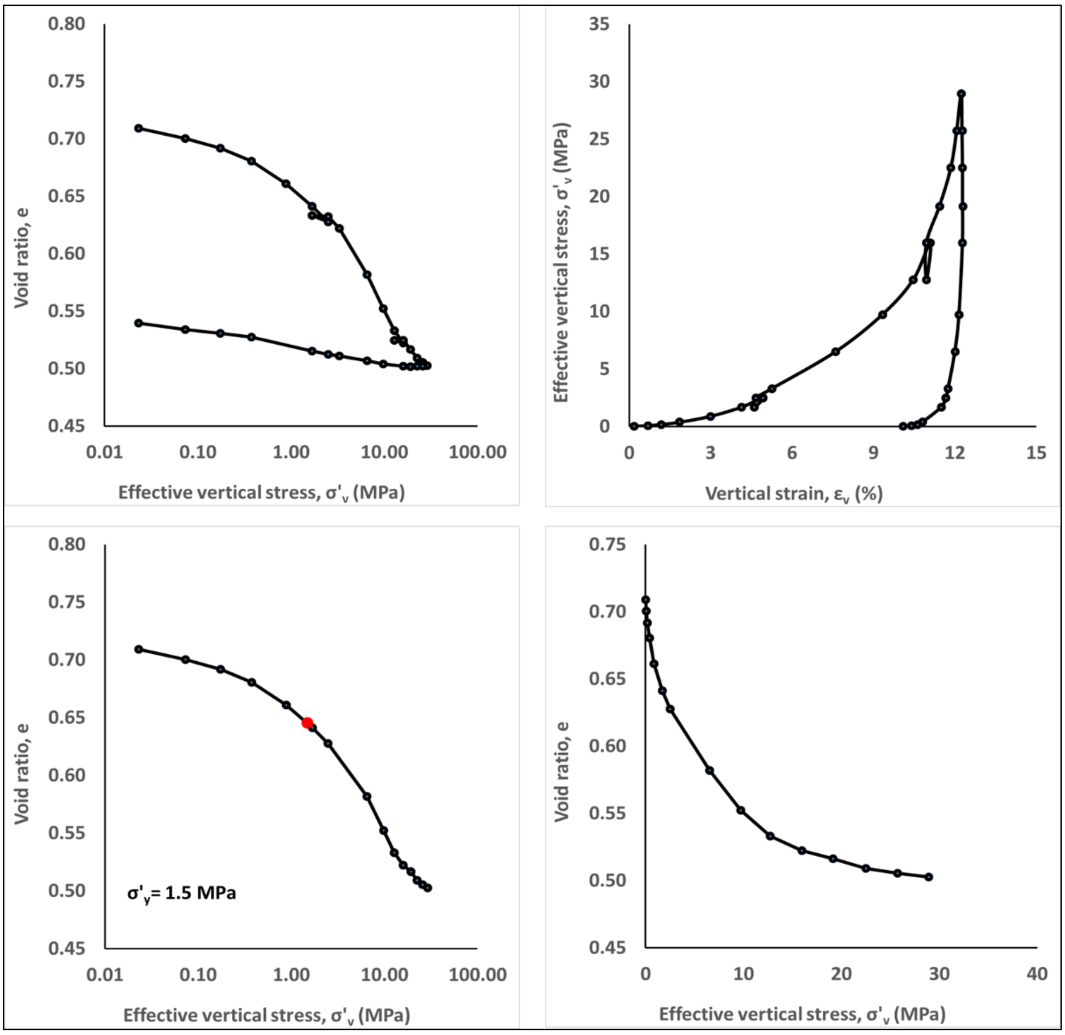

Figure 4.43. Oedometer test results of 35 % relative density sample

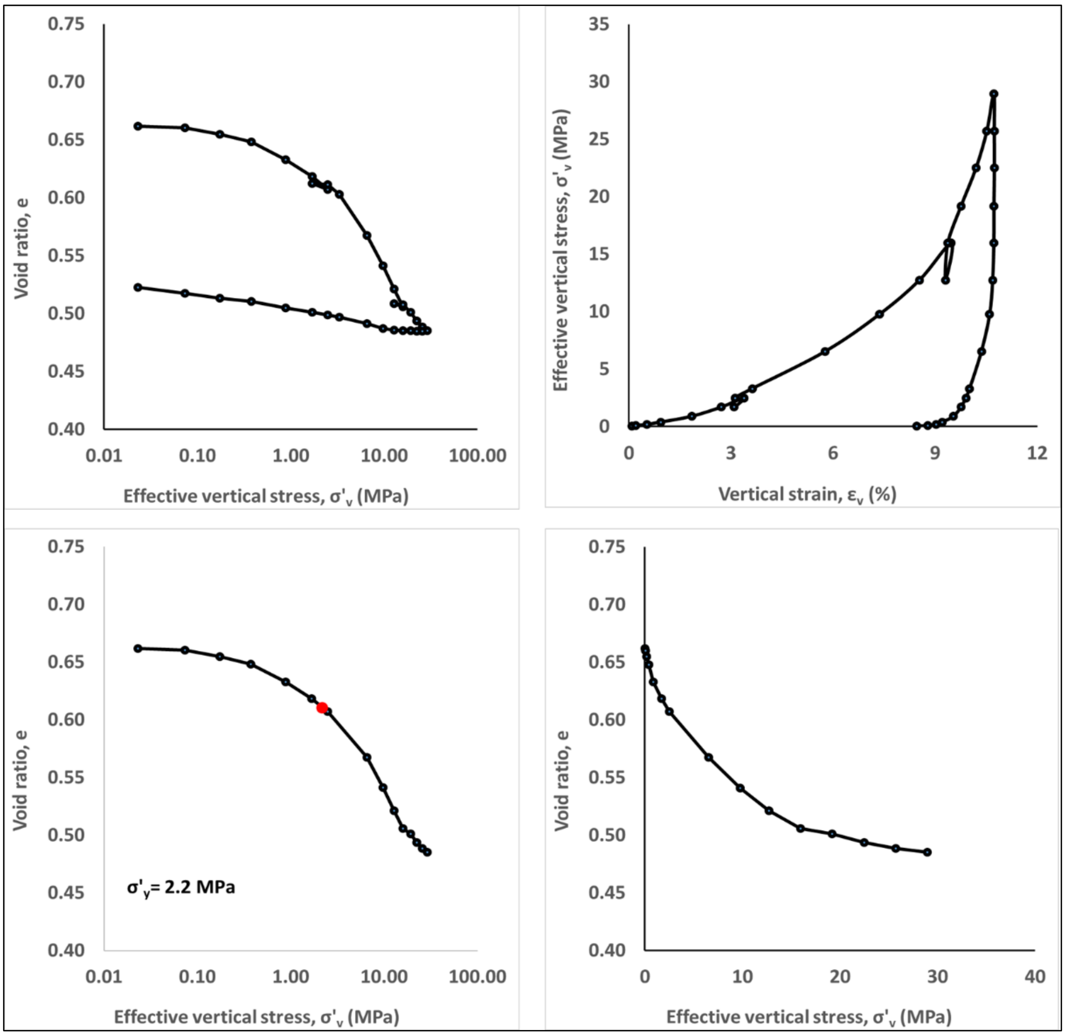

Figure 4.44. Oedometer test results of 50 % relative density sample

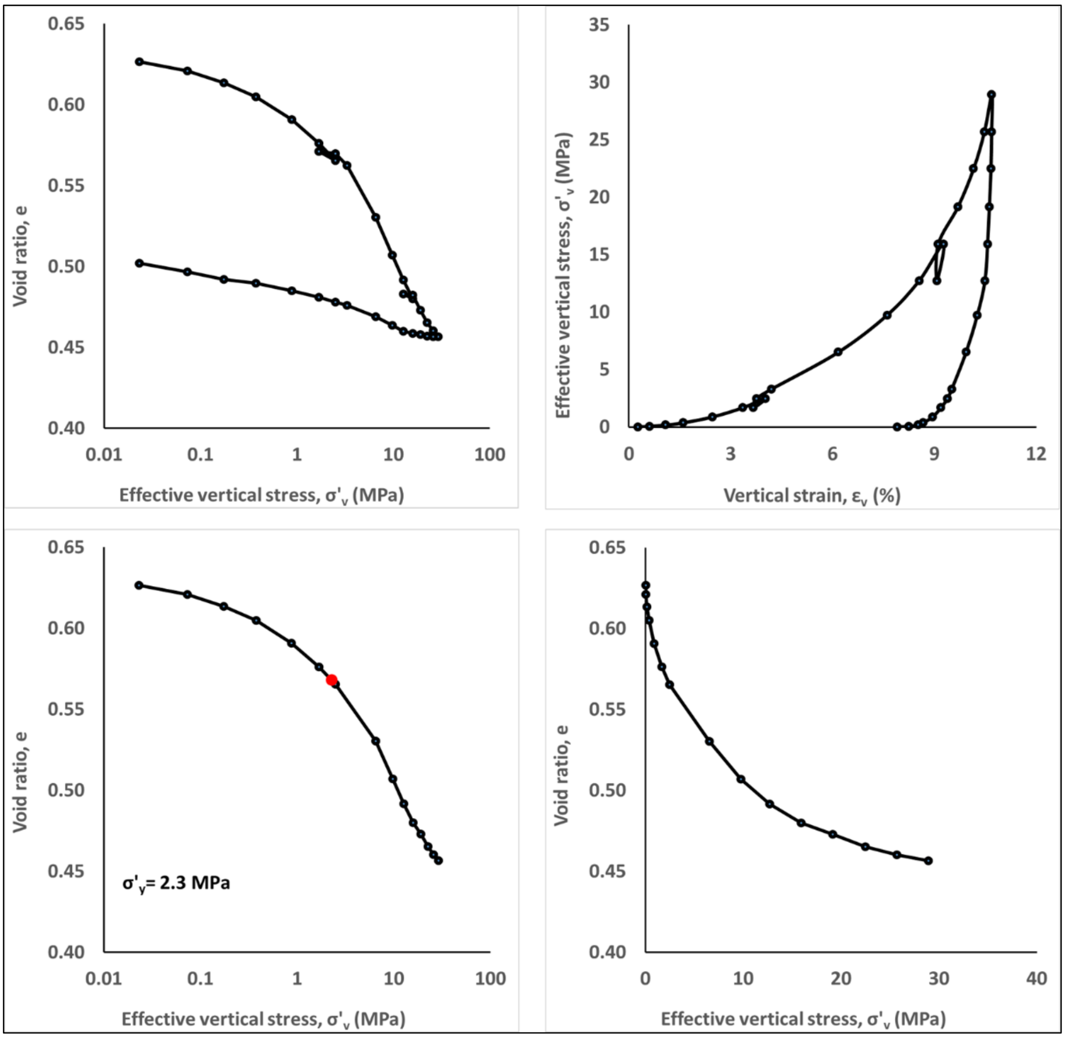

Figure 4.45. Oedometer test results of 60 % relative density sample

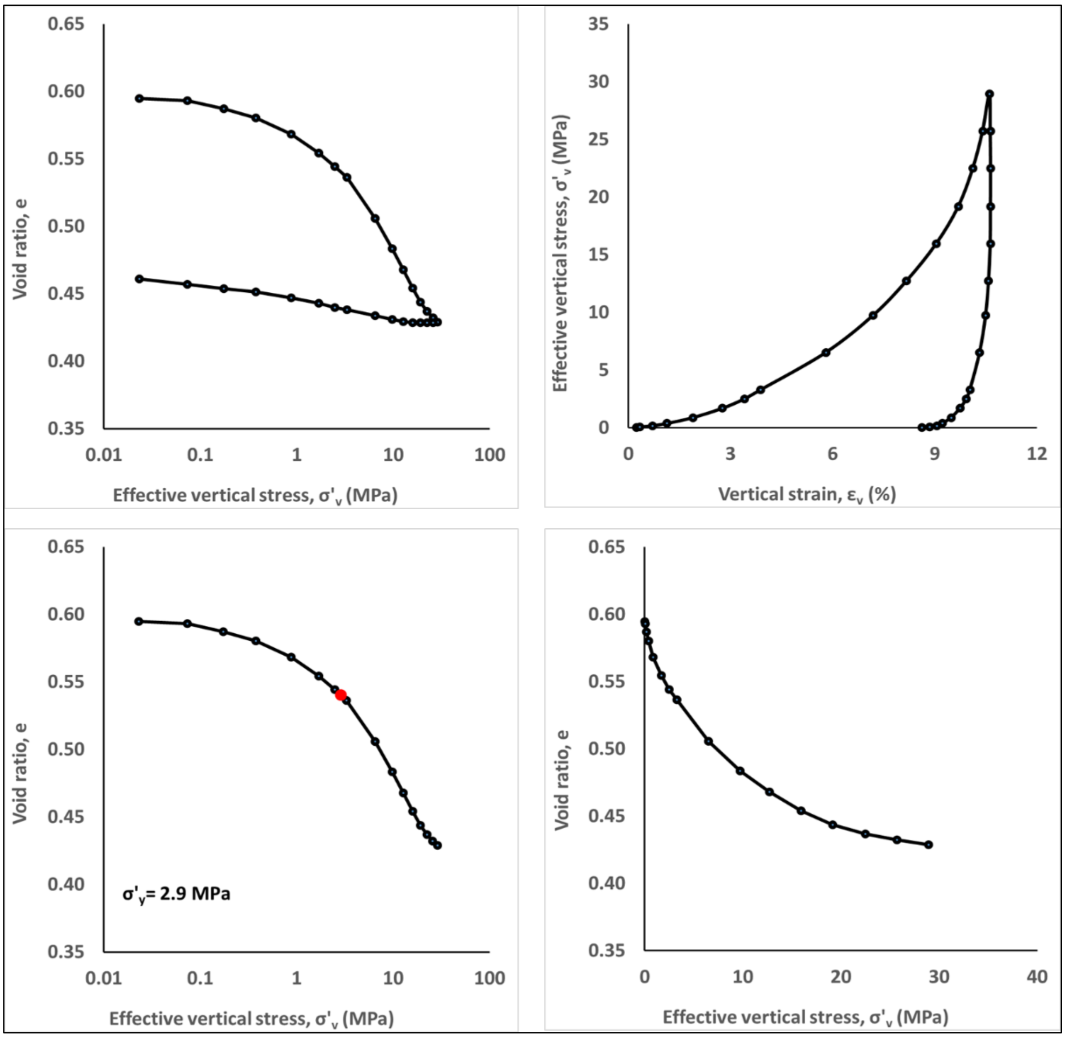

Figure 4.46. Oedometer test results of 70 % relative density sample

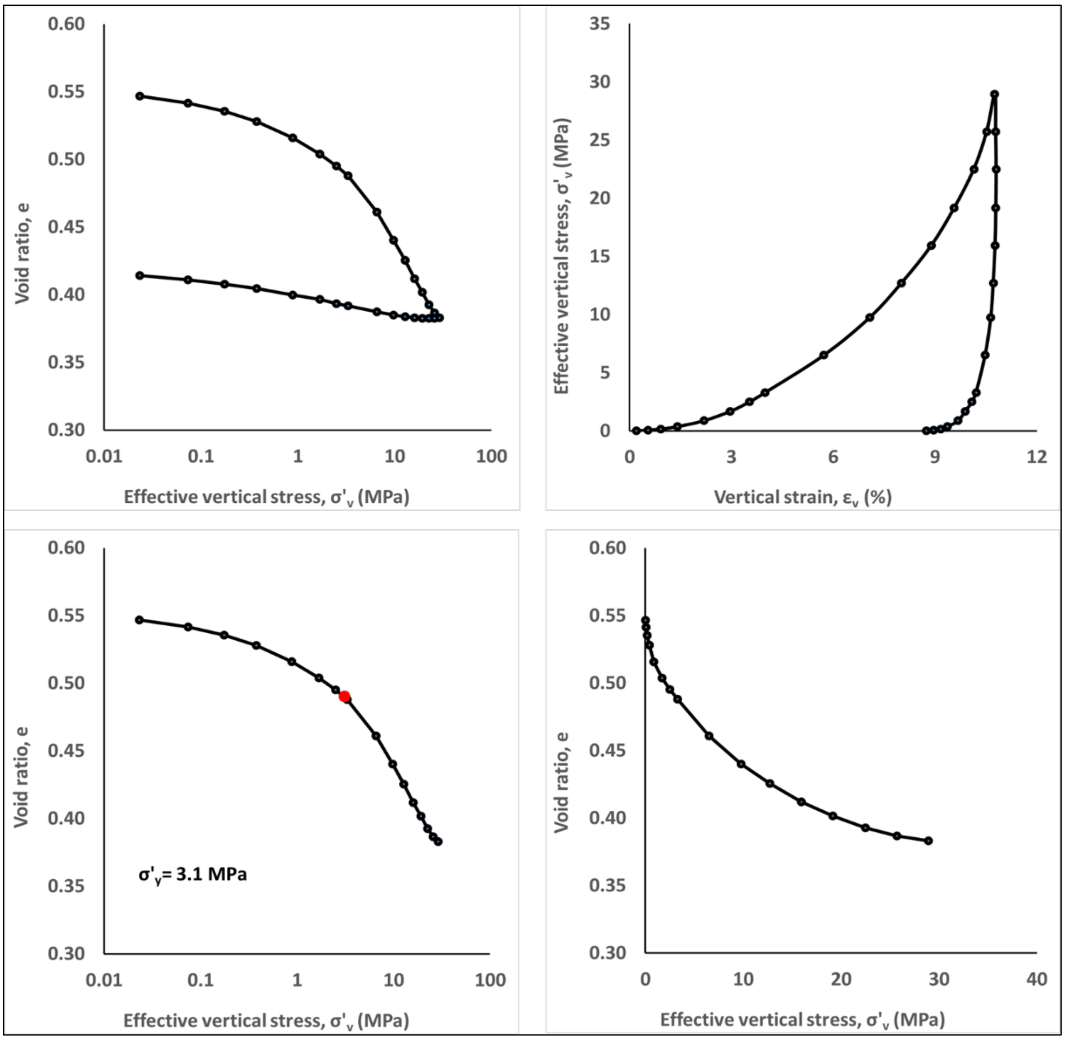

Figure 4.47. Oedometer test results of 85 % relative density sample

4.4 Interpretation of Oedometer Test Results

Six different oedometer tests were performed to understand effect of void ratio on one dimensional compression behavior of Çine sand. In Figure 4.48, effect of void ratio on the yield stress is shown. As can be seen from the Figure, as the initial void ratio decreases, yield stress increases. The yield stresses were defined with respect to maximum curvature of the void ratio-effective vertical stress (in logarithmic scale). The yield stresses change between 1.3 and 3.1 MPa range for 25–85 % relative density samples.

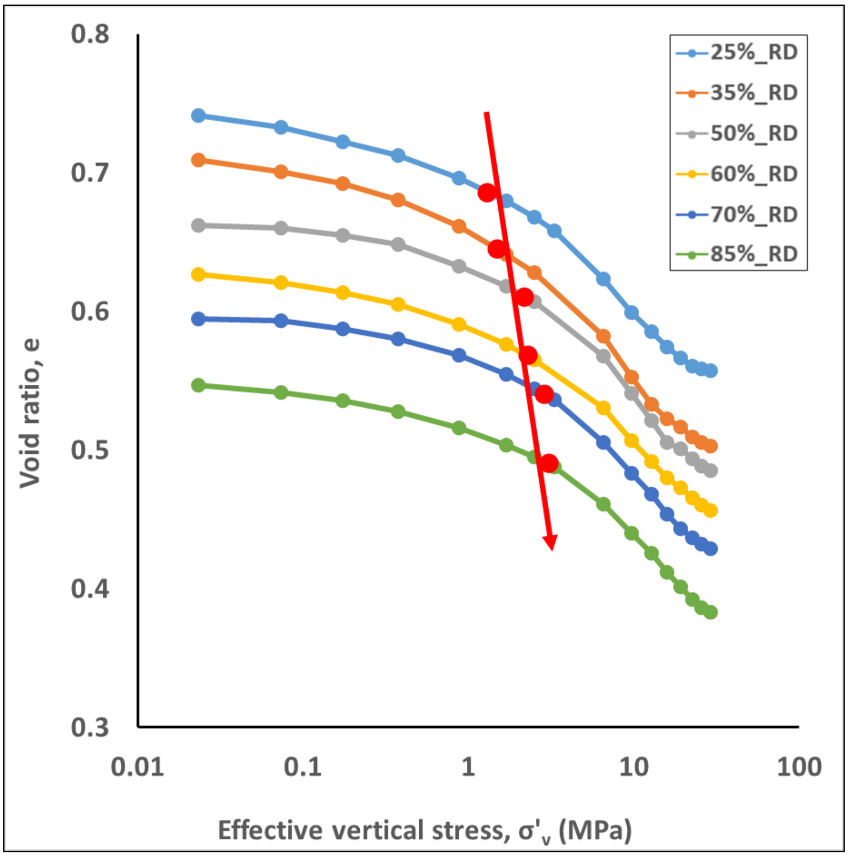

Figure 4.48. Comparison of yield stresses with respect to void ratio

In Figures 4.49 to 4.54, changes in constrained modulus, compression index, and recompression index – compression index ratio with effective vertical stress are shown. Also, the relation between the secondary compression and compression index is shown.

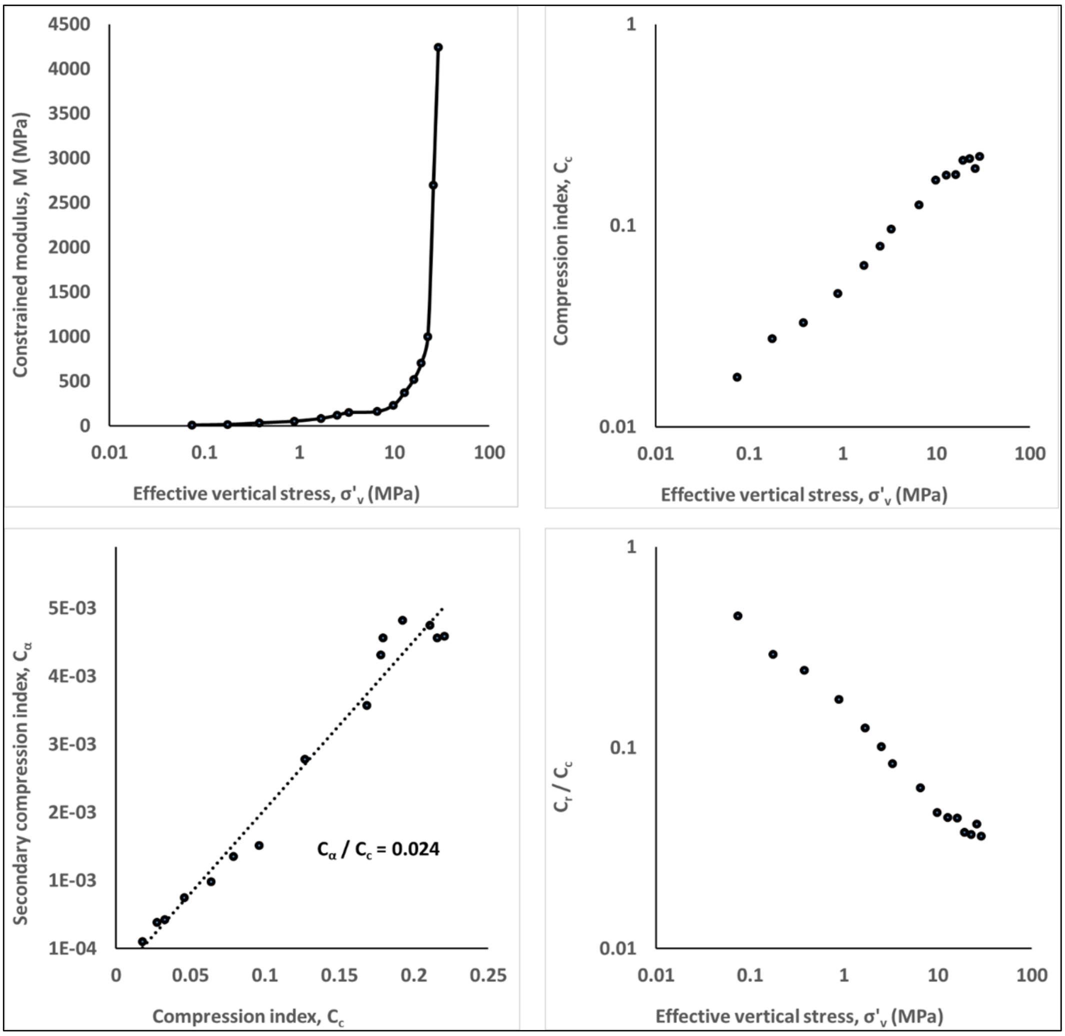

Figure 4.49. Results of 25% relative density sample

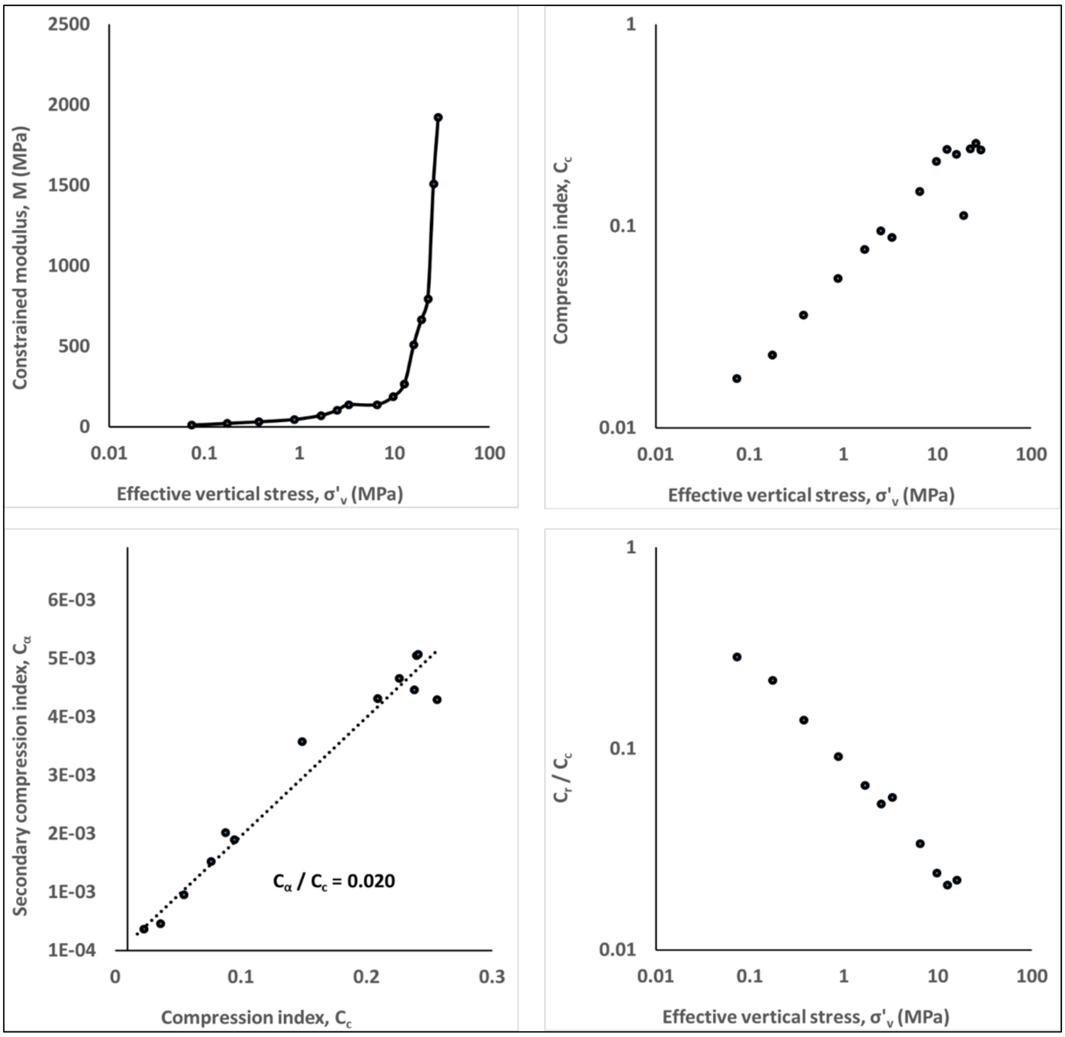

Figure 4.50. Results of 35% relative density sample

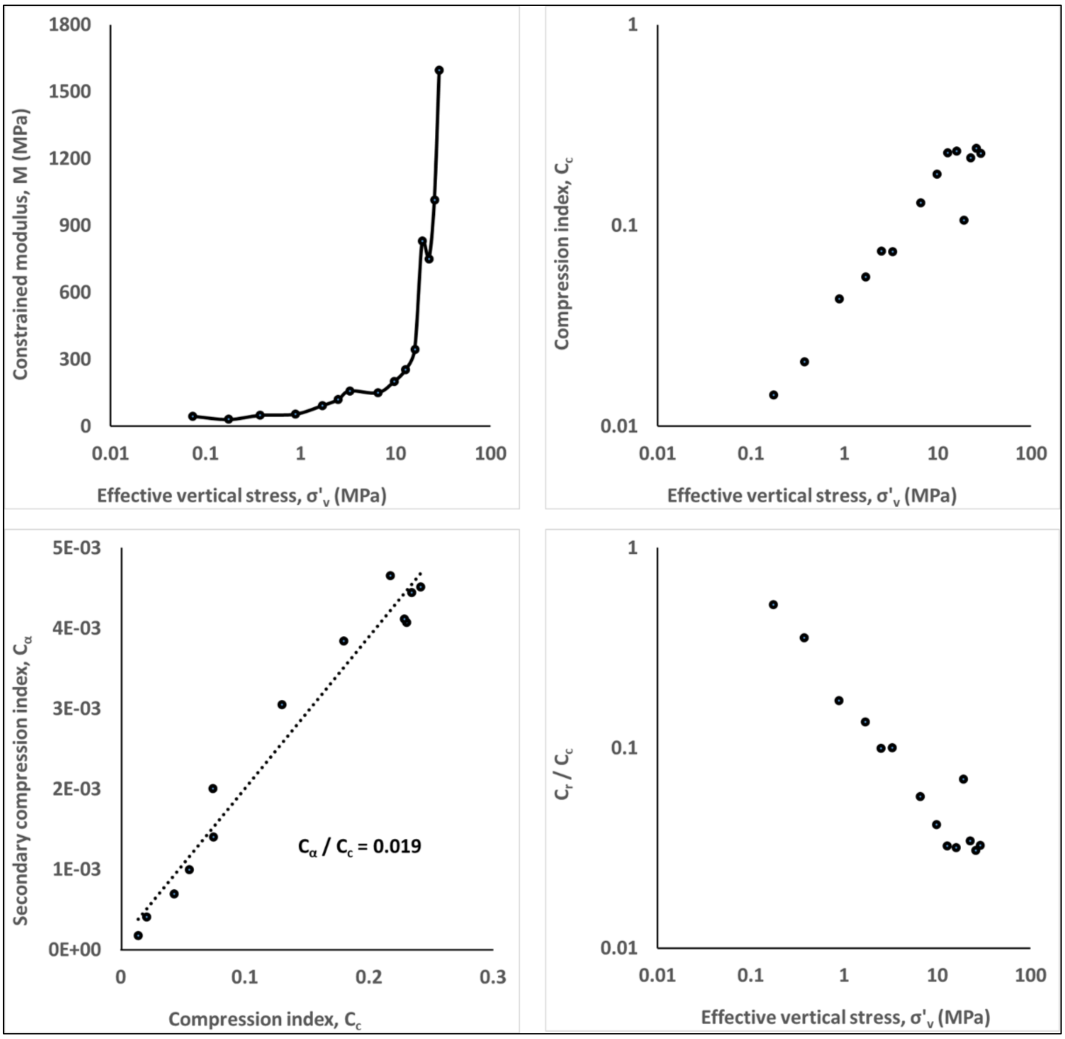

Figure 4.51. Results of 50% relative density sample

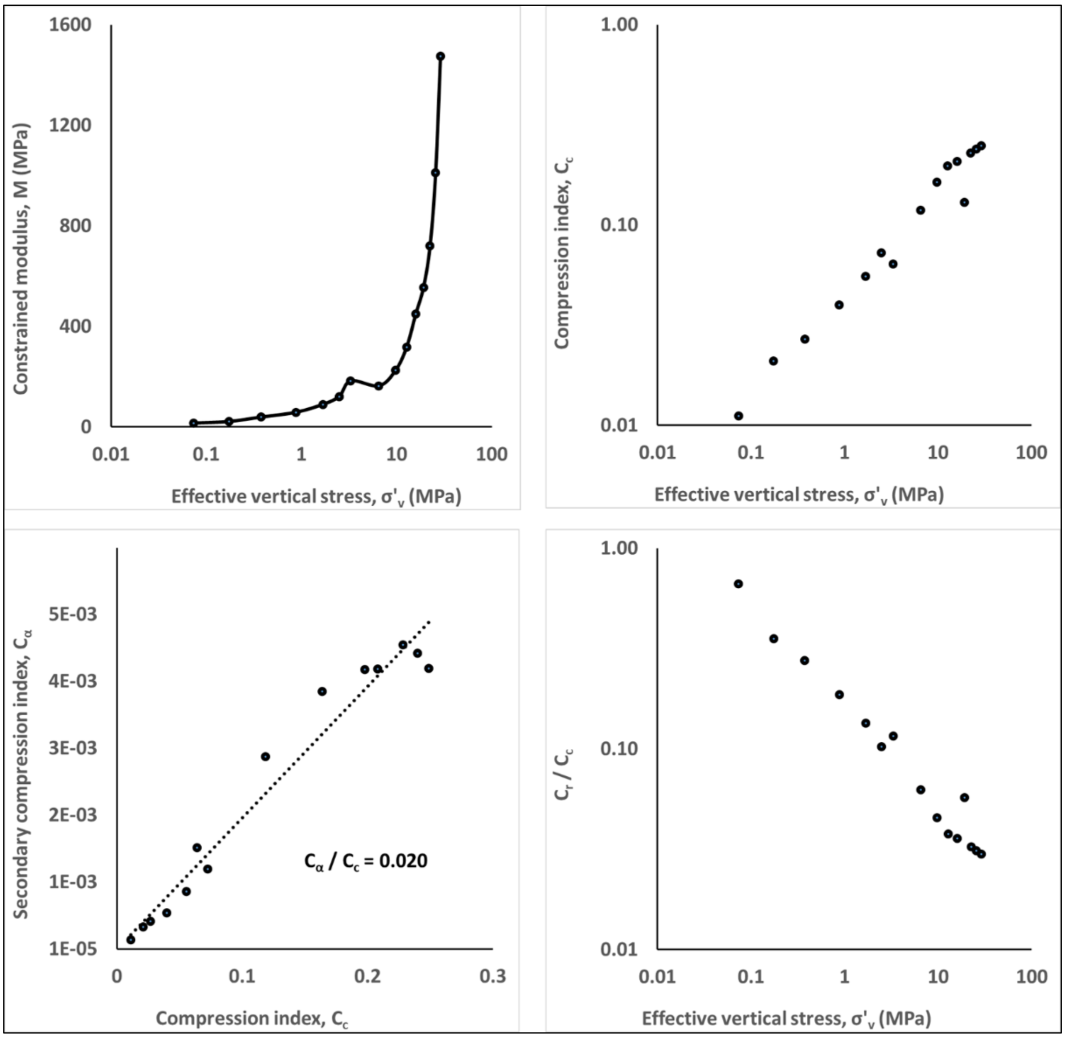

Figure 4.52. Results of 60% relative density sample

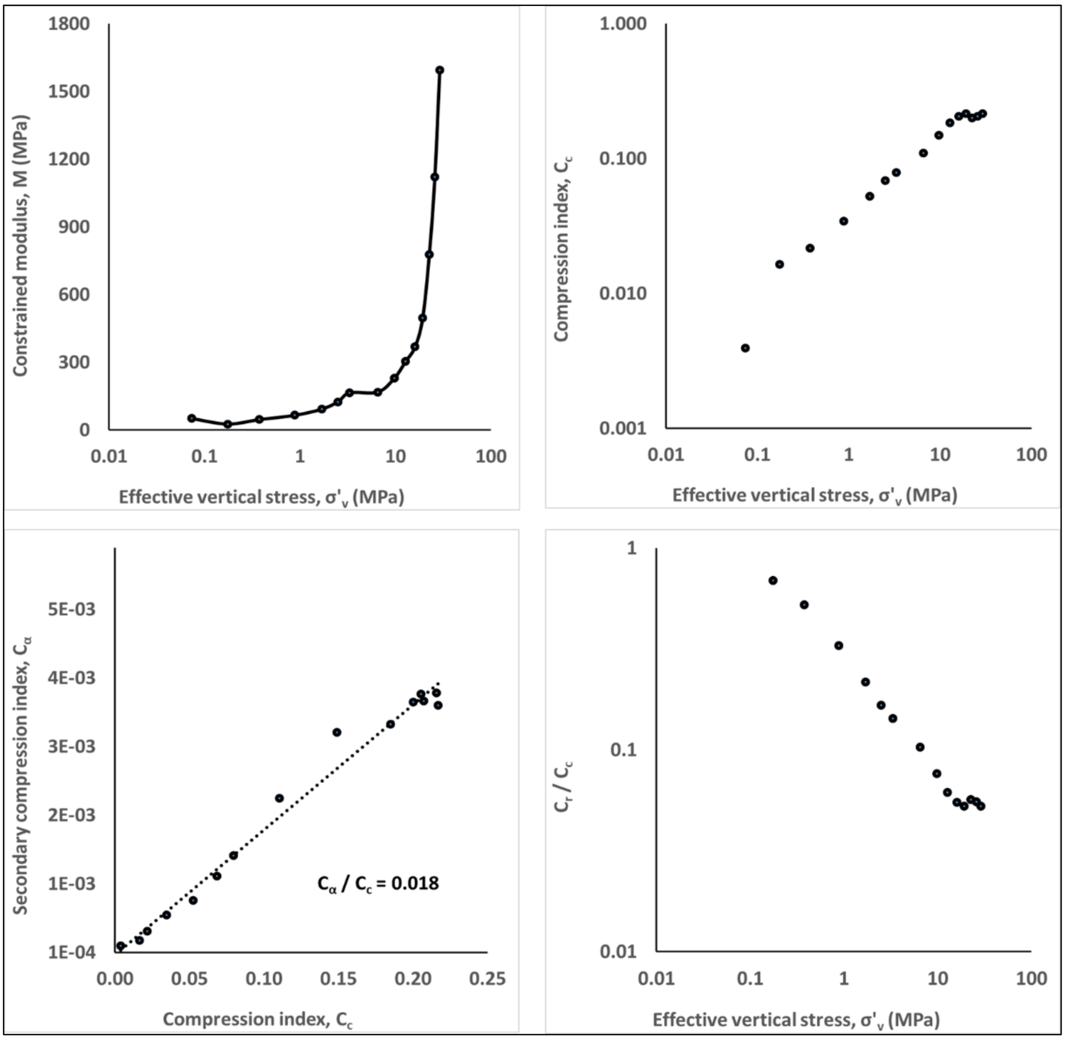

Figure 4.53. Results of 70% relative density sample

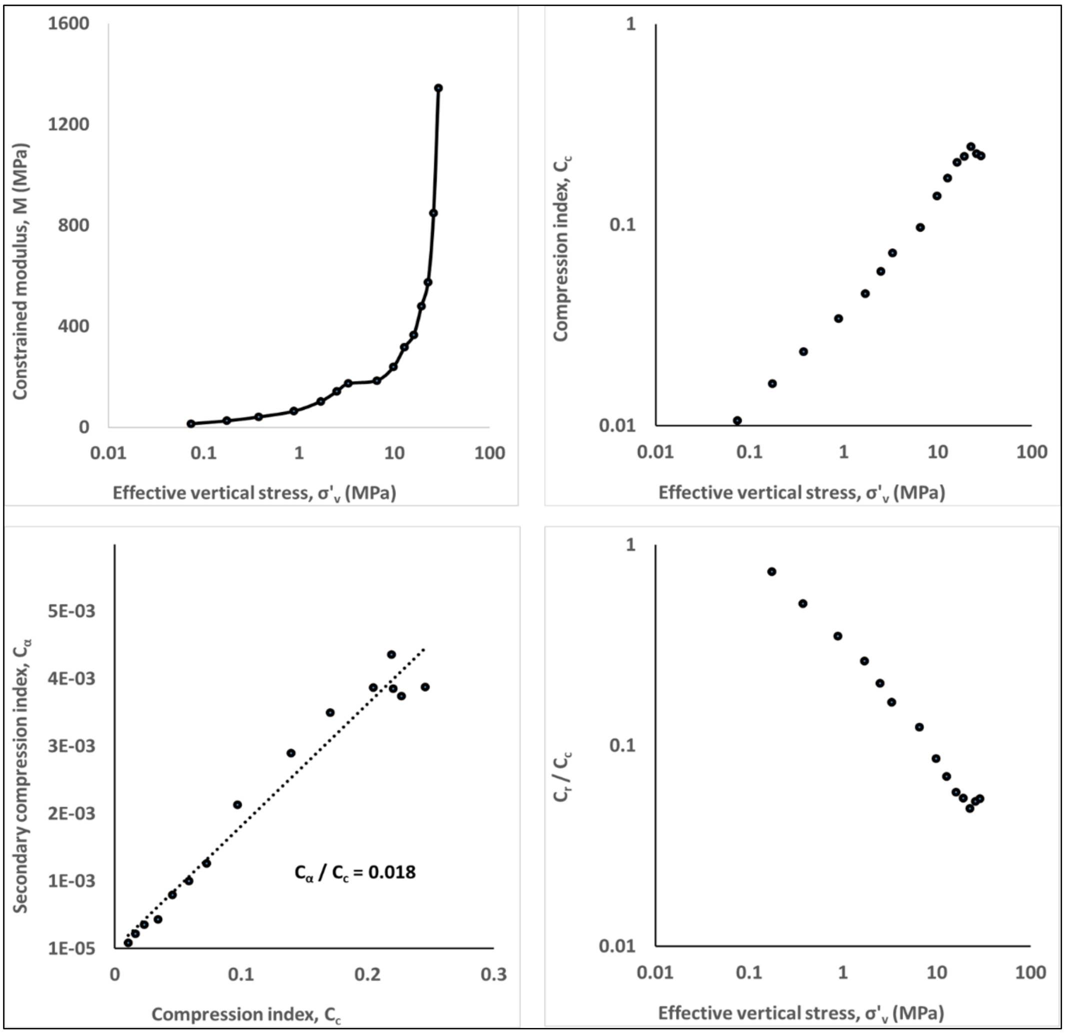

Figure 4.54. Results of 85% relative density sample

Mesri and Vardhanabhuti (2009) compiled the data from literature, and they summarized the primary compression behavior of granular soils under 3 different types: A, B, and C. During primary compression, type A soils show 3 different stages while type B and type C soils show 3 and 1 stage respectively. The properties of these 3 types of soils are shown in Table 4.3.

Table 4.3 Type A, B, and C soil behavior during primary compression

Type A, B, and C behavior during primary compression	**Type A**			**Type B**			**Type C**
	Stage 1	**Stage 2**	**Stage 3**	**Stage 1**	**Stage 2**	**Stage 3**	**Stage 1**
Level I particle damage	+		+	+		+	+
Level II particle damage	+		+	+		+	+
Level III particle damage		+	+		+	+	+
Locking - Unlocking equilibrium	L > UL	UL > L	L > UL	L > UL	UL ≈ L	L > UL	L > UL
Constrained Stiffness (M) change with increasing effective stress	Increases	Decreases	Increases	Increases	Constant	Increases	Increases

Çine sand shows an increase in stiffness in the first stage since locking behavior dominates unlocking behavior. In the second stage, constant stiffness with increasing effective vertical stress is observed due to equilibrium in locking and unlocking behavior. In the final stage, Çine sand starts to show an increase in stiffness again with locking behavior dominance. Therefore, according to Mesri and Vardhanabhuti's (2009) classification, Çine sand shows similar behavior with type B soil.

From test results, it can be seen that C_α / C_c ratio changes between 0.024 and 0.018. As the initial void ratio decreases, the C_α / C_c ratio also decreases. It is also shown in the Figures that as the vertical stress increases, the C_c value also increases. Towards to end of the experiments, C_c value tends to stay constant or decrease with increasing effective stress.

CHAPTER 5

CONSTITUTIVE MODELING PARAMETERS FOR ÇİNE SAND

When a system is designed or analyzed in engineering works, the system should first be modeled. In geotechnical engineering, there are several constitutive models that model soils responses with a certain accuracy. Since soils are very heterogeneous, it is impossible to model soils with 100 % accuracy. Besides, the data obtained with soil investigations are limited for geotechnical projects. Therefore, occasionally soil behavior must be predicted with limited data.

On the basis of the results of the experimental studies conducted within this research's scope, linear elastic perfectly plastic and nonlinear elastic perfectly plastic soil models will be constituted, and the parameters belonging to the models will be determined. With triaxial test results, it will be tried to find the most realistic model parameters by using available data. Comparison of models with actual behavior will also be shown.

5.1 Linear Elastic Perfectly Plastic Model

In the linear elastic perfectly plastic model, it is considered that soils behave linear elastic until failure, and after failure, soils behave perfectly plastic, as shown in Figure 5.1. Since soils have a very heterogeneous structure, they never show a linear elastic and perfectly plastic behavior in reality, as compared to this model. However, its use could be ideal for preliminary assessments. In this model, the linear part is based on Hooke's law of linear elasticity, and failure stress is defined with the Mohr-Coulomb failure criterion. Therefore the correct designation of the model is the linear elastic perfectly plastic model with Mohr-Coulomb failure criterion.

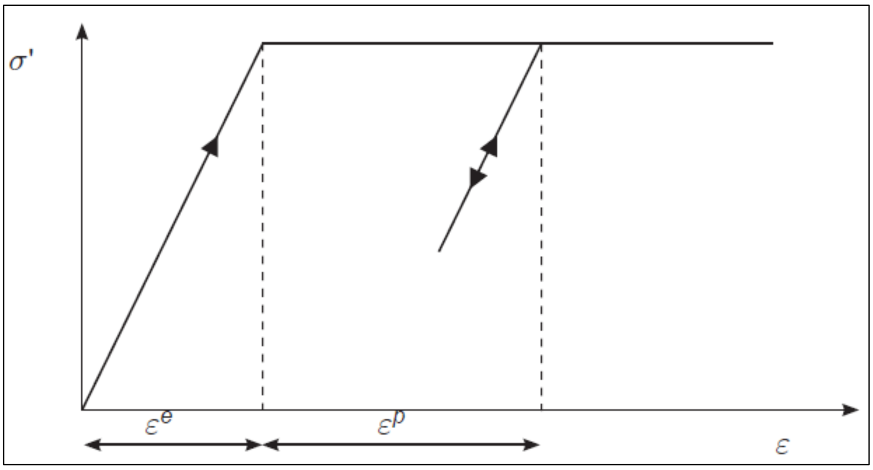

Figure 5.1. Linear elastic perfectly plastic model

Within this research scope, the linear part of the linear elastic perfectly plastic soil model was created by extending the stress-strain graphs' initial linear part to failure stress. Failure stresses were found by the obliquity concept for samples showing strain hardening response and by maximum deviatoric stress for samples that show strain-softening response. Strains formed in the linear part are considered recoverable. In the plastic part, strain increases under constant deviatoric stress (failure stress), and these strains are considered nonrecoverable. The plastic part is modeled according to the Mohr-Coulomb failure criterion, as shown in the equation below.

$$F(\sigma) = \frac{\sigma_1 - \sigma_3}{2} - \frac{\sigma_1 + \sigma_3}{2} \times \sin\varphi - \frac{2c\cos\varphi}{2} \qquad \text{Eqn. 5.1}$$

In Figure 5.2 to 5.6, linear elastic perfectly plastic models constituted with triaxial test results are shown. Blue dots show real behavior while black lines show linear elastic perfectly plastic model.

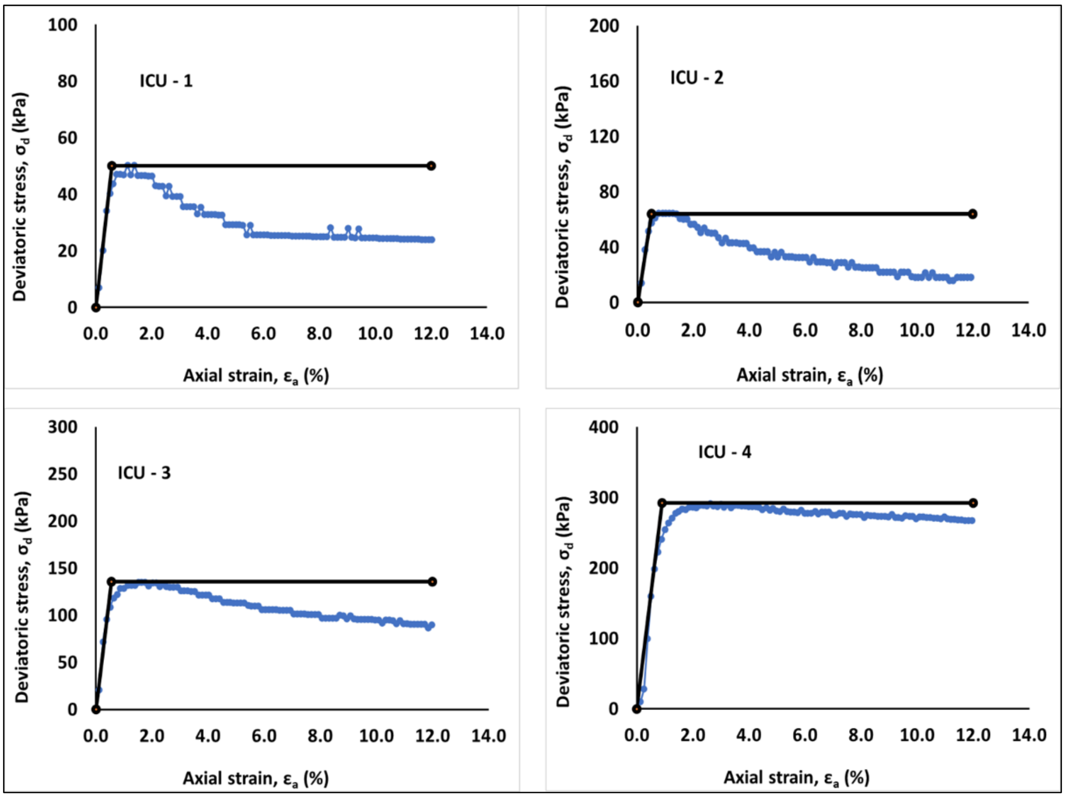

Figure 5.2. Comparison of true Çine sand behavior (21 – 26 % relative density samples) and linear elastic perfectly plastic model with Mohr-Coulomb failure criterion

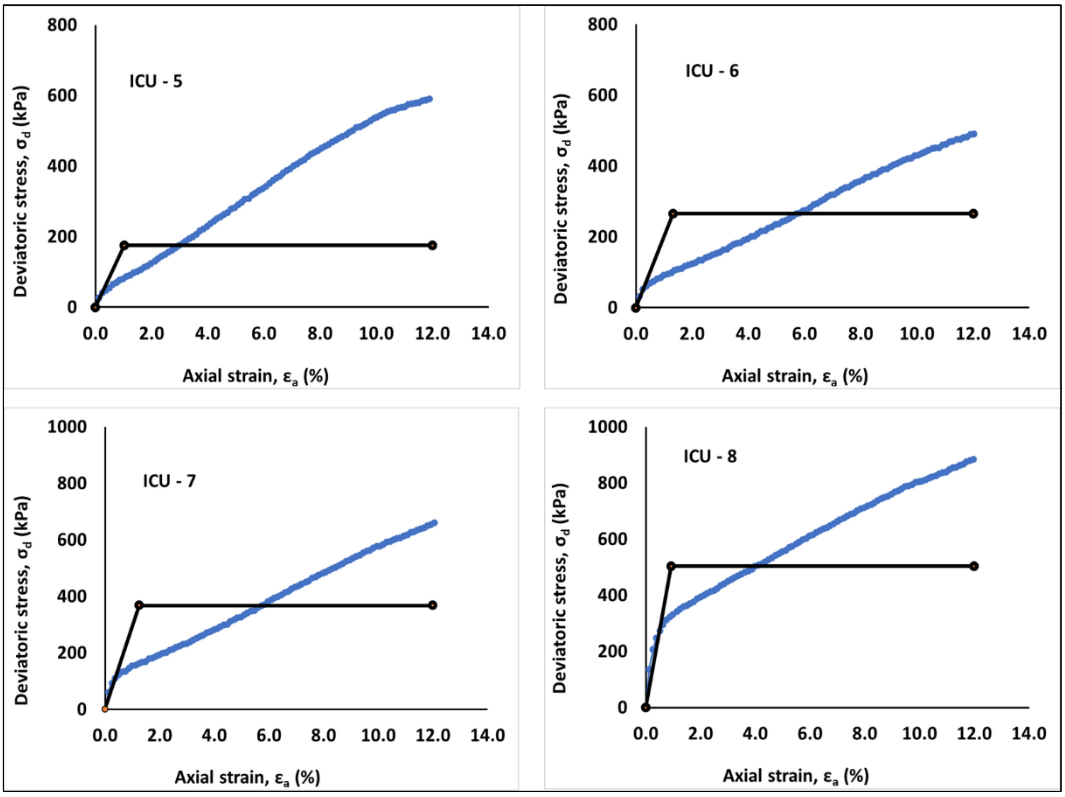

Figure 5.3. Comparison of true Çine sand behavior (47 % relative density samples) and linear elastic perfectly plastic model with Mohr-Coulomb failure criterion

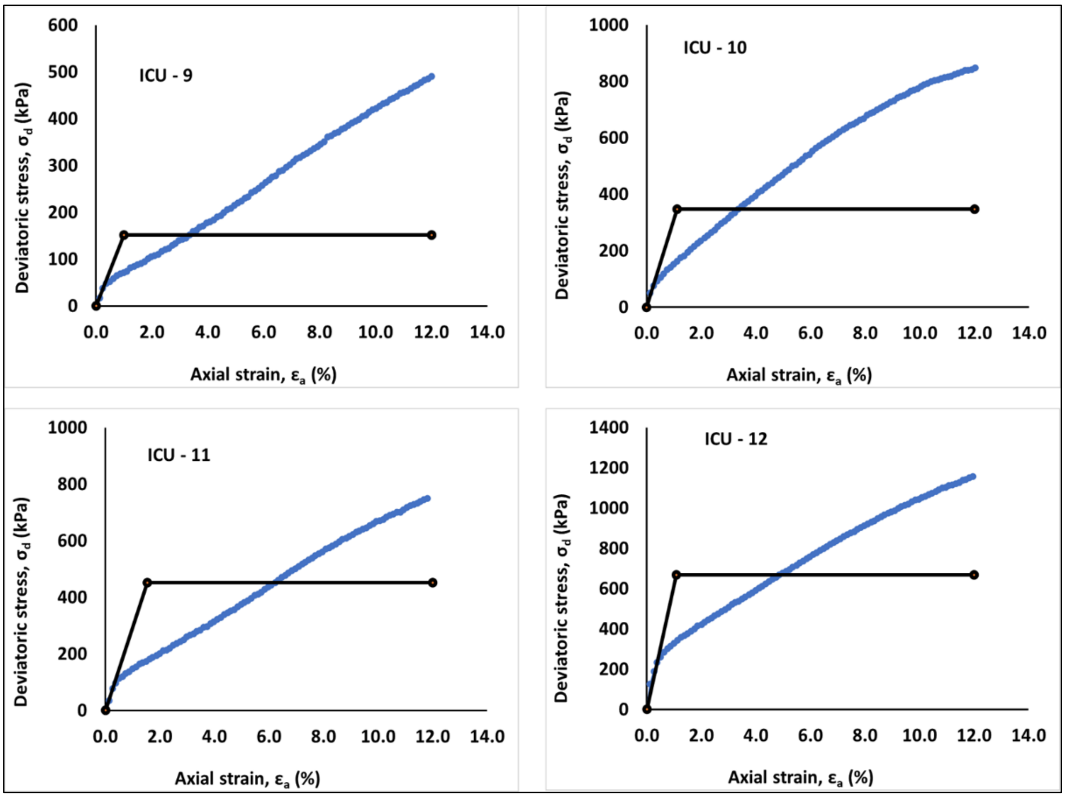

Figure 5.4. Comparison of true Çine sand behavior (60 % relative density samples) and linear elastic perfectly plastic model with Mohr-Coulomb failure criterion

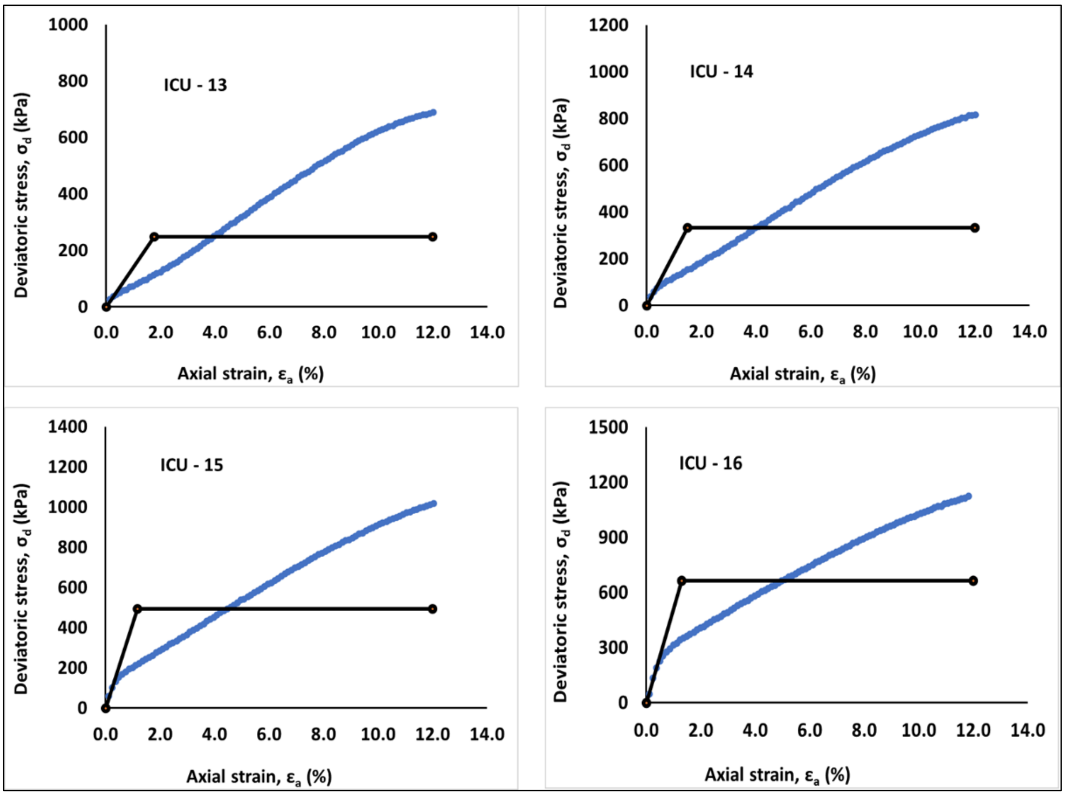

Figure 5.5. Comparison of true Çine sand behavior (70 % relative density samples) and linear elastic perfectly plastic model with Mohr-Coulomb failure criterion

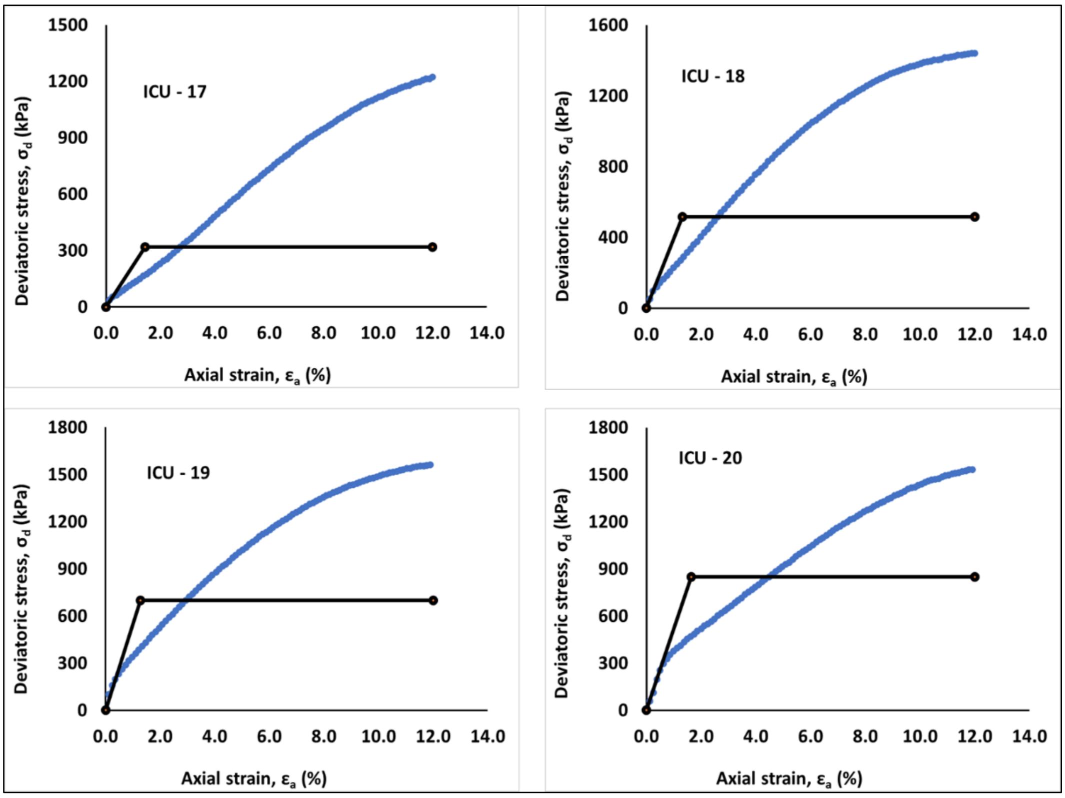

Figure 5.6. Comparison of true Çine sand behavior (83 - 88 % relative density samples) and linear elastic perfectly plastic model with Mohr-Coulomb failure criterion

As shown from Figures, the linear elastic perfectly plastic model with the Mohr-Coulomb failure criterion is not a suitable model type that reflects soil's true behavior. For samples that show strain-softening or hardening responses, the model accuracy is poor. Since the model does not take into consideration of strain hardening, it is a conservatively biased for strain hardening sois. The opposite is true for strain softening soil samples.

There are five parameters for the linear elastic perfectly plastic model with Mohr-Coulomb failure criterion. 2 parameters (E_{trx} and υ) for the elastic part and three parameters (φ, c, and ψ) for the plastic part. Explanation of parameters and their values from each test are tabulated in Table 5.1.

Table 5.1 Linear elastic perfectly plastic model with Mohr-Coulomb failure criterion parameters from test results

Test ID	D_R (%)	σ'_c (kPa)	E_{trx} (MPa)	ϕ' (°)
ICU-1	21	50	9	27.2
ICU-2	24	100	13.4	20.5
ICU-3	21	200	25	24.2
ICU-4	26	400	32	27.8
ICU-5	47	50	17.1	36.6
ICU-6	47	100	20	33.7
ICU-7	47	200	29.5	33.7
ICU-8	47	400	54.8	35.2
ICU-9	60	50	15.4	36.6
ICU-10	60	100	31.3	35.9
ICU-11	60	200	29.6	33.7
ICU-12	60	400	61.3	34.4
ICU-13	70	50	14.2	35.9
ICU-14	70	100	22.3	35.3
ICU-15	70	200	42.5	35.1
ICU-16	70	400	51.1	33.1
ICU-17	84	50	22.1	38.0
ICU-18	88	100	39.6	39.5
ICU-19	84	200	55	37.3
ICU-20	83	400	52.1	35.2

E_{trx}: Elastic modulus from triaxial results. It was found by the initial relatively linear part of the test results.

υ: Poisson’s ratio. Since there is no volume change in undrained tests, it is taken as 0.5.

φ': Effective friction angle.

c: Cohesion, which is zero for clean Çine sand.

ψ: Dilatancy angle. Since there is no volume change in undrained tests, it is taken as zero.

Since initial tangent modulus, E_i, and strength parameter angle of friction, φ is stress-dependent, it is also possible to standardize these parameters under the same void ratio conditions. To standardize E_i, Janbu (1963) suggests a formulation that represents the change of E_i with confining pressure.

$$E_i = K \times P_a \left(\frac{\sigma_3}{P_a}\right)^n \qquad \text{Eqn. 5.2}$$

K: modulus number

n: modulus exponent

P_a: atmospheric pressure

Different consolidation pressures are used on the same relative density samples to determine K and n. E_i values are determined for each test. Then (E_i / P_a) and (σ_3 / P_a) values are plotted on a log-log scale. Then K and n values are calculated as shown in Figure 5.7, which shows the results of Oroville Dam shell material (Wong & Duncan 1970).

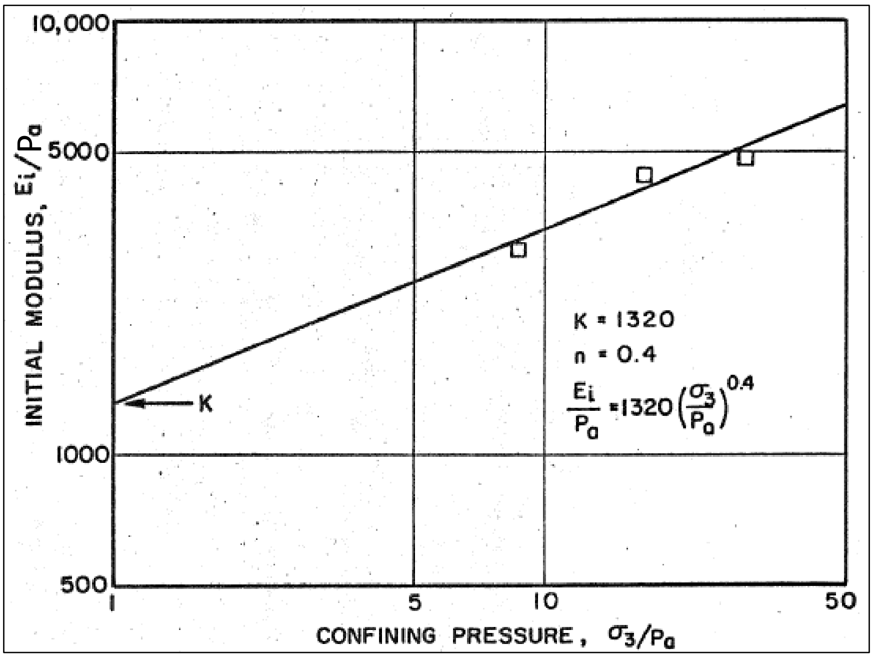

Figure 5.7. Determination of K and n parameters for Oroville Dam shell material (Wong & Duncan 1970)

K is the value of E_i when σ_3 is equal to atmospheric pressure. n is calculated from the graph or by the following formula:

$$n = \frac{\Delta log(E_i/P_a)}{\Delta log(\sigma_3/P_a)} \qquad \text{Eqn. 5.3}$$

For each relative density, K and n values were found, as shown in Table 5.2

Table 5.2 K and n values of Çine sand for different relative densities

D_R (%)	**K**	**n**
21-26	141	0.6
47	224	0.6
60	250	0.6
70	230	0.6
83-88	364	0.7

The angle of friction, φ is stress dependent. As the confining pressure increases, the angle of friction decreases for the same void ratio. The following formula is used to standardize this parameter, as Wong & Duncan (1970) stated.

$$\varphi = \varphi_0 - \Delta\varphi log_{10}\left(\frac{\sigma_3}{P_a}\right) \qquad \text{Eqn. 5.4}$$

φ_0 = angle of friction when confining pressure is equal to atmospheric pressure

Δφ = change in the angle of friction because of change in confining pressure

For each relative density, ranges of φ_0 and Δφ parameters were defined in Table 5.3.

Table 5.3 φ_0 and Δφ parameters for Çine sand

D_R (%)	**φ_0 (°)**	**Δφ (°)**
21-26	24-26	3−4
47	33-35	3−4
60	34-36	2−3
70	35-37	2−3
83-88	37-39	3−4

5.2 Nonlinear Elastic Perfectly Plastic Model

Nonlinear elastic perfectly plastic model or hyperbolic stress-strain relationship approximate soil behavior more accurately than linear elastic perfectly plastic soil models. The nonlinear elastic perfectly plastic soil model considers strain hardening behavior up to a certain level. Kondner (1963) and Kondner & Zelasko (1963) stated that the hyperbolic stress-strain relationship in Figure 5.8 reasonably reflects a general soil behavior.

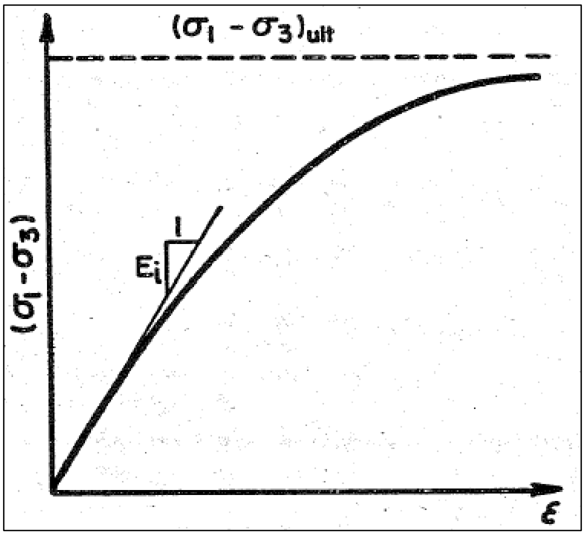

Figure 5.8. Hyperbolic stress-strain relationship of soils

In this hyperbolic stress-strain behavior, Ei is the initial slope of the real stress-strain curve. $(\sigma_1 - \sigma_3)_{ult}$ is the asymptotic value of stress difference. Owing to ease of defining the parameters from real test data, the hyperbolic stress-strain relationship is widely and conveniently used. The formulation of this hyperbolic behavior is shown below:

$$(\sigma_1 - \sigma_3) = \frac{\varepsilon}{\frac{1}{E_i} + \frac{\varepsilon}{(\sigma_1 - \sigma_3)_{ult}}} \qquad \text{Eqn. 5.5}$$

E_i was estimated by taking the initial linear part of stress-strain test data, and the value of it for each test was determined previously. $(\sigma_1 - \sigma_3)_{ult}$ is the asymptotic value of stress difference. Wong & Duncan (1970) determine the asymptotic value of stress difference as the following formula.

$$(\sigma_1 - \sigma_3)_f = R_f(\sigma_1 - \sigma_3)_{ult} \qquad \text{Eqn. 5.6}$$

R_f: failure ratio

Wong & Duncan (1970) state that R_f changes between 0.5 and 0.9 for most soils. R_f was taken as 0.7 for modeling Çine sand. Failure stress differences were already determined previously. As a result of determining $(\sigma_1 - \sigma_3)_{ult}$ and E_i values, nonlinear elastic perfectly plastic models for each test are shown in Figures 5.9 to 5.13. Blue lines show true Çine sand behavior while black curves show nonlinear elastic perfectly plastic model.

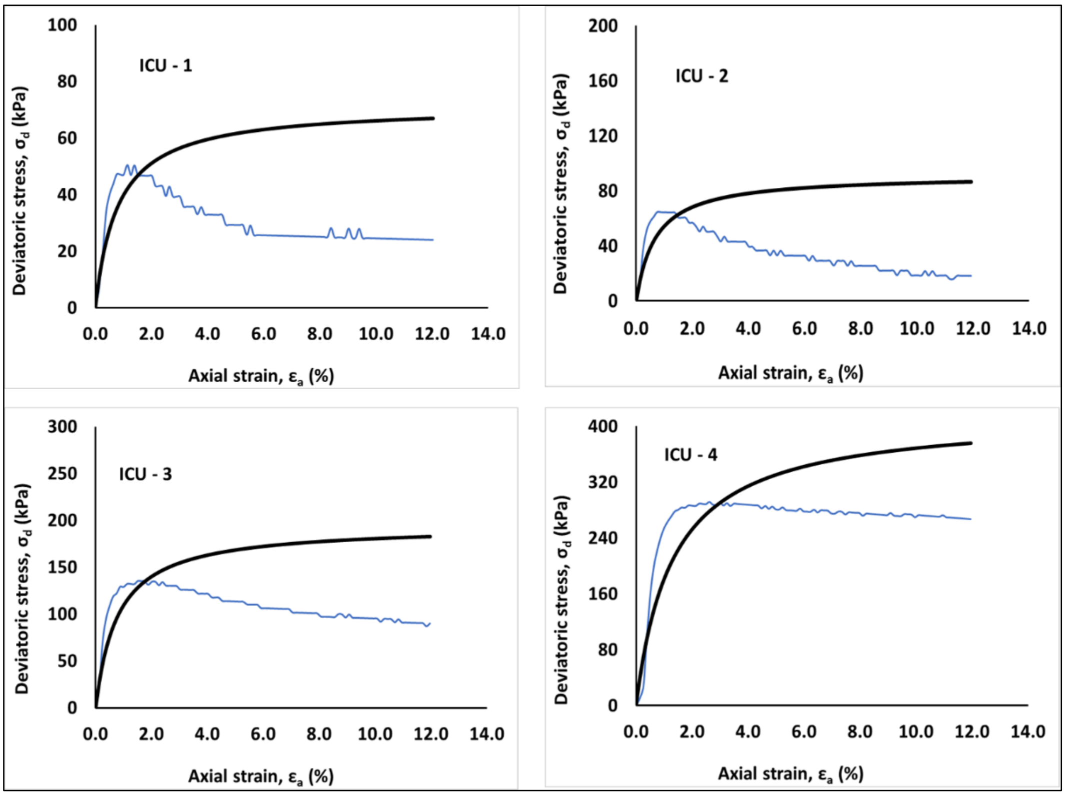

Figure 5.9. True Çine sand behavior (21 – 26 % relative density samples) and nonlinear elastic perfectly plastic model

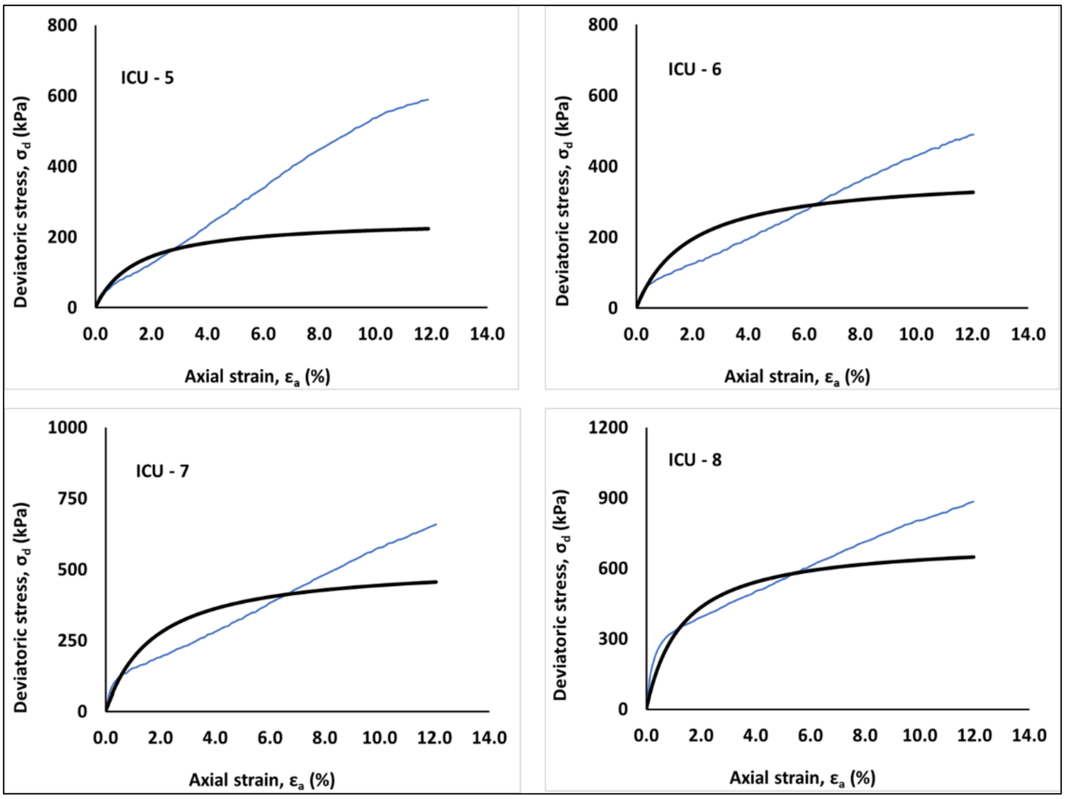

Figure 5.10. True Çine sand behavior (47 % relative density samples) and nonlinear elastic perfectly plastic model

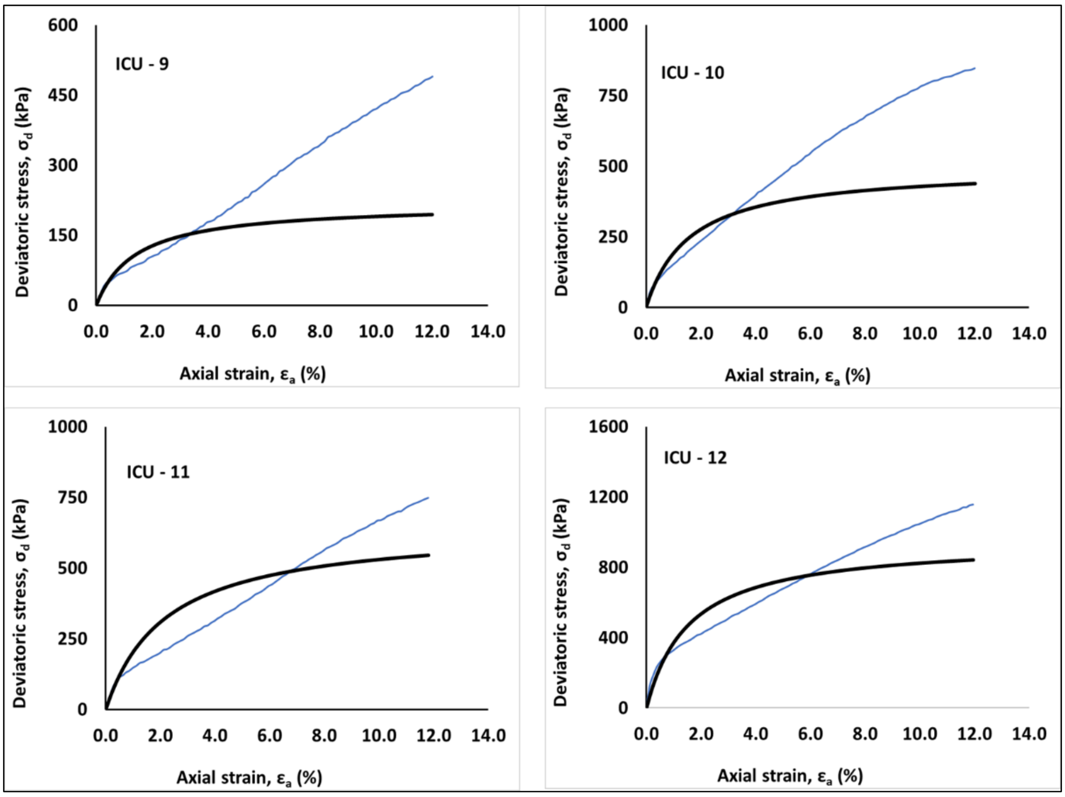

Figure 5.11. True Çine sand behavior (60 % relative density samples) and nonlinear elastic perfectly plastic model

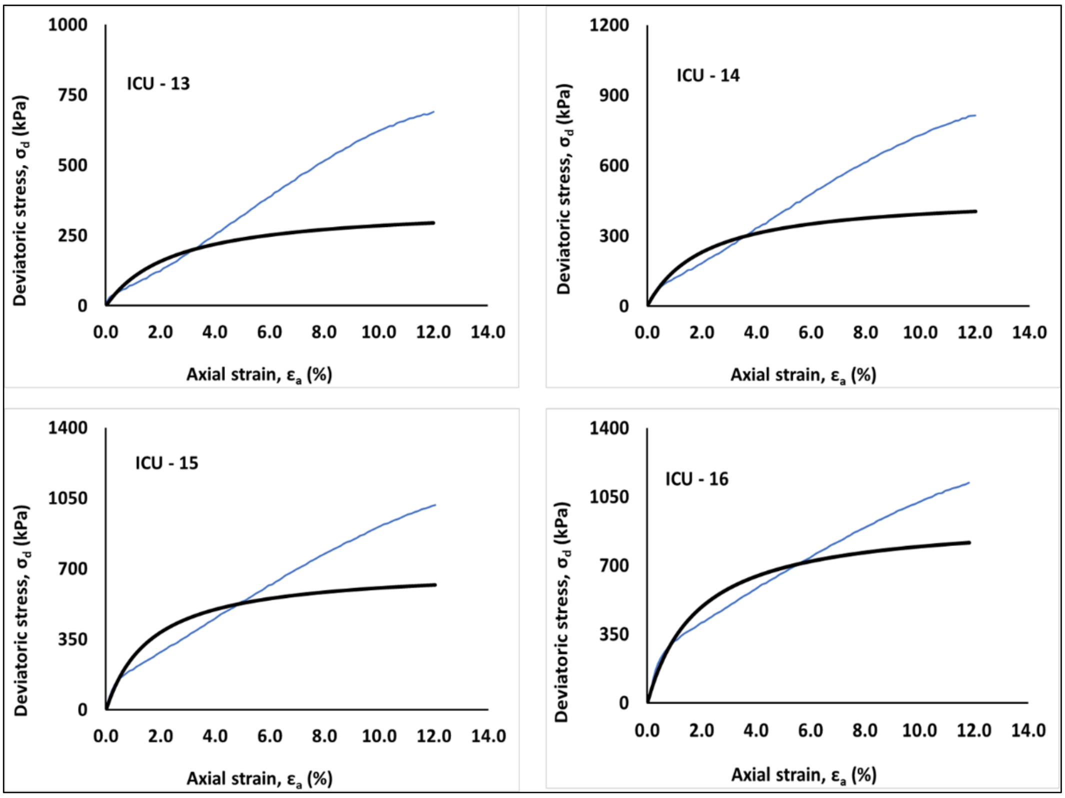

Figure 5.12. True Çine sand behavior (70 % relative density samples) and nonlinear elastic perfectly plastic model

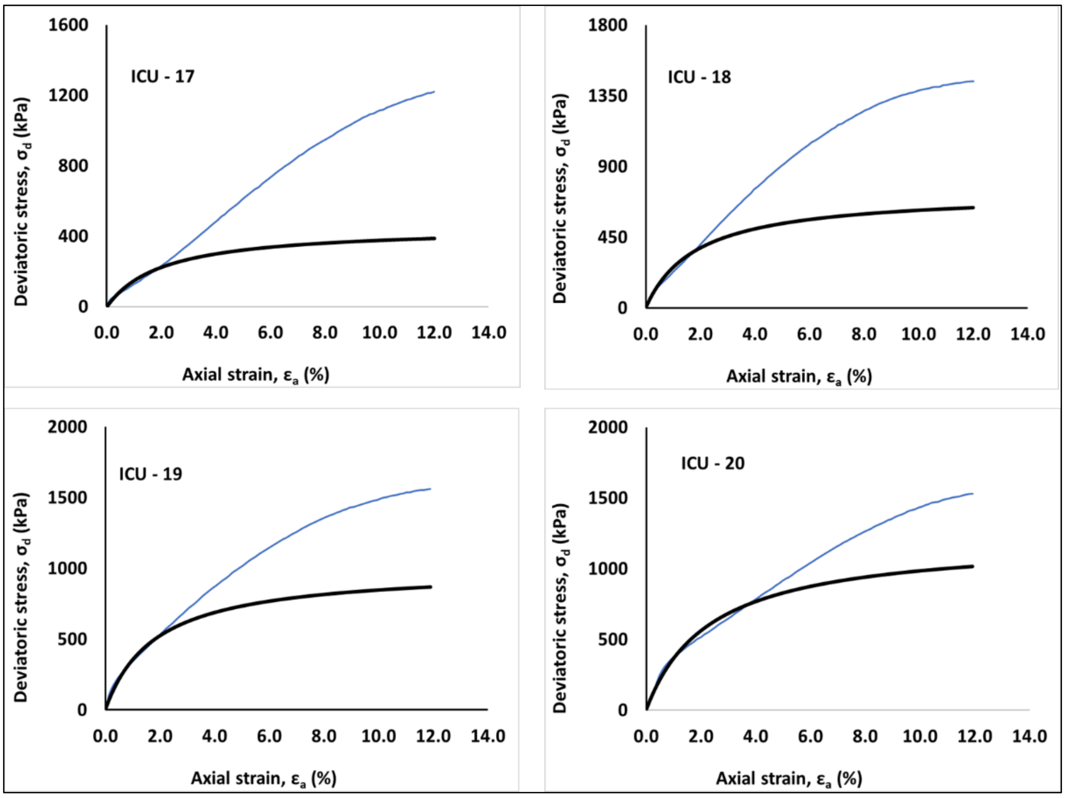

Figure 5.13. True Çine sand behavior (83 - 88 % relative density samples) and nonlinear elastic perfectly plastic model

As shown in the Figures, nonlinear elastic perfectly plastic model accuracy increases as the initial void ratio and consolidation pressure increases. The reason is that model considers the strain hardening behavior of soil up to a certain level. After that level, the model underestimates the strength of the soil. For the loosest set, however, the model overestimates the soil's strength because of the strain-softening behavior of true soil behavior.

There are six parameters for this hyperbolic soil model. These are K, n, c, φ_0, $\Delta\varphi$, and R_f. For different relative densities, all parameters for Çine sand were determined as shown in Table 5.4.

Table 5.4 Hyperbolic soil model parameters of clean Çine sand for different relative densities

D_R (%)	K	n	c (kPa)	φ_0 (°)	$\Delta\varphi$ (°)	R_f
21-26	141	0.6	0	24-26	3−4	0.7
47	224	0.6	0	33-35	3−4	0.7
60	250	0.6	0	34-36	2−3	0.7
70	230	0.6	0	35-37	2−3	0.7
83-88	364	0.7	0	37-39	3−4	0.7

CHAPTER 6

CONCLUSION

Shearing and volumetric straining responses of local, Çine sand, were investigated with the intent to introduce a new "standard sand" to the literature from Turkey. Index, shear strength and stiffness parameters were studied and estimated.

Çine sand was classified as a poorly graded sand (SP) according to USCS, and its specific gravity was estimated as 2.66. Similarly, the minimum and the maximum void ratios were estimated as 0.501 and 0.826, respectively.

20 consolidated undrained triaxial tests were performed to assess shearing response of Çine sand. In these triaxial tests, reconstituted specimens were prepared at 25-47-60-70-85 % relative densities, and consolidated to 50-100-200-400 kPa cell pressures.

6 oedometer tests were performed to examine one-dimensional response of Çine sand. In these tests, reconstituted specimens were prepared at 25-35-50-60-70-85 % relative densities and they were loaded up to an axial stress of ~29 MPa. It was observed that yield stresses of specimens varied in the range of 1.3-3.1 MPa.

Linear elastic and nonlinear elastic-perfectly plastic constitutive modeling parameters were developed based on triaxial test results. Additionally, other constitutive modeling and critical state parameters were determined specifically for Çine sand.

The major findings of this study are listed tables and figures below.

Table 6.1 Index properties of Çine sand

Specific Gravity, G_s	2.66
e_{min}	0.826
e_{max}	0.501
D_{60} (mm)	0.50
D_{30} (mm)	0.26
D_{10} (mm)	0.15
C_u	0.89
C_c	3.30

Table 6.2 Mechanical properties of Çine sand

	~ 25 % RD	**~ 35 % RD**	**~ 47 % RD**	**~ 60 % RD**	**~ 70 % RD**	**~ 85 % RD**
Peak friction angle, φ' (°)	23-27	-	32-36	33-37	34-38	36-39
Yield stress, σ'_y (MPa)	1.3	1.5	2.2	2.3	2.9	3.1
$C_{c,max}$	0.220	0.256	0.242	0.249	0.217	0.246
C_α/C_c	0.024	0.020	0.019	0.020	0.018	0.018

Table 6.3 Nonlinear elastic perfectly plastic model parameters of Çine sand

D_R (%)	K	n	c (kPa)	φ_0 (°)	$\Delta\varphi$ (°)	R_f
21-26	141	0.6	0	24-26	3−4	0.7
47	224	0.6	0	33-35	3−4	0.7
60	250	0.6	0	34-36	2−3	0.7
70	230	0.6	0	35-37	2−3	0.7
83-88	364	0.7	0	37-39	3−4	0.7

Due to the dilative nature of Çine sand under studied stress and density states, perfectly plastic models are judged to be overly conservative to model post failure. Hence, they are not recommended to assess the response of Çine sand in an unbiased manner.

Çine sand shows an increase in stiffness in the first stage since locking behavior dominates unlocking behavior. In the second stage, constant stiffness with increasing effective vertical stress is observed due to equilibrium in locking and unlocking behavior. In the final stage, Çine sand starts to show an increase in stiffness again with locking behavior dominance. Therefore, according to Mesri and Vardhanabhuti's (2009) classification, Çine sand shows similar behavior with type B soil.

Characteristic curves for Çine sand are presented in Figure 6.1.

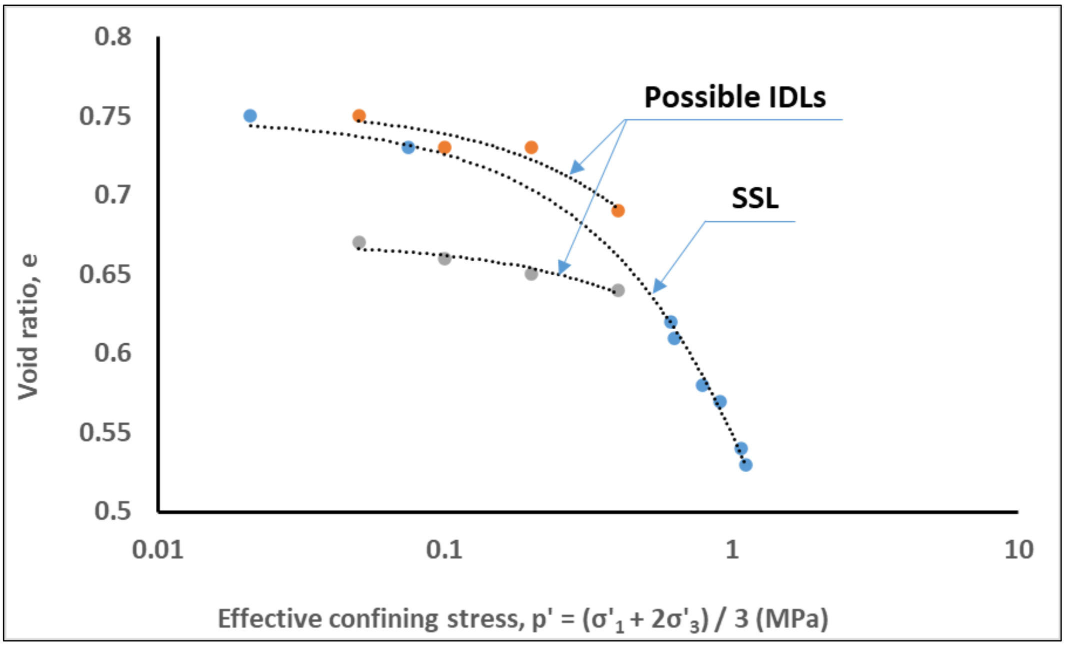

Figure 6.1. Characteristic curves for Çine sand

Isotropic consolidation data which are taken from consolidation stages for each relative density set are shown in the Figure 6.2.

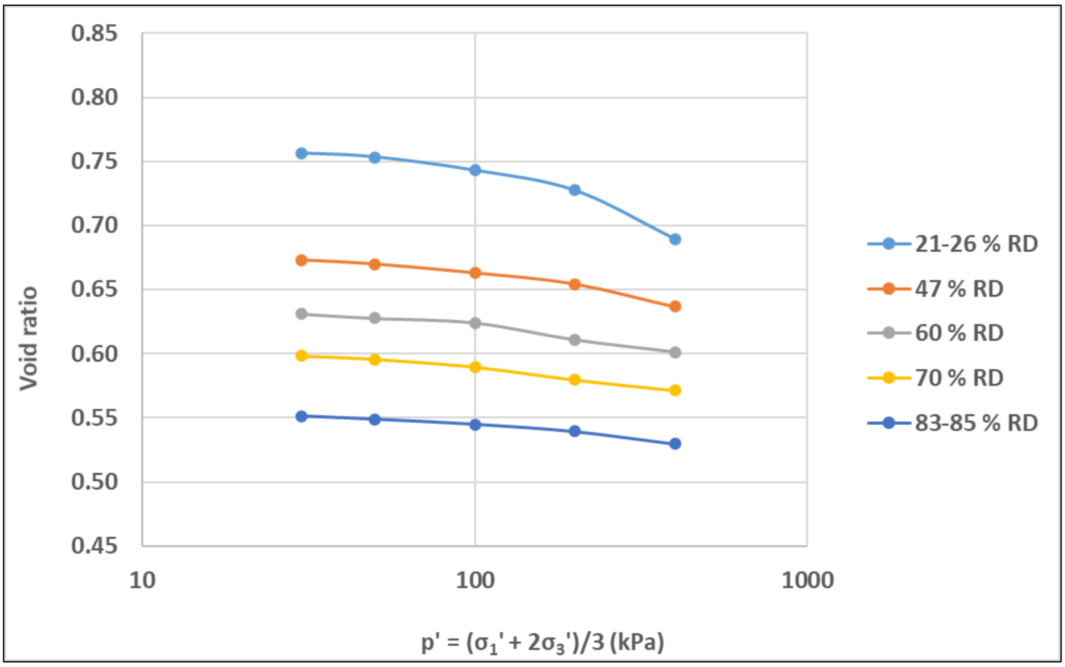

Figure 6.2. Isotropic consolidation data of Çine sand for different relative density

Effective stress friction angle vs. relative density values were compared with the test data presented by Andersen and Schjetne (2013), as shown in Figure 6.3. Triangles represent Çine sand, whereas circles are the data from Andersen and Schjetne (2013).

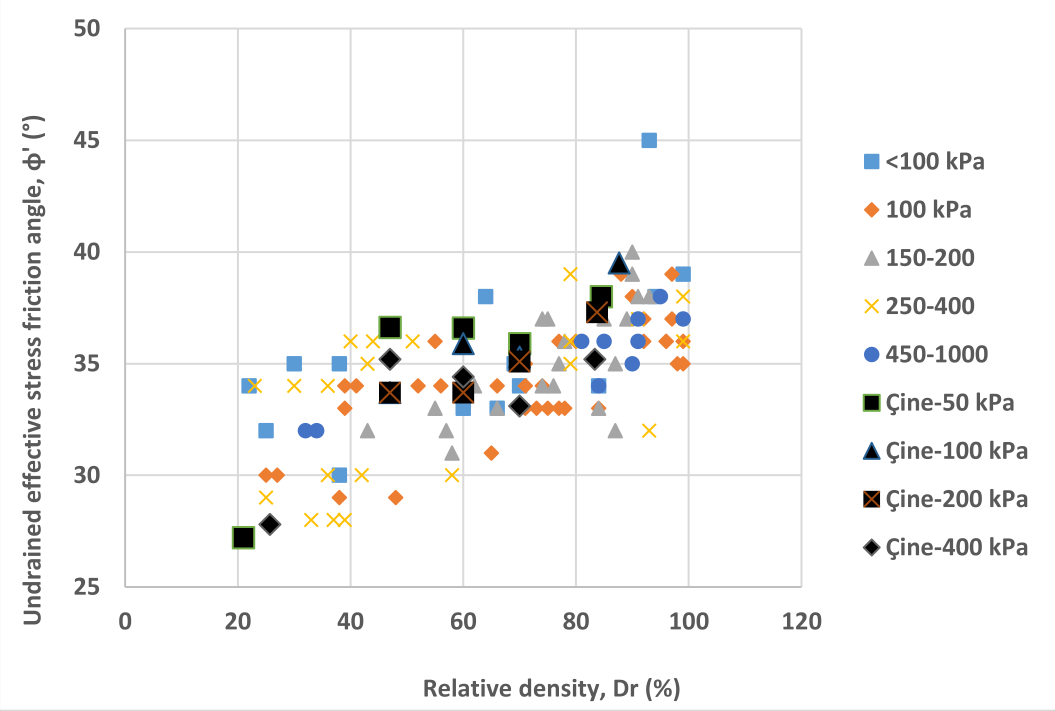

Figure 6.3. Relative density vs. effective stress friction angles adapted from Andersen and Schjetne (2013) as compared with the findings of this study for Çine sand

Future works:

In this study, the conclusions were listed based on consolidated undrained triaxial and one-dimensional oedometer tests, which were loaded up to a maximum stress level of ~29 MPa. Experiments with different failure modes and boundary conditions, using simple shear or torsional shear apparatus, and compression or extension loading schemes are recommended to be performed on Çine sand to test the uniqueness of the parameters presented herein. Additionally, one-dimensional compression tests may be repeated under higher stress levels.

Since Çine sand shows dilative response in dense conditions and under relatively low confining stresses, it hardens with shear straining. Therefore, linear-elastic and nonlinear elastic perfectly plastic models are not adequate to model Çine sand's post failure shearing behavior. Alternatively, strain hardening/softening constitutive models can be considered for an improved modeling of Çine sand's shearing response.

Last but not least, a Çine sand specific constitutive model, addressing particle yielding at larger stress levels for the assessment of shear and volumetric straining responses, are recommended to be developed.

REFERENCES

Andersen, K. H., & Schjetne, K. (2013). Database of friction angles of sand and consolidation characteristics of sand, silt, and clay. *Journal of Geotechnical and Geoenvironmental Engineering*, *139*(7), 1140-1155.

ASTM International. (2014). *D854-14 Standard Test Methods for Specific Gravity of Soil Solids by Water Pycnometer*. Retrieved from https://doi.org/10.1520/D0854-14.

ASTM International. (2016). *D4254-16 Standard Test Methods for Minimum Index Density and Unit Weight of Soils and Calculation of Relative Density*. Retrieved from https://doi.org/10.1520/D4254-16.

ASTM International. (2017). *D6913/D6913M-17 Standard Test Methods for Particle-Size Distribution (Gradation) of Soils Using Sieve Analysis*. Retrieved from https://doi.org/10.1520/D6913_D6913M-17.

ASTM International. (2020). *D4767-11(2020) Standard Test Method for Consolidated Undrained Triaxial Compression Test for Cohesive Soils*. Retrieved from https://doi.org/10.1520/D4767-11R20.

Castro, G. (1969). Liquefaction of sands. *ph. D. Thesis, Harvard Soil Mech*.

Chuhan, F. A., Kjeldstad, A., Bjørlykke, K., & Høeg, K. (2002). Porosity loss in sand by grain crushing—Experimental evidence and relevance to reservoir quality. *Marine and Petroleum Geology*, *19*(1), 39-53. doi:10.1016/S0264-8172(01)00049-6.

Chuhan, F. A., Kjeldstad, A., Bjørlykke, K., & Høeg, K. (2003). Experimental compression of loose sands: relevance to porosity reduction during burial in sedimentary basins. *Canadian Geotechnical Journal*, *40*(5), 995-1011. doi:10.1139/t03-050.

Coop, M. R. (1990). The mechanics of uncemented carbonate sands. *Géotechnique*, *40*(4), 607-626. doi: 10.1680/geot.1990.40.4.607.

Deák, F., Ván, P., & Vásárhelyi, B. (2012). Hundred years after the first triaxial test. *Periodica Polytechnica Civil Engineering*, *56*(1), 115-122. https://doi.org/10.3311/pp.ci.2012-1.13.

Duncan, J. M., & Seed, H. B. (1967). Corrections for strength test data. *Journal of Soil Mechanics & Foundations Div*, *93*(SM5), 121-137.

Hagerty, M. M., Hite, D. R., Ullrich, C. R., & Hagerty, D. J. (1993). One-dimensional high-pressure compression of granular media. *Journal of Geotechnical Engineering*, *119*(1), 1-18.

Hardin, B. O. (1985). Crushing of soil particles. *Journal of Geotechnical Engineering*, *111*(10), 1177-1192. doi: 10.1061/(ASCE)0733-9410(1985)111:10(1177).

Hendron Jr, A. (1963). *The behavior of sand in one-dimensional compression* (No. RTD-TDR63 3089). ILLINOIS UNIV AT URBANA-CHAMPAIGN CHAMPAIGN United States.

Ishihara, K. (1993). Liquefaction and flow failure during earthquakes. *Geotechnique*, *43*(3), 351-415.

Ishihara, K. (1996). *Soil behaviour in earthquake geotechnics*. New York: Oxford University Press Inc.

Ishihara, K., Tatsuoka, F., & Yasuda, S. (1975). Undrained deformation and liquefaction of sand under cyclic stresses. *Soils and Foundations*, *15*(1), 29–44. https://doi.org/10.3208/sandf1972.15.29.

Janbu, N. (1963). Soil compressibility as determined by odometer and triaxial tests. In *Proc. Europ. Conf. SMFE* (Vol. 1, pp. 19-25).

Kondner, R. L. (1963). A hyperbolic stress-strain formulation for sands. In *Proc. 2 nd Pan Am. Conf. on Soil Mech. and Found. Eng., Brazil, 1963* (Vol. 1, pp. 289-324).

Kondner, R. L. (1963). Hyperbolic stress-strain response: cohesive soils. *Journal of the Soil Mechanics and Foundations Division*, *89*(1), 115-143.

Konrad, J. M. (1990). Minimum undrained strength of two sands. *Journal of Geotechnical Engineering*, *116*(6), 932-947. doi:10.1061/(asce)0733-9410(1990)116:6(932).

Lade, P. (2016). *Triaxial testing of soils*. Chichester, West Sussex: John Wiley & Sons.

Lade, P. V., & Abelev, A. V. (2005). Characterization of cross-anisotropic soil deposits from isotropic compression tests. *Soils and Foundations*, *45*(5), 89-102.

Lade, P. V., & Wasif, U. (1988). Effects of height-to-diameter ratio in triaxial specimens on the behavior of cross-anisotropic sand. In *Advanced triaxial testing of soil and rock.* ASTM International. https://doi.org/10.1520/STP29109S.

Lade, P.V., Yamamuro, J.A., & Bopp, P.A. (1997). Influence of time effects on instability of granular materials. *Computers and Geotechnics*, *20*(3-4), 179–193. doi:10.1016/S0266-352X(97)00002-5.

Lambe, T. W. and Whitman, R. V. (1969). *Soil mechanics*. New York: John Willey & Sons. Inc.

Lee, K. L., & Farhoomand, I. (1967). Compressibility and crushing of granular soil in anisotropic triaxial compression. *Canadian Geotechnical Journal*, *4*(1), 68-86. doi: 10.1139/t67-012.

Marachi, N.D., Chan, C.K., and Seed, H.B. (1972). Evaluation of properties of rockfill materials. *Journal of the Soil Mechanics and Foundations Division*, *98*(1), 95-114.

Marsal, R. J. (1967). Large scale testing of rockfill materials. *Journal of Soil Mechanics and Foundations Division, 93*(2), 27-43.

McDowell, G.R. (2002). On the yielding and plastic compression of sand. *Soils and Foundations, 42*(1): 139–145.

McDowell, G.R., Bolton, M.D., & Robertson, D. (1996). The fractal crushing of granular materials. *Journal of the Mechanics and Physics of Solids, 44*(12), 2079–2102. doi:10.1016/S0022-5096(96) 00058-0.

Mesri, G., & Godlewski, P. M. (1977). Time and stress-compressibility interrelationship. *ASCE J Geotech Eng Div, 103*(5), 417-430.

Mesri, G. & Vardhanabhuti, B. (2009). Compression of granular materials. *Canadian Geotechnical Journal, 46*(4), 369-392. doi: 10.1139/T08-123.

Nakata, Y., Kato, Y., Hyodo, M., Hyde, A. F. L., & Murata, H. (2001). One-dimensional compression behavior of uniformly graded sand related to single particle crushing strength. *Soils and Foundations, 41*(2), 39-51.

Pestana, J. M. & Whittle, A. J. (1995). Compression model for cohesionless soils. *Geotechnique*, *45*(4), 611-634. doi: 10.1680/geot.1995.45.4.611.

Rahim, A. (1989). *Effect of morphology and mineralogy on compressibility of sands* (Doctoral dissertation, PhD thesis, Indian Institute of Technology Kanpur, Kanpur, India).

Roberts, J. E., & de Souza, J. M. (1958). The compressibility of sands. *Proceedings of the American Society for Testing and Materials, 58*.

Skempton, A.W. (1954). The pore pressure coefficients A and B. *Geotechnique, 4*(4), 143-147.

Terzaghi, K., & Peck, R.B. (1948). *Soil mechanics in engineering practice*. New York: John Wiley & Sons.

Vaid, Y., & Negussey, D. (1984). Relative density of pluviated sand samples. *Soils and Foundations*, *24*(2), 101-105. doi:10.3208/sandf1972.24.2_101.

Vaid, Y. P., & Negussey, D. (1988). Preparation of reconstituted sand specimens. In *Advanced triaxial testing of soil and rock*. ASTM International. doi:10.1520/stp29090s.

Vaid, Y. P., Sivathayalan, S., and Stedman, D. (1999). Influence of specimen-reconstituting method on the undrained response of sand. *Geotechnical Testing Journal*, *22*(3), 187–195.

Verdugo, R., & Ishihara, K. (1996). The steady state of sandy soils. *Soils and Foundations*, *36*(2), 81-91.

Vesic, A.S., & Clough, G.W. (1968). Behavior of granular materials under high stresses. *Journal of the Soil Mechanics and Foundations Division, 94*(3), 661–688.

Wang, B.Q., & Lade, P. V. (2001). Shear banding in true triaxial tests and its effect on failure in sand. *Journal of Engineering Mechanics, 127*(8), 754-761.

Wong, K. S., & Duncan, J. M. (1974). *Hyperbolic stress-strain parameters for nonlinear finite element analyses of stresses and movements in soil masses*. College of Engineering, Office of Research Services, University of California.

Wong, R.T., Seed, H.B., and Chan, C.K. (1975). Cyclic loading liquefaction of gravelly soils. *Journal of the Geotechnical Engineering Division, 101*(GT6), 561-583.

Wood, F. M., Yamamuro, J. A., & Lade, P. V. (2008). Effect of depositional method on the undrained response of silty sand. *Canadian Geotechnical Journal*, *45*(11), 1525–1537. https://doi.org/10.1139/T08-079.

Yamamuro, J. A., Bopp, P. A., and Lade, V. L. (1996). One-dimensional compression of sands at high pressures. *Journal of the Geotechnical Engineering*, *122*(2), 147-154.

Yoshimine, M., & Ishihara, K. (1998). Flow potential of sand during liquefaction. *Soils and Foundations*, *38*(3), 189-198.

APPENDICES

A. Appendix A

Table A-1: Results of Specific Gravity Tests for Çine Sand

SPECIFIC GRAVITY TEST RESULTS	**Sample No**			
	1	**2**	**3**	**4**
M_p, the avarage calibrated mass of the dry pycnometer (g)	76.78	78.55	75.41	74.62
M_{pw}, the mass of the pycnometer and water at the test temperature (g)	327.14	331.33	326.77	328.94
M_s, the mass of the oven dry soil solids (g)	66.81	66.34	65.66	63.74
M_{pws}, the mass of pycnometer, water, and soil at the test temperature (g)	368.91	372.76	367.76	368.80
T, the test temperature (°C)	28.00	28.00	28.00	28.00
K, the temperature coefficient	0.99803	0.99803	0.99803	0.99803
Gs	2.663	2.658	2.656	2.664

B. Appendix B

Table B-1: Results of maximum and minimum void ratio tests

Diameter of Mold (mm)	152.05
Height of Mold (mm)	115.61
Mass of Mold (g)	4538.2
Volume of Mold (mm3)	2099220.85
e_{max}	
Mass of mold + specimen (g)	7587.8
Mass of specimen (g)	3049.6
Gs	2.66
ρ_{water} (g/cm^3)	0.997
e_{max}	0.826
e_{min}	
Mass of mold + specimen (g)	8247.1
Mass of specimen (g)	3708.9
Gs	2.66
ρ_{water} (g/cm^3)	0.997
e_{min}	0.501